이학박사 학위논문

Fluxes and behaviors of groundwater-borne nutrients in the ocean

해양에서 지하수 기원 영양염의 플럭스와 거동

2017 년 8 월

서울대학교 대학원

지구환경과학부

조 형 미

Abstract

Fluxes and behaviors of groundwater-borne nutrients in the ocean

Hyung-Mi Cho
School of Earth and Environmental Sciences
The Graduate School
Seoul National University

Submarine groundwater discharge (SGD) into coastal waters is an important pathway for transporting nutrients to the ocean. Although the fluxes of SGD and associated nutrient discharge to the ocean at local and regional scales have been well studied, detailed estimates and models of SGD-related nutrient inputs to coastal waters on a global scale are few in number. Therefore, in this study, the global magnitude of SGD and its associated nutrient fluxes into the global ocean were estimated using a radium isotope (^{228}Ra). The re-estimated magnitude of global SGD flux was approximately 1–1.5 times the river discharge and SGD-derived nutrient fluxes were comparable to the river-driven fluxes to the global ocean. These results imply that SGD is a critical source of nutrients to the ocean and therefore plays a critical role in marine productivity.

Nutrient fluxes through SGD can be calculated by multiplying the endmember concentrations of nutrients in groundwater by the SGD flux. However, groundwater nutrient concentrations are altered through biogeochemical reactions in the subterranean estuary (STE), where mixing between groundwater and aquifer solids occurs, prior to entering the ocean. Furthermore, the adsorption and desorption behaviors of silicon (Si) and phosphorus (P) in the STE have not been investigated although these processes influence Si and P fluxes through SGD. Based on laboratory experiments, rapid desorption of P (5–20 μmol/L) occurred from the sediment columns when Si was 40−90% removed in the initial stage within the first 24 hours. These results suggest that Si adsorption can result in significant P desorption from sediments in the STE into seeping groundwater.

Nutrient inputs via SGD play a significant role in nutrient cycling and primary productivity in the coastal ocean. This study based on seasonal sampling campaigns shows that SGD plays a critical but different role in nutrient budgets and stoichiometry in coastal waters off a volcanic island depending on open-ocean nutrient conditions. When bay seawater was influenced by the N-limited Tsushima Current, SGD was the major source of DIN in N-limited bay waters. SGD was also the absolute source of DIP in P-depleted bay waters that were influenced by P-limited Changjiang River diluted water (CDW). In addition, excessive inputs of nutrients from SGD resulted in an almost complete transfer of SGD-derived nutrients to the open ocean during the season in which a large flux of SGD occurs.

Keywords: submarine groundwater discharge (SGD), nutrients, subterranean estuary, nutrient fluxes, coastal ocean, global ocean

Student number: *2009-22956*

Table of Contents

List of Tables

List of Figures

1. Introduction

1.1. Submarine groundwater discharge

River discharge has been known to be a major pathway for water discharge from land to ocean. Rivers are highly visible open channels and their contributions to the oceans are easily quantifiable (Taniguchi et al., 2002). Recently, however, submarine groundwater discharge (SGD) has been paid attention from oceanographic community recent decades (Taniguchi et al., 2002). SGD occurs as springs and diffusive flow on continental margins, usually at or below the water surface (Taniguchi et al., 2002; Kim et al., 2003). A compilation of observed SGD on a worldwide scale shows that groundwater seepage from the land to the ocean occurs in many environments along the world's continental margins. SGD is both volumetrically and chemically important to coastal water and chemical budgets since the length of coastline where SGD occurs is great, and will occur whether or not rivers are present (Taniguchi et al., 2002).

The term SGD has been used in different ways over the years. According to Zekster et al. (1983), SGD was defined as the net groundwater discharge to the ocean, which comes from aquifer recharge. On the other hand, Church (1996) defined SGD to be "direct groundwater outflow across the ocean-land interface into the ocean" which would include recirculated seawater. Due to the ambiguity of the definition of SGD with or without recirculated seawater, misunderstandings could

occur when comparing SGD with other freshwater discharges. Finally, SGD is defined as any and all flow of water on continental margins from the seabed to the coastal ocean, regardless of fluid composition or driving force (Burnett et al., 2003). Therefore, the total SGD consists of submarine fresh groundwater discharge (SFGD) and recirculated saline groundwater discharge (RSGD) (Figure 1.1).

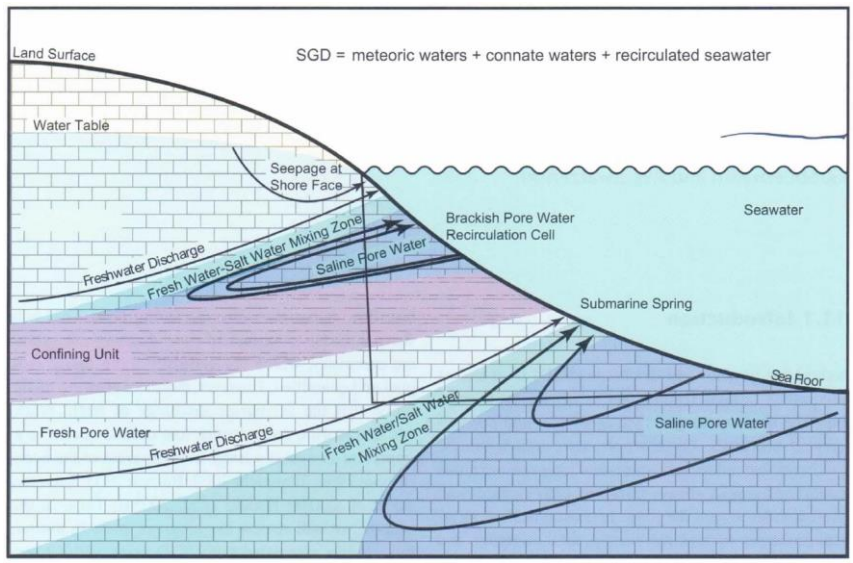

Figure 1.1. Schematic overview of an idealized SGD-influenced hydrogeological land-ocean interface (from Kim and Swarzenski, 2010).

1.2. Behaviors of nutrients in the subterranean estuary

Mixing between meteoric water and seawater produces brackish to saline water in many coastal aquifers. In this mixing zone, chemical reactions of the salty water with aquifer solids modify the composition of the water. To emphasize the importance of mixing and chemical reaction in these coastal aquifers, Moore (1999) defined the mixing zone as subterranean estuary (STE).

In contrast to surface estuaries, STEs are usually characterized by longer residence times, lower dissolved oxygen content, and stronger particle-water interactions and biogeochemical reactions (Santos et al., 2008). Although the biogeochemical processes regulating the input, recycling, and removal in surface estuaries and their transfer to the oceans are relatively well known, biogeochemical behaviors of nutrients in STEs have begun to be studied in recent decades.

The biogeochemistry of nutrients (e.g. NO_3^-, NH_4^+, and PO_4^{3-}) in STEs and the groundwater nutrient fluxes to coastal waters are strongly affected by the redox conditions of the freshwater and seawater (e.g. Slomp and Van Cappellen, 2004; Spiteri et al., 2008). Nitrate (NO_3^-) can be reduced to nitrite (NO_2^-) under anaerobic conditions and ultimately formed molecular nitrogen (N_2) through a series of intermediate gaseous nitrogen oxide products (NO and N_2O) under anoxic conditions. The anaerobic oxidation of ammonium (anammox) is a relatively recent discovery, which is a “short circuit” in the nitrogen (N) cycle because N_2 gas can be formed

without complete oxidation of ammonium (NH_4^+) to NO_3^- (Santoro, 2010). On the other hand, under oxic conditions, NH_4^+ is effectively removed through nitrification while phosphorus (P) is attenuated through sorption onto iron and aluminum oxides. As a result of P adsorption onto iron- and aluminum oxides in aquifers and coastal sands, P loading through SGD is typically well attenuated.

The major source of dissolved inorganic silicon (DSi) to groundwater is the rocks, sediments, and soils making up the aquifer substrate. The concentrations of DSi in groundwater are less variable than those of nitrate, phosphate, or other dissolved constituents (Davis, 1964), but varying somewhat based on rock type. The groundwater silica concentrations are mainly determined by the mineral characteristics of the aquifer substrate (Davis, 1964) and how long the water has been in contact with that aquifer substrate (Haines and Lloyd, 1985), while the concentrations of nitrate and phosphate are influenced by anthropogenic sources and by groundwater chemistry.

1.3. Nutrient fluxes via submarine groundwater discharge and biological effects in the coastal ocean

Surface runoff through rivers has been considered the most important terrestrial nutrient pathway supporting primary production in coastal oceans. However, recent local and regional studies suggested that SGD is even more important than river discharge with respect to the delivery of nutrients to coastal waters (Table 1.1). For example, Johannes (1980) may be the first who showed that SGD-derived N flux is several fold higher than that through river discharges in the Perth, Australia. In some locations where rivers are present, groundwater nutrient loads are comparable to, or greater than, riverine fluxes (e.g., Garrison et al., 2003; Burnett et al., 2007).

Over a basin scale, Kim et al. (2005) showed that Si flux through SGD in the Yellow Sea is 20−100% of the riverine input. Rodells et al. (2015) recently showed that nutrient inputs through SGD is comparable to, or higher than those through rivers in the Mediterranean Sea.

The groundwater-borne nutrient loads are relatively more important at some sites with little or no surface flow and SGD is the only pathway for terrestrial nutrients transport to the sea. These sites include volcanic islands such as Hawaii, USA (Kay et al., 1977; Oki, 1999), the island of Majorca, Spain (Rodellas et al., 2014), Mauritius Island (Povinec et al., 2012), and Jeju Island, Korea (Kim et al.,

2003) and karst environments such as the Yucatan Peninsula of Mexico (Young et al., 2008), Florida (Corbett et al., 1999), and etc.

Nutrients delivered to estuaries, bays, and coastal waters by SGD can have important ecological effects. Thus, SGD-derived nutrients to coastal oceans enhance primary production (Luo et al., 2014) and benthic production (Waska and Kim, 2011). Moreover, groundwater-borne nutrients may have significant effects on phytoplankton community composition (Lapointe, 1997; Lee and Kim, 2007b) and water quality in coastal oceans (Reay et al., 1992). Since nutrient concentrations in groundwater correlate with land use and population density (Cole et al., 2006), excess nutrients from SGD can lead to significant eutrophication problems in coastal region (Hwang et al., 2005b). SGD-related eutrophication has occurred in enclosed or semi-enclosed nature, which restricts circulation and exchange with lower-nutrient offshore seawater. Hwang et al. (2005b) reported that SGD provided the majority of nutrients and was determined to be the cause of benthic eutrophication in Bangdu Bay on the volcanic Jeju Island. Discharge of high-nutrient groundwater was also implicated in eutrophication in the Florida Keys (Lapointe and Clark, 1992) and in Tolo Harbor, Hong Kong (Tse and Jiao, 2008).

Another potential negative consequence of SGD-related nutrient subsidies are red tides and brown tides (Gobler and Sañudo-Wilhelmy, 2001; Hu et al., 2006; Lee et al., 2010), known as harmful algal blooms (HABs). Hu et al. (2006) observed

that nutrient loads from rivers were insufficient to support a HAB in coastal waters off west-central Florida, and suggested that SGD was the most likely source of the additional nutrients. SGD was identified as the most likely source of nutrients supporting recurrent HABs also in many sites in Korea (e.g. Yeoja Bay, Hwang et al., 2005a; Masan Bay, Lee et al., 2009).

Finally, SGD-borne nutrients can damage to coral reefs and 'phase shifts' from coral-dominated to macroalgae-dominated reef areas. Paytan et al. (2006) evaluated nutrient input via SGD to six coral reef sites in the Indian, Atlantic and Pacific Oceans, and Gulf of Aqaba and confirmed that SGD was an important source of new nutrients to these coral reef ecosystems. However, enhanced nutrient loading by human activity via SGD can lead to reef degradation (Paytan et al., 2006).

Table 1.1. A comparison of SGD-derived nutrient fluxes and riverine fluxes into the coastal ocean.

Site	Geology	Nutrient	Ratio of SGD nutrient fluxes to riverine inputs	Reference
Perth Region, West Australia		DIN DIP	3 : 1 5 : 1	*Johannes, 1980*
Kahana Bay, Oahu, Hawaii	Alluvium	TDN TDP	2 : 1 5 : 1	*Garrison et al., 2003*
Tampa Bay, Florida	Permeable sand	TDN TDP	0.4 : 1 1 : 1	*Kroeger et al., 2007*
Lynch Cove, WA		DIN	(1-2) : 1	*Swarzenski et al., 2007a*
Gulf of Mexico STE	Limestone & dolomite	TDN	1 : 1	*Santos et al., 2008*
Masan Bay, Korea	Silt & clay	DIN DIP, DSi	(0.2-1.7) : 1 (2-3) : 1	*Lee et al., 2009*
Gulf of Thailand		DIN DIP	0.5 : 1 0.7 : 1	*Burnett et al., 2007*
Yeongil Bay, Korea	Sand & gravel	DIN DIP DSi	950 : 1 24 : 1 52 : 1	*Kim et al., 2008*
Tolo Harbour, Hong Kong	Alluvium	DIN DIP DSi	955 : 1 25 : 1 93 : 1	*Lee et al., 2012*
Total South Carolina Marshes	Fine-grained sand	DIN DIP	1 : 1 1.2 : 1	*Krest et al., 2000*

DIN: Dissolved inorganic nitrogen

DIP: Dissolved inorganic phosphorus

TDN: Total dissolved nitrogen

DSi: Dissolved inorganic silicon

1.4. Aims and the scope of study

The aim of this study is to investigate the flux, behavior, and role of groundwater-borne nutrients in the ocean (Figure 1.2). The simplest approach to estimating SGD-associated nutrient fluxes to coastal waters is multiplying the SGD flux by the endmember value of nutrients concentrations of the discharging groundwater. However, the total SGD (fresh and saline) and associated nutrients fluxes into the coastal oceans on a global scale have not yet been studied well due to the lack of the global dataset. Thus, in this study, the global magnitude of total SGD is re-evaluated using radium isotope data from global ocean and groundwater in coastal aquifers. In addition, the SGD-derived net nutrient fluxes into the global ocean are estimated and compared with riverine fluxes.

However, the endmember concentrations of Ra isotopes and nutrients are greatly dependent on groundwater salinity. The SGD-derived chemical species usually undergo transformation by geochemical reactions in the STE, which can significantly alter nutrient concentrations that are discharged into the ocean via SGD. While the biogeochemical behaviors of N have been studied well, the behaviors of P and Si in the STEs are relatively unknown. Therefore, the biogeochemical behaviors (adsorption/desorption) of P and Si in STEs are investigated in this study.

The SGD-derived nutrients are important in coastal primary production. Especially, SGD-derived nutrient fluxes from highly permeable volcanic islands

standing in oligotrophic oceans could be very important for feeding nutrients to coastal organisms. Therefore, the temporal changes in groundwater-borne nutrient contributions to coastal waters are investigated on a volcanic Jeju Island, where nutrient conditions of open-ocean waters passing alongside the island are different for different seasons.

Overall, the objectives this study are:

(1) to estimate the flux of SGD to the global ocean

(2) to estimate the nutrients input fluxes to the global ocean via total SGD

(3) to investigate the behaviors of silicate and phosphate in the STE

(4) to investigate the different roles of groundwater-borne nutrients to coastal waters off a volcanic Jeju Island for different seasons.

Thus, these studies are composed of a series of global fluxes, behaviors, and roles of SGD and SGD-derived nutrients in the marine environments.

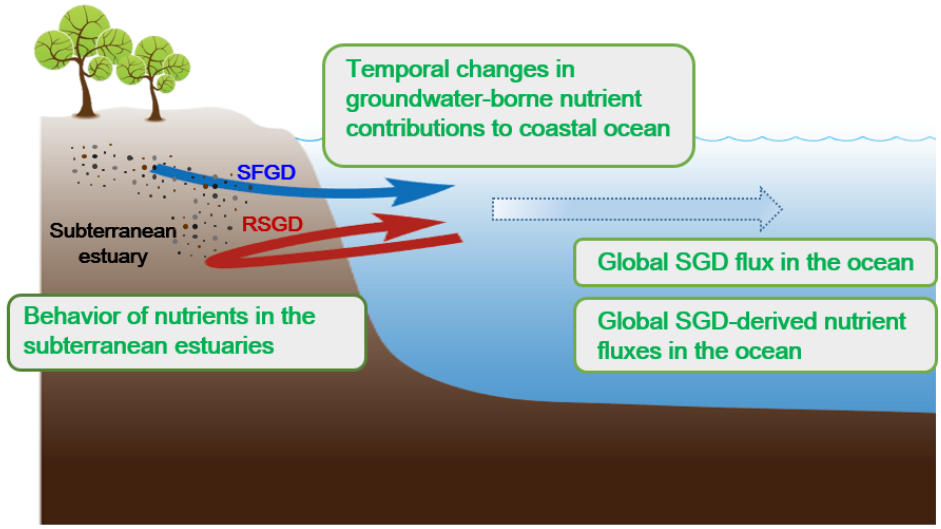

Figure 1.2. Schematic overview of the goals of this study.

2. Estimation of global magnitude of submarine groundwater discharge

2.1. Introduction

SGD is the flow of water from coastal aquifers into oceans that takes place at continental margins. The total SGD comprises meteoric water combined with seawater that has infiltrated coastal aquifers (which subsequently flows back into the ocean after mixing with meteoric water). The direct estimation of SGD is almost impossible over a large scale since it is unseen and very variable over different temporal and spatial scales. Taniguchi et al. (2002) concluded that fresh SGD can span a range of approximately three orders of magnitude, or 0.01–30% of the total river discharge, based on water balance or hydrogeological considerations. However, Moore (1996) documented that SGD contributes at least 40% of the river flux into the South Atlantic Bight using ^{226}Ra (half-life: 1600 years) as a tracer. As such, Moore et al. (2008) showed that the SGD into the Atlantic basin is 0.8−1.6 times the river discharge using a ^{228}Ra (half-life: 5.75 years) tracer. More recently, Kwon et al. (2014) showed that the SGD into the global ocean (Indo-Pacific Ocean and Atlantic Ocean) is estimated to be $(12 \pm 3) \times 10^{13}$ $m^3 \cdot yr^{-1}$, which is 3−4 times the riverine freshwater flux, using ^{228}Ra tracer modeling. This difference is, in part, due to the difference in the definition of SGD (i.e., fresh vs. saline groundwater). In terms of the transport of chemical constituents (i.e., nutrients, trace elements, carbon,

radionuclides, etc.), saline groundwater fluxes are known to be, in general, far more important than fresh groundwater fluxes (Li et al., 1999; Kim and Hwang, 2002; Burnett et al., 2003; Kim et al., 2003).

Geochemical tracer methods are powerful tools in to the estimation of the total SGD (fresh plus saline groundwater) over a large scale, since SGD tracers (i.e., Rn and Ra isotopes) are 1−2 orders of magnitude more enriched in groundwater, soluble in seawater, and decay on the same scale as oceanic turnover. In particular, ^{228}Ra has been used successfully for tracing SGD throughout the Atlantic Ocean (Moore et al., 2008) and the global ocean (Kwon et al., 2014). Moore et al. (2008) estimated the magnitude of total SGD across the entire Atlantic Ocean using the endmember value of ^{228}Ra in coastal groundwater and SGD-derived ^{228}Ra flux into the ocean. In this estimation, the SGD-derived ^{228}Ra flux into the ocean was calculated by subtracting riverine, atmospheric, and sedimentary diffusive fluxes from the total ^{228}Ra flux into the ocean, which were derived from the decay of the ^{228}Ra inventory in the entire Atlantic Ocean. Using a similar ^{228}Ra mass balance model, Kwon et al. (2014) estimated the SGD magnitude in the global ocean. They obtained the coastal ^{228}Ra fluxes using inverse modeling of the ^{228}Ra in surface waters. This inverse model used ^{228}Ra decay (after subtracting the atmospheric input of ^{228}Ra) and an ocean circulation field, which was constrained by observed temperature, salinity, sea surface height, air-sea exchange of heat and freshwater, radiocarbon, and chlorofluorocarbon-11.

In a manner similar to ^{228}Ra, long-lived ^{226}Ra has also been successfully used to trace SGD at coastal and regional scales (Kim et al., 2005; Moore, 1996). In addition, the short-lived ^{224}Ra (half-life: 3.4 days) and ^{223}Ra (half-life: 11.3 days) have been successfully used at coastal scales (Hwang et al., 2005a; 2005b). The mass balance models of ^{226}Ra, ^{224}Ra, and ^{223}Ra for SGD estimation use information on the SGD-derived flux of these isotopes and their coastal groundwater endmembers. The SGD-derived fluxes are estimated by subtracting the other fluxes, such as atmospheric, benthic diffusive, and riverine fluxes, from the total fluxes, which are determined by the inventory of excess concentrations of Ra isotopes and the residence time of the water masses.

These geochemical SGD tracing methods have the greatest uncertainty with respect to constraining the tracer endmember concentration in groundwater. Most of the previous methods calculate Ra endmembers by averaging tracer values in the groundwater (Beck et al., 2007a; Moore et al., 2008; Rapaglia et al., 2010; Lee et al., 2012; Kwon et al., 2014). However, Moore (1996) and Stewart et al. (2015) used the maximum ^{226}Ra concentration for the groundwater endmember to avoid overestimations.

The concentrations of tracers can be affected greatly by the complex interactions among hydrogeological, oceanic, and geochemical processes that occur

in STEs, such as the redox conditions of groundwater, biogeochemical and geochemical conditions, and the residence times of water in the aquifer. Thus, in this study, the characteristics of ^{228}Ra and ^{226}Ra in coastal groundwater were examined and then the influence of the endmember characteristics and the geographical heterogeneity of data density on determining the SGD magnitude were re-evaluated.

2.2 Data compilations

Data were compiled for ^{228}Ra (n = 552) and ^{226}Ra (n = 708) in global coastal groundwater (Figure 2.1), which have been updated from Kwon et al. (2014) and Moore et al. (2008), in order to calculate the basin-scale endmembers of Ra isotopes in groundwater.

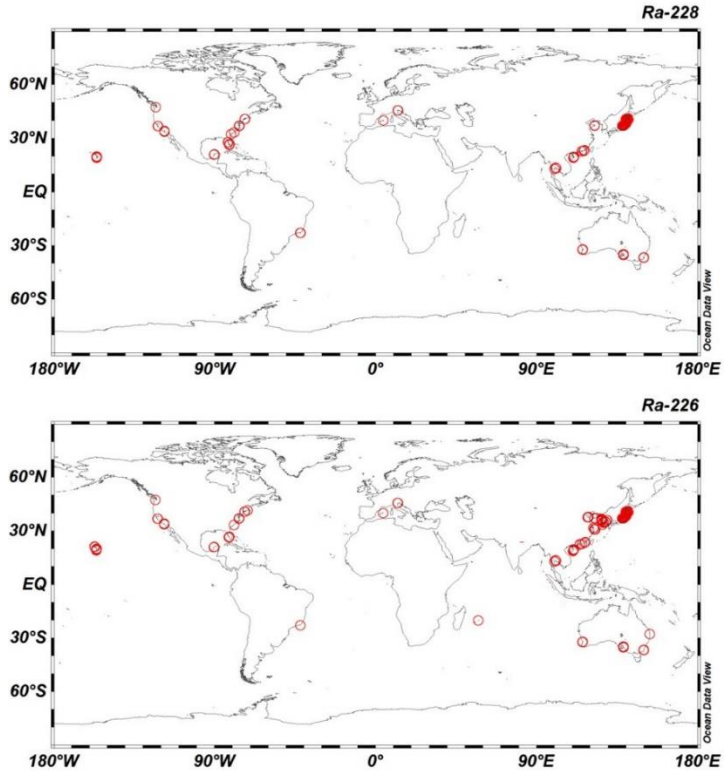

Figure 2.1. The global distributions of data collection sites for ^{228}Ra (n = 552) and ^{226}Ra (n = 708) concentrations in groundwater from coastal aquifers. The compiled data, which have been updated from Kwon et al. (2014) and Moore et al. (2008), are shown in Appendix Table A.

2.3. Results and discussion

2.3.1. Effects of geographical gridding methods

The endmember of Ra isotopes has been traditionally calculated using the lognormal average of all data obtained from the area of interest, regardless of hydrogeological conditions and heterogeneity of data (Moore et al., 2008; Kwon et al., 2014). However, sampling locations are heavily biased towards the western coast of the Pacific and Atlantic Oceans, and data are particularly rare in South America, Africa, and Europe (Figure 2.1). Thus, in this study, the endmember values were calculated using two different methods (with and without gridding), since the endmember values could potentially be affected significantly by the geographical heterogeneity of the data density. The method without gridding estimates the globally averaged Ra endmember of the SGD using the mean of a lognormal distribution of all the collected data (Figure 2.2). The method with gridding uses three steps to estimate the endmember value of Ra: (1) the entire area is divided into the horizontal resolution of a 2° × 2° grid in order to split all the data into grid squares before averaging; (2) the average value for each grid square is calculated; (3) the averaged Ra value of the SGD of the global ocean is calculated using the averaged values in each grid square. For both methods, lognormal distributions of all data were assumed to account for the skewness.

The lognormal averages of the ^{228}Ra endmember (without gridding), as calculated previously by Moore et al. (2008) and Kwon et al. (2014), were estimated

to be 1109 ± 94 and 920 ± 64 dpm m^{-3} in the Atlantic and global oceans, respectively. These values agree well, within uncertainties, with 1097 ± 300 and 934 ± 208 dpm m^{-3} as calculated by the 2° × 2° gridding method in the Atlantic and global oceans, respectively (Figure 2.3a). These endmember values of ^{228}Ra in the Atlantic Ocean and the global ocean agreed with those obtained by Moore et al. (2008) (1273–1592 dpm m^{-3}) and Kwon et al. (2014) (986–1147 dpm m^{-3}), respectively, after the data were updated. The lognormal averages of the ^{226}Ra endmember (without gridding) were estimated to be 1113 ± 104 and 643 ± 42 dpm m^{-3} for the Atlantic and global oceans, respectively. These ^{226}Ra endmember values agree with the results (1050 ± 338 and 594 ± 132 dpm m^{-3}) obtained by the gridding method (Figure 2.3b). Overall, the results from the gridding method agree well with those obtained without the gridding method for both ^{228}Ra and ^{226}Ra, suggesting that the geographical skewness of data distributions does not significantly affect the endmember values. Therefore, it can possible to use either method, or the average of both methods, to determine a representative value for each element.

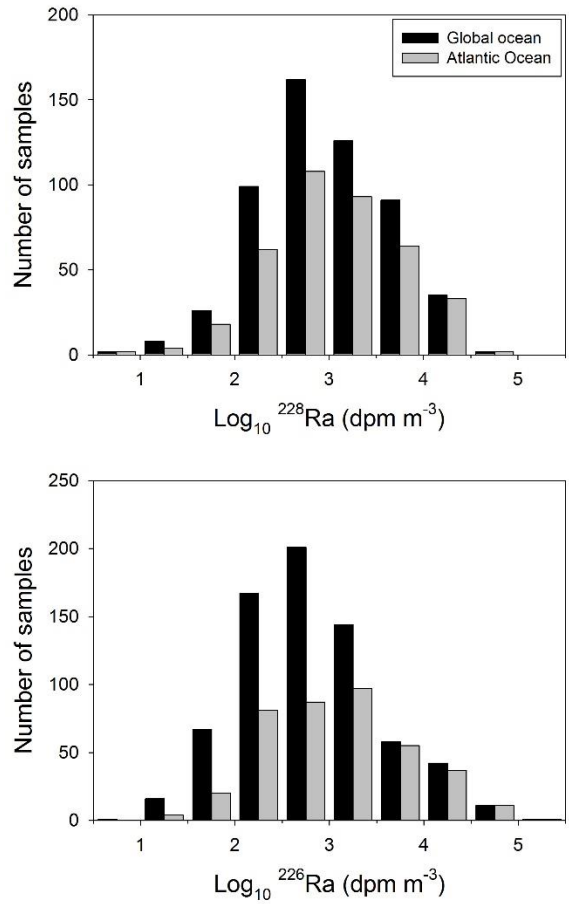

Figure 2.2. The distributions of ^{228}Ra and ^{226}Ra in coastal groundwater samples from the Atlantic Ocean and the global ocean using the compiled data.

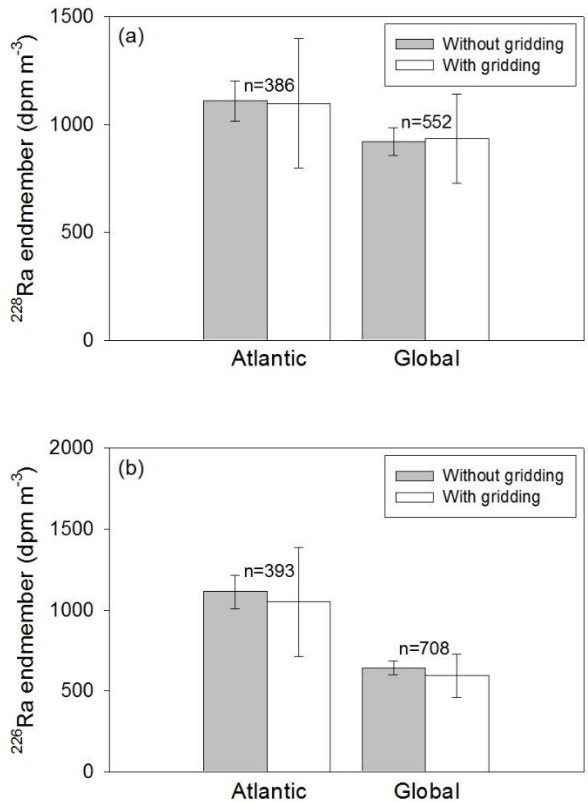

Figure 2.3. The endmember values of ^{228}Ra and ^{226}Ra in coastal groundwater for the Atlantic Ocean and the global ocean. The graphs show the results obtained from both with and without the use of gridding methods. The error bars show ± one standard deviation of the results.

2.3.2. Effects of groundwater salinity

Because the SGD fluxes obtained using Ra tracers are for the total groundwater, which includes saline and fresh groundwater, the effect of salinity on Ra endmember values can bias the magnitude of SGD. Therefore, the average Ra concentrations in groundwater for different ranges of salinity were calculated, and then the effect of sample salinity on SGD estimations was examined. For this purpose, the data (^{228}Ra, n = 360; ^{226}Ra, n = 516) that had salinity information were only used. The salinity of groundwater for the compiled ^{228}Ra and ^{226}Ra samples ranged from 0 to 59. For a simple comparison, the concentrations of ^{228}Ra and ^{226}Ra were sorted into four different salinity ranges (0−10, 10−20, 20−30, and >30).

The endmember concentrations of ^{228}Ra for the salinity ranges of 0−10, 10−20, 20−30, and >30 were 433 ± 69 (n = 100), 1806 ± 375 (n = 41), 2441 ± 376 (n = 81), and 2821 ± 501 dpm m^{-3} (n = 71), respectively, in the Atlantic Ocean and 492 ± 70 (n = 149), 1727 ± 340 (n = 47), 2403 ± 360 (n = 85), and 2506 ± 430 dpm m^{-3} (n = 79), respectively, in the global ocean (Figure 2.4a). The data from the Atlantic Ocean dominate the global data set for high salinity groundwater. In general, the endmember concentrations of ^{228}Ra are higher for higher salinity waters.

The endmember concentrations of ^{226}Ra for the salinity ranges of 0−10, 10−20, 20−30, and >30, were 394 ± 57 (n = 103), 1392 ± 429 (n = 42), 1342 ± 311 (n = 83), and 1351 ± 198 dpm m^{-3} (n = 72), respectively, in the Atlantic Ocean, and

336 ± 36 (n = 191), 646 ± 131 (n = 82), 891 ± 144 (n = 129), and 870 ± 108 dpm m^{-3} (n = 114), respectively, in the global ocean (Figure 2.4b). The endmember ^{226}Ra concentrations for salinity values >10 were consistently approximately three-fold greater than those for fresh groundwater in the Atlantic Ocean. However, the endmember concentrations increase as salinity increases if the data from Yucatan, which show unusually high concentrations of ^{226}Ra, are omitted.

Overall, in the global ocean, the concentrations of ^{228}Ra and ^{226}Ra are higher in higher salinity ranges, with much lower activities in fresh groundwater relative to saline groundwater (salinity >10) (Figure 2.4). The increases in Ra observed in higher salinity water seem to be associated with higher ionic strength, showing lower particle reactivity due to competition with other ions for the adsorption sites of sediments. This concept is well supported by various laboratory studies and estuarine studies (Gonneea et al., 2008; Webster et al., 1995). For general estuaries, Ra isotopes are preferentially desorbed relative to their parents as fluvial sediments encounter seawater, resulting in maximum ^{226}Ra concentrations in water with a mid-salinity range between 10 and 25 (Li et al., 1977; Moore, 1981; Elsinger and Moore, 1984; Burnett et al., 1990; Moore et al., 1995; Gonneea et al., 2008). The decrease of Ra in estuaries with a salinity higher than 25 seems to be due to dilution by the open-ocean water following the maximum desorption (Figure 2.5). However, Ra concentrations increase as salinity increases in STEs (Figure 2.5), since seawater directly invades fresh rocks and sediments.

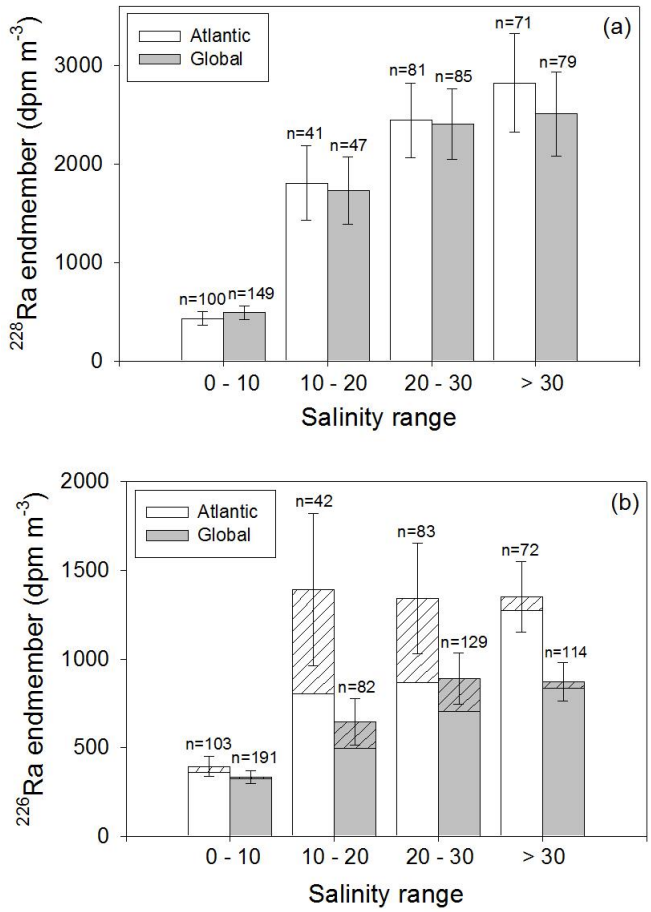

Figure 2.4. The distribution of the endmember values of (a) ^{228}Ra and (b) ^{226}Ra in coastal groundwater, according to the groundwater salinity ranges in the Atlantic Ocean and the global ocean, respectively. The bar marked with dashes indicates the Yucatan data (n = 17) in the Atlantic Ocean, which showed unusually high ^{226}Ra values in the salinity range of 10−30. The concentrations of ^{228}Ra and ^{226}Ra increased for higher salinity ranges in the global ocean, with much lower activities in fresh groundwater relative to saline groundwater (salinity >10).

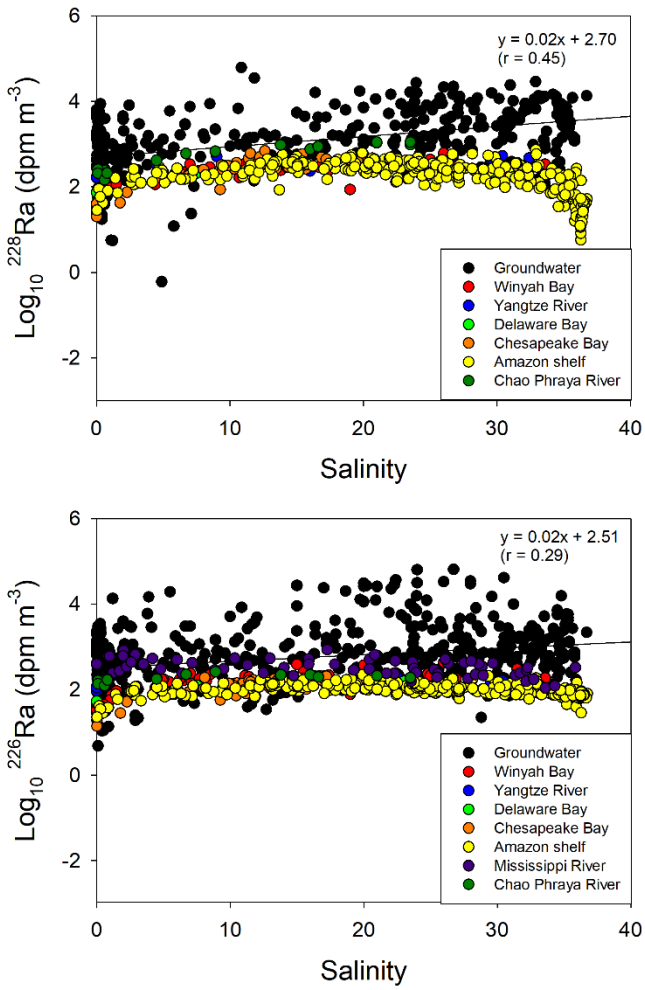

Figure 2.5. ^{228}Ra and ^{226}Ra concentrations as a function of salinity for groundwater and river water samples. The river water data in Winyah Bay, Yangtze River, and Delaware Bay are from Elsinger and Moore (1984). The river water data in Chesapeake Bay, Amazon shelf, Mississippi River, and Chao Phraya River are from Moore (1981), Moore et al. (1995), Moore and Scott (1986), and Nozaki et al. (2001), respectively.

2.3.3. Revisiting basin-scale SGD magnitude estimations

Since ^{228}Ra endmember values are greatly dependent on salinity, Ra endmember values of SGD for three different salinity ranges (>10, >20, and >30; Table 2.1) were calculated and compared. The endmember values of ^{228}Ra in the Atlantic Ocean were similar among the higher salinity ranges (2415 ± 239, 2612 ± 297, and 2821 ± 501 dpm m^{-3} for salinity >10, >20, and >30, respectively) but approximately six-fold higher than the endmember value in the lower salinity range (salinity <10). For the compiled global data, the endmember values of ^{228}Ra were similar among the higher salinity ranges (2268 ± 216, 2452 ± 271, and 2506 ± 430 dpm m^{-3} for salinity >10, >20, and >30, respectively), but they were approximately five-fold higher than those in the lower salinity range (salinity <10).

Thus, the salinity effect may bias the ^{228}Ra and ^{226}Ra endmember values given that the previous studies did not consider salinity in the endmember calculations. In fact, previously compiled data (Kwon et al., 2014) show that fresh groundwater data account for almost half of the entire dataset. Although it is impossible to separate fresh and saline groundwater in SGD, the salinity of the majority of groundwater is likely to be greater than 10 based on seepage experiments conducted throughout the world (Lewis, 1987; Cable et al., 1997; Kim et al., 2003; Stieglitz et al., 2007; Taniguchi et al., 2007; Rapaglia and Bokuniewicz, 2009; Taniguchi et al., 2009) and the fact that about 10% of SGD is composed of fresh groundwater throughout the world (Burnett et al., 2003; Kim et al., 2003; Taniguchi

et al., 2006; Kwon et al., 2014). Taniguchi et al. (2009) reported that the magnitude of total SGD is generally dependent on the distance from shore, with higher discharges and higher fresh water proportions in shallow waters. This trend is associated with decreasing hydraulic connectivity between terrestrial groundwater and seawater with increasing distance from shore. The proportions of fresh groundwater in SGD are ~40% and ~5% at 100 and 1000 m offshore, respectively (Taniguchi et al., 2009). Thus, it is reasonable to use the data for salinity >10 rather than determining more narrow salinity range since the magnitudes of SGD are similar within 15% for different higher salinity ranges (>10, >20, and >30).

Thus, I compared the calculated SGD results of the total dataset (using the traditional methods without consideration of salinity effects) with the higher salinity data set (salinity >10) for the entire Atlantic Ocean and the global ocean. If the Ra endmember value in saline groundwater (salinity >10) are used, SGD becomes (1.7 ± 0.4) × 10^{13} m^3 yr^{-1}, which is approximately 50% of the value determined using the full dataset, in the Atlantic Ocean. For the global ocean, if the low salinity groundwater (salinity <10) data were exclude, the magnitude of global SGD is estimated to be (5.6 ± 1.5) × 10^{13} m^3 yr^{-1}, which is approximately 40% of the value determined using the full dataset. The results are similar for different higher salinity ranges (>10, >20, and >30) for groundwater Ra endmember values in the Atlantic and global oceans (Table 2.1).

The basin-scale SGD fluxes in the literature that use different methods for calculating groundwater Ra endmember values are compared with the calculated SGD fluxes that use lognormal Ra average in higher salinity (>10) groundwater (Table 2.2). Various approaches have been used to obtain groundwater Ra endmember values in previous studies (Moore, 1996; Kim et al., 2005; Moore et al. 2008; Kwon et al., 2014; Rodellas et al., 2015). The SGD fluxes (Table 2.2) in the Yellow Sea (Kim et al., 2005) and the Mediterranean Sea (Rodellas et al., 2015) were calculated using a range of groundwater Ra data, which allowed large uncertainties. In the South Atlantic Bight, the highest average of groundwater Ra data was used (Moore, 1996), resulting in approximately two-fold lower SGD rates compared to the results from the method used in this study. For the entire Atlantic Ocean, Moore et al. (2008) suggested that the magnitude of SGD is (2−4) × 10^{13} m^3 yr^{-1}, which is 80−160% of the river discharge to the Atlantic Ocean, based on the groundwater Ra endmember calculated using the mean value of a lognormal distribution for the complete ^{228}Ra dataset. If higher salinity data (salinity >10) are used, the SGD becomes (1.3 ± 0.6) × 10^{13} m^3 yr^{-1}, which is approximately 50% of the river flux. For the global ocean, Kwon et al. (2014) suggested that the magnitude of SGD, based on the total ^{228}Ra dataset, is (12 ± 3) × 10^{13} m^3 yr^{-1}, which is approximately 3−4 times the river discharge. However, if the low salinity groundwater (salinity <10) data were exclude, the magnitude of global SGD is estimated to be (4.4 ± 1.2) × 10^{13} m^3 yr^{-1}, which is approximately 60% lower and therefore is approximately 1−1.5 times the river discharge.

During the last few decades, through the use of Ra tracers, SGD has been emphasized as the main pathway for the input of nutrients, dissolved organic matter, and trace elements in the near-coast ocean (Burnett et al., 2003; Kim et al., 2005; Moore, 2006; Kim et al., 2012; Rodellas et al., 2014). Using Ra-based SGD estimation, nutrient inputs via SGD are found to be comparable with inputs via rivers in the Mediterranean Sea (Rodellas et al., 2015) and the Yellow Sea (Kim et al., 2005). At small scales (i.e., bays, harbors, and islands), nutrient inputs through SGD, determined using Ra isotopes, are often an order of magnitude higher than those through surface run-off (Lee et al., 2012; Wang et al., 2014). Thus, careful consideration of the groundwater Ra endmember is necessary in order to estimate more accurate SGD and associated fluxes of chemical species into the ocean.

Table 2.1. Comparison between ^{228}Ra endmembers and SGD fluxes for different salinity ranges in the Atlantic Ocean and the global ocean.

	^{228}Ra endmember (dpm m^{-3})		SGD flux (10^{13} m^3 yr^{-1})	
	Atlantic	Global	Atlantic	Global
Total	1103 ± 197	927 ± 136	3.8 ± 1.1	14 ± 4
Salinity >10	2415 ± 239	2268 ± 216	1.7 ± 0.4	5.6 ± 1.5
Salinity >20	2612 ± 297	2452 ± 271	1.6 ± 0.4	5.2 ± 1.4
Salinity >30	2821 ± 501	2506 ± 430	1.5 ± 0.4	5.1 ± 1.5

Table 2.2. Comparison of SGD fluxes from the literature calculated using different methods for defining groundwater Ra endmember values with the revised SGD fluxes calculated using this method.

Region	SGD flux (m^3 yr^{-1}) in the original report	SGD flux (m^3 yr^{-1}) calculated using this method[a]
Yellow Sea	(1–6.7) × 10^{11} (Kim et al., 2005)[b]	(3.5 ± 0.5) × 10^{11}
Mediterranean Sea	(0.3–4.8) × 10^{12} (Rodellas et al., 2015)[c]	n.a.
South Atlantic Bight	1.1 × 10^{10} (Moore, 1996)[d]	1.9 × 10^{10}
Atlantic Ocean	(2–4) × 10^{13} (Moore et al., 2008)[e]	(1.3 ± 0.6) × 10^{13}
Global ocean	(12 ± 3) × 10^{13} (Kwon et al., 2014)e	(4.4 ± 1.2) × 10^{13}

n.a.: Salinity data are not available.

[a] The mean value of lognormal distribution for saline groundwater (salinity >10) is used for groundwater Ra endmember.

[b] The range of all the groundwater dataset is used for groundwater Ra endmember.

[c] The range between the first and third quartiles of the groundwater dataset is used for groundwater Ra endmember.

[d] The highest mean value in brackish groundwater is used for groundwater Ra endmember.

[e] The mean value of a lognormal distribution for all data is used for groundwater Ra endmember.

2.4. Conclusions

The effect of the geographical bias of data distributions on determining the endmember values of Ra in groundwater is found to be insignificant for SGD estimation using Ra mass balance methods. However, groundwater Ra endmember values are dependent on salinity, showing higher values at higher salinities. Based on these analyses, it is concluded that Ra data obtained from coastal groundwater with salinity less than 10 should be excluded from the Ra endmember values for SGD estimation. Using the newly calculated Ra endmember for coastal groundwater (salinity >10), it could be suggested that the previous estimation of the magnitudes of SGD in the Atlantic Ocean and global ocean (without considering the salinity effect) are overestimated approximately 2−3 fold. A similar overestimation can happen in local studies when using Ra isotopes. Because previously used methods can also misrepresent the SGD-derived fluxes of chemical constituents into the ocean, which have a great impact on coastal biogeochemistry, more extensive studies are necessary to accurately determine the endmember values of Ra in coastal groundwater.

3. Nutrients fluxes via submarine groundwater discharge to the global ocean

3.1. Introduction

In the coastal ocean, nutrients could be supplied by advective inputs from aquifers and pore water, in addition to atmospheric and riverine inputs (Figure 3.1). The advective fluxes may include the nutrients from terrestrial sources and the remineralization of organic matter within the sediments (Figure 3.1). In this study, SGD is defined as any upward water advection through the submarine ocean boundaries, which includes the discharge of fresh and saline groundwater as well as pore water advection.

While global estimates are now available on the fluxes of nutrients to the global ocean via rivers and atmosphere deposition, no estimates are available for the SGD contribution to nutrient cycles in the global ocean. However, recently, the total water flux of SGD has been revealed to be comparable to the river discharge to the Atlantic (Moore et al., 2008) and global oceans (Kwon et al., 2014; Cho and Kim, 2016) using ^{228}Ra (half life: 5.75 years) as a tracer. Several local studies have suggested that saline groundwater often delivers larger fluxes of solutes to the ocean than fresh groundwater (Li et al., 1999; Burnett et al., 2007; Swarzenski et al., 2007a; Anschutz et al., 2016). For a basin scale, nutrient inputs through total SGD were

found to be comparable to those via rivers in the Mediterranean Sea (Rodellas et al., 2015) and Yellow Sea (Kim et al., 2005). Over the global ocean, while saline groundwater is the dominant component of the total SGD (Li et al., 1999; Burnett et al., 2003), estimates only exist for the contributions of "fresh" groundwater to DIN (Beusen et al., 2013) and DSi (Frings et al., 2016; Tréguer and De La Rocha, 2013) fluxes.

It is hypothesized that SGD is a major global source of nutrients to the oceans. The main challenge to assess this hypothesis is to determine a globally-significant groundwater endmember concentration for estimating SGD-driven nutrient fluxes. In this study, a global compilation of nutrient data is combined with the observationally constrained ^{228}Ra flux estimate through SGD (Kwon et al., 2014) and compare the estimated fluxes with the river sources.

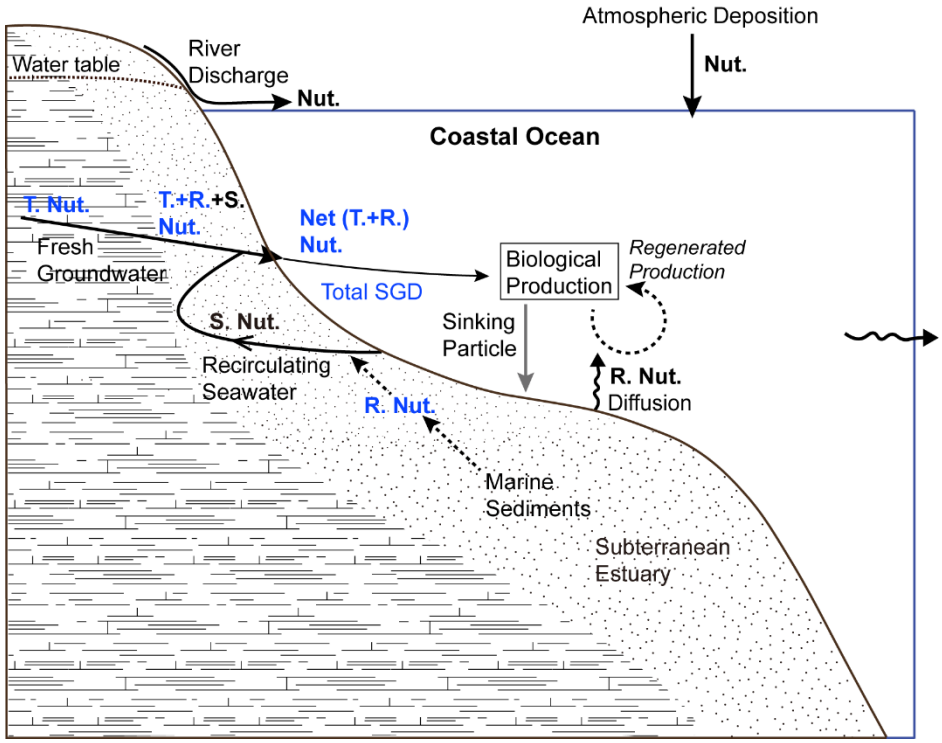

Figure 3.1. A schematic of biological production in the euphotic zone supported by nutrients from atmosphere, rivers, and groundwater in the coastal ocean. T. Nut., R. Nut., and S. Nut. denote nutrient sources from meteoric groundwater, recirculating seawater, and sediment remineralization, respectively. Net Nut. denotes net nutrient inputs via SGD to coastal waters. In the coastal ocean, the diffusive fluxes of nutrients from bottom sediments in the euphotic zone are included in the regenerated nutrients.

3.2. Materials and methods

3.2.1. Data compilations and the SGD-driven net nutrient fluxes

Data for DIN (n = 943), DIP (n = 980), DSi (n = 762), and ^{228}Ra (n = 552; Cho and Kim, 2016) for global coastal groundwater (Figure 3.2) and seawater (Figure 3.3) are compiled.

In order to calculate the net nutrient fluxes from continental margins to the coastal ocean through SGD Consider a land-ocean domain consisting of two boxes: The 'gw' box represents coastal aquifers and pore waters, and the 'sw' box represents the shelf shallower than 200 m (Figure 3.4). The 'sw' box includes the grid points adjacent to the lands and islands in horizontal resolution of 2°×2° for ^{228}Ra and 1°×1° for nutrients, shallower than 200 m.

The volumes of the boxes are V_{gw} and V_{sw} (Figure 3.4). There are two tracers, R and N, representing ^{228}Ra and nutrients of interest, respectively, with units of mol m^{-3}. The concentrations of the tracers in each box can be denoted as R_{gw} and R_{sw}, and N_{gw} and N_{sw}. The exchange rate of waters between the two boxes is f in a unit of m^3 yr^{-1}. The negative f represents the SGD recharge (from sw to gw) and the positive f represents the SGD discharge (from gw to sw). The fresh groundwater fluxes from the gw to sw boxes are neglected in this box model as it accounts for only ~4% of the total SGD.

Then, the net fluxes of R and N from the gw to sw boxes become:

$$Net\ R\ Flux = f\left(R_{gw} - R_{sw}\right) \quad (1)$$

$$Net\ N\ Flux = f\left(N_{gw} - N_{sw}\right) \quad (2)$$

Combining equations (S1) and (S2), the net N flux can be obtained by

$$Net\ N\ Flux = Net\ R\ Flux \times \frac{\left(N_{gw} - N_{sw}\right)}{\left(R_{gw} - R_{sw}\right)} \quad (3)$$

The net R Flux from the gw box to the sw box can be approximated by the SGD-driven ^{228}Ra fluxes to the global ocean obtained by Kwon et al. (2014), resulting in equation (4)

$$\frac{Nutrient_{gw} - Nutrient_{sw}}{^{228}Ra_{gw} - {}^{228}Ra_{sw}} \times {}^{228}Ra\ flux = Net\ Nutrient\ Flux \quad (4)$$

where $Nutrient_{gw}$ and $^{228}Ra_{gw}$ (dpm m^{-3}) are the concentrations (mol m^{-3}) of DIN, DIP, and DSi and the endmember value of ^{228}Ra in coastal groundwater aquifers, respectively. $^{228}Ra_{gw}$ (dpm m^{-3}) is obtained from Cho and Kim (2016). $Nutrient_{sw}$ and $^{228}Ra_{sw}$ are the concentrations of nutrients and ^{228}Ra in the coastal seawater. The World Ocean Atlas 2013 (Garcia et al., 2014) is used to estimate the globally averaged concentrations of DIN, DIP, and DSi in coastal seawater. From the globally gridded 1°×1° nutrient data (Figure 3.3), the coastal grids adjacent to the lands and islands between 0−200 m (60°S−70°N) are only taken. The volume weighted mean concentrations are then obtained from the coastal grid points. The nutrient and ^{228}Ra concentrations for coastal seawater are averaged from grid points adjacent to lands and islands and hence represent the values resulting from terrestrial

sources, chemical and biological decays within the coastal regions, and oceanic mixing and advection. The seawater components of nutrients and ^{228}Ra are important to the net flux, since it is assumed that the SGD fluxes are dominated by saline rather than fresh SGD (Li et al., 1999; Burnett et al., 2003). *^{228}Ra flux* (dpm yr^{-1}) is the flux of ^{228}Ra into the global ocean through SGD, which was estimated to be $(1.3 \pm 0.3) \times 10^{17}$ dpm yr^{-1} using a numerical model combined with a global compilation of ^{228}Ra observations (Kwon et al., 2014).

3.2.2. Geographical gridding method and the effects of salinity

Approximately 800 sampling sites for groundwater nutrient ($Nutrient_{gw}$) data cluster along the east coasts of Asia and North America, including also the Mediterranean Sea, with scarce data elsewhere (Figure 3.2). This clustering can affect the endmember concentrations of nutrients in groundwater. Therefore, a gridding method is used to examine the effect of the heterogeneity of geographical data distributions on determining the nutrient endmember values in groundwater. This method divides the globe into 2°×2° grid points, as examined previously by chapter 2.3.1 in this study and Cho and Kim (2016) for ^{228}Ra. All of the data within each grid point are averaged to represent the mean value at each grid point, assuming lognormal distributions of the tracers. Furthermore, the sensitivity of the groundwater endmember values of nutrients to salinity is examined. The endmember values are calculated for different salinity ranges (0−10, >10, >20, >30).

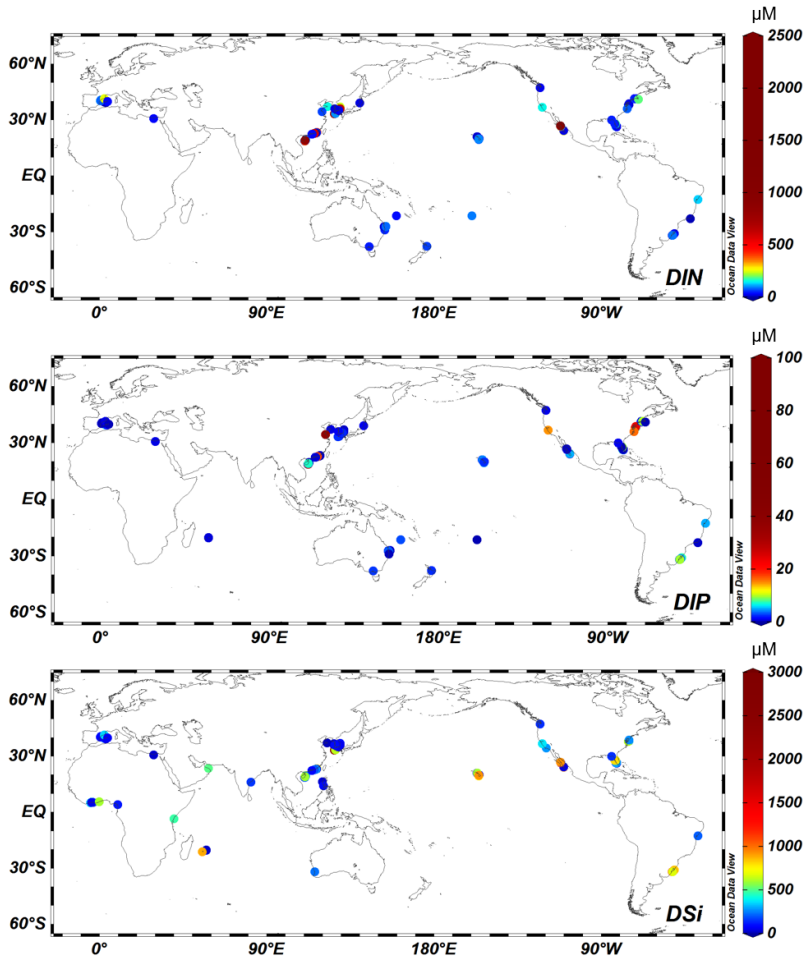

Figure 3.2. The distributions of data collection sites and concentrations for DIN (n = 943), DIP (n = 980), and DSi (n = 762), respectively, in world-wide coastal groundwater. A list of data sources for DIN, DIP, and DSi is shown in Appendix Table B.

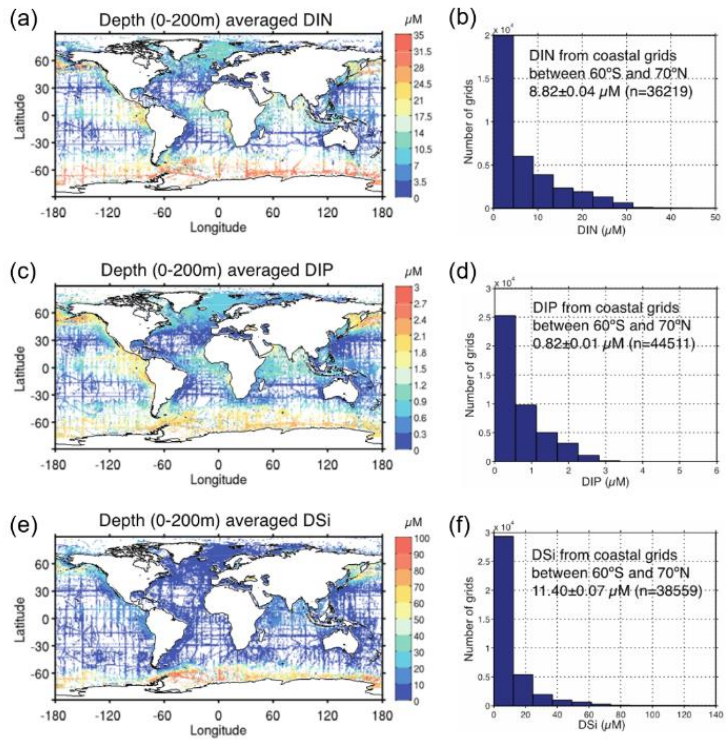

Figure 3.3. World Ocean Atlas 2013 coastal seawater concentrations (μM) of DIN, DIP, DSi. (a) The global distribution of 1°×1° DIN averaged from the surface to 200 m. (b) The histogram of coastal seawater DIN subsampled from the grid points adjacent to the lands and islands, 0−200 m, 60°S−70°N. The mean DIN concentration for the coastal sweater used in this study is shown inside the panel with ±one standard error. The number of grid points (n) used for the average is shown in parenthesis. (c and d) The same as (a and b) except that the cases for DIP are shown. (e and f) The same as (a and b) except that the cases for DSi are shown.

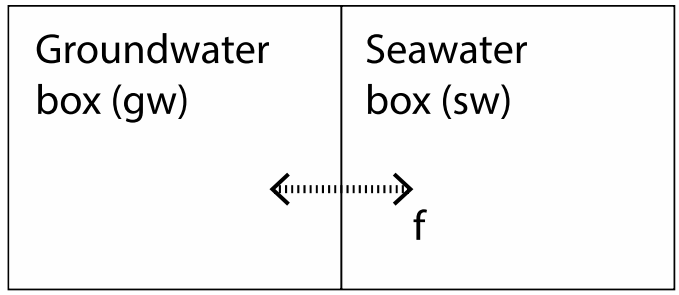

Figure 3.4. Two-box model used to conceptualize the derivations of ($Nutrient_{gw}$ - $Nutrient_{sw}$)/($^{228}Ra_{gw}$ - $^{228}Ra_{sw}$) ratios for different land-ocean exchange processes.

3.3. Results and discussion

3.3.1. Effects of geographical gridding methods

The gridding method does not make a discernible difference in terms of the global mean value compared to a bulk averaging (mean of the lognormal distribution) method without gridding (Figure 3.5). The estimated endmember values of DIN, DIP, and DSi in groundwater using the gridding method are 87 ± 18, 1.3 ± 0.3, and 125 ± 33 μM in the Pacific; 49 ± 11, 1.3 ± 0.4, and 109 ± 29 μM in the Atlantic; and 67 ± 10, 1.4 ± 0.4, and 126 ± 21 μM in the global ocean, respectively (Figure 3.5). In general, the gridding method yields larger uncertainties for all nutrients (Figure 3.5). However, the endmember values of nutrients agree well with the without-gridding method within the uncertainty ranges (73 ± 5, 1.7 ± 0.1, and 149 ± 12 μM in the Pacific; 46 ± 3, 1.3 ± 0.1, and 121 ± 6 μM in the Atlantic; and 58 ± 3, 1.4 ± 0.1, and 129 ± 5 μM in the global ocean, respectively). Thus, in this study, the global mean groundwater endmember obtained by the mean of the lognormal distribution without gridding is used for the calculation of SGD-driven nutrient fluxes.

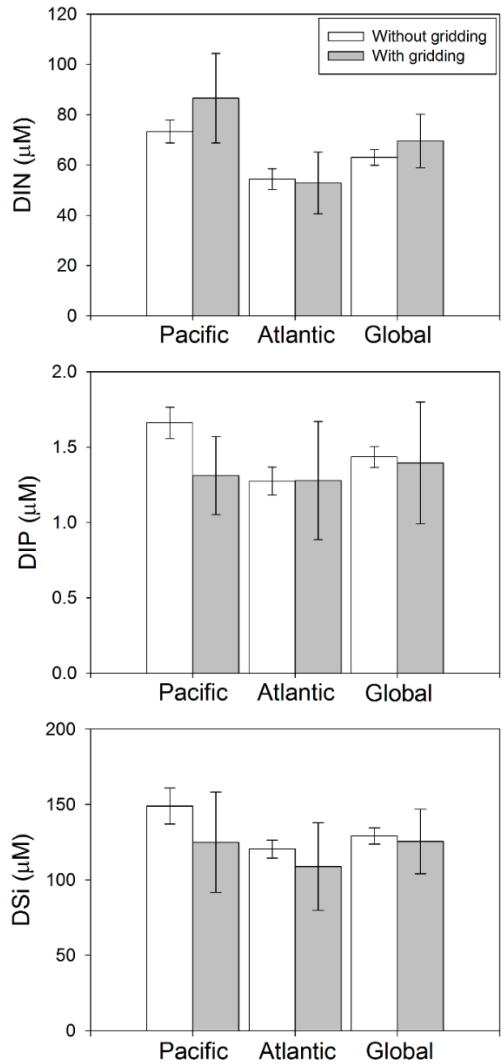

Figure 3.5. The graphs show the average concentrations of DIN, DIP, and DSi in coastal groundwater for the Pacific, Atlantic, and global oceans obtained with and without the use of gridding methods. The error bars show ± one standard error of the results.

3.3.2. Effects of groundwater salinity

The sampling sites for the compiled $Nutrient_{gw}$ data cover a wide range of environments including beach pore water, seepage zone, and inland wells near marginal seas, corresponding to a wide range of salinity. In order to examine the sensitivity of the groundwater endmember values of nutrients to salinity, the endmember values are calculated for different salinity ranges (0−10, >10, >20, >30; Figure 3.6 and Table 3.1). The concentrations of DIN and DSi are much higher in fresh groundwater (salinity <10) relative to saline groundwater (Figure 3.6). The higher DIN concentrations in lower salinity groundwater may be associated with anthropogenic inputs, such as waste materials, fertilizers, manure, etc. (Van Drecht et al., 2003; Basterretxea et al., 2010). However, the higher concentrations of DSi in lower salinity groundwater could be due to the enrichment of DSi by rock weathering and the dissolution of biogenic silica in sediments (e.g., Struyf et al., 2006). In contrast, the activity of ^{228}Ra is much higher in saline groundwater (salinity >10; Figure 3.6) as explained by Cho and Kim (2016). This trend is well known and originates from the low particle reactivity due to competition with other ions in saline water and continuous ingrowth from its parent (^{232}Th) in the geological matrix. The concentrations of DIP are highest in groundwater with salinity between 10 and 30 (Figure 3.6). The difference in DIP concentrations for different salinity ranges is unclear because it is affected by various factors: (1) groundwater contamination with DIP, (2) effects of DIP adsorption-desorption equilibria at the ambient salinity, and (3) DIP remineralization by decomposing organic matter in coastal aquifers. Owing

to such different behaviors and anthropogenic source inputs for DIN and DIP, DIN:DIP ratios in groundwater are much higher for lower salinity waters (N:P = 73, salinity 0–10; N:P = 26, salinity > 10; N:P = 23, salinity > 20; N:P = 17, salinity > 30).

The salinity dependency of nutrient concentrations indicates that the salinity range assumed for the SGD can significantly affect these estimates for the SGD-driven nutrient fluxes. To offer a conservative estimate of nutrient fluxes via total SGD, observations from fresh groundwater (salinity <10) are excluded from the dataset under consideration (Cho and Kim, 2016). This choice is supported by the fact that fresh groundwater is a minor fraction of SGD (<10%, Li et al., 1999; Burnett et al., 2003). Indeed, several local studies have shown that salinity is often greater than 10 in seeping groundwater (Kim et al., 2003; Stieglitz et al., 2007; Rapaglia and Bokuniewicz, 2009; Taniguchi et al., 2009). By focusing on the less scattered data from saline groundwater, the uncertainty arising from the complex geochemical transformations and modulation occurring to nutrients within coastal aquifers is reduced. Thus, it is assumed that nutrient concentrations in samples with salinity >10 represent the values at the interface between seabed and the coastal seawater (Figure 3.7).

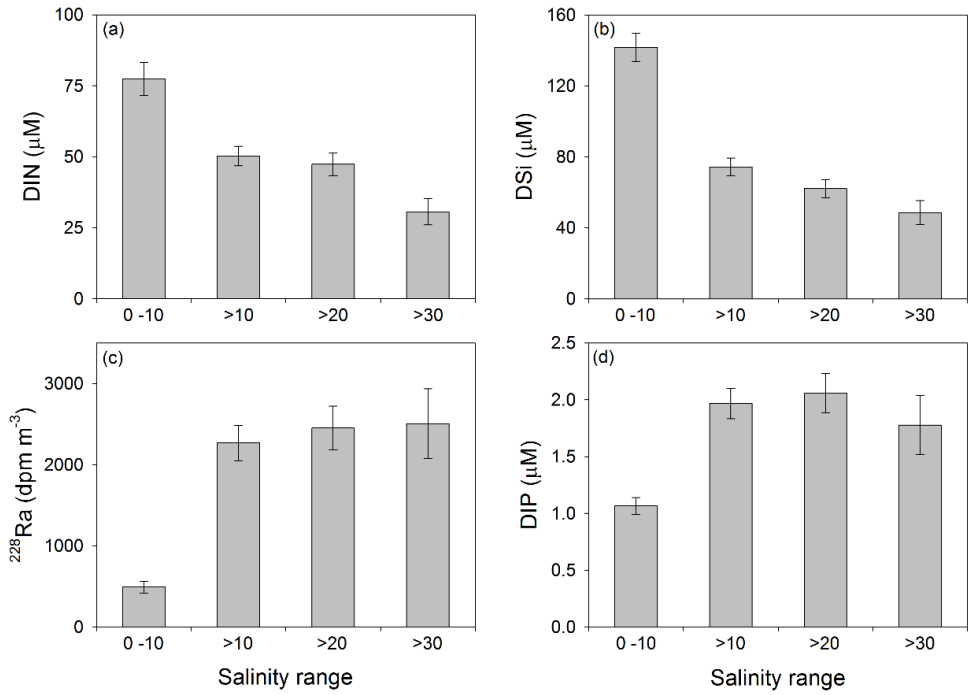

Figure 3.6. The bars represent the endmember values of (a) DIN, (b) DSi, (c) ^{228}Ra, and (d) DSi in global coastal groundwater for the different salinity ranges of groundwater. The error range represents ± one standard error from the average.

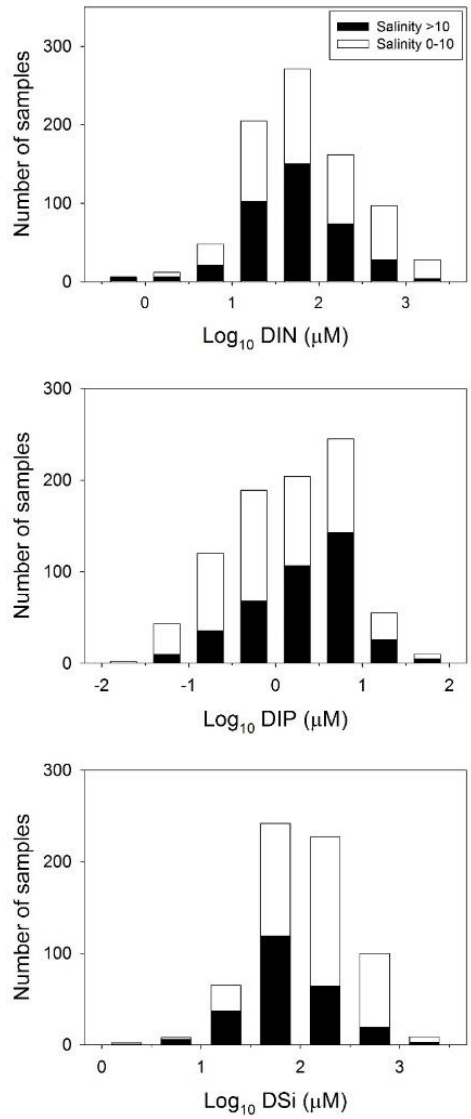

Figure 3.7. The histograms represent the distributions of DIN, DIP, and DSi in coastal groundwater of the global ocean. The white and black bars represent salinity values lower and higher than 10, respectively.

Table 3.1. The endmember values of DIN, DIP, and DSi in groundwater for different salinity groups.

Salinity group	DIN (n = 829)	DIP (n = 868)	DSi (n = 653)
0–10	77 ± 6 (n = 439)	1.1 ± 0.1 (n = 473)	142 ± 8 (n = 404)
> 10	50 ± 3 (n = 390)	2.0 ± 0.1 (n = 395)	74 ± 5 (n = 249)
> 20	47 ± 4 (n = 267)	2.1 ± 0.2 (n = 270)	62 ± 5 (n = 158)
> 30	31 ± 5 (n = 99)	1.8 ± 0.3 (n = 102)	49 ± 7 (n = 62)

3.3.3. Global SGD-driven nutrient fluxes

The estimated net SGD-driven DIN, DIP, and DSi fluxes into the global ocean are 2.4 ± 0.7 Tmol yr^{-1}, 0.07 ± 0.02 Tmol yr^{-1}, and 3.6 ± 1.0 Tmol yr^{-1}, respectively. The uncertainty represents one standard error from the average. The estimated SGD-driven nutrient fluxes are the net advective transport from continental margins to the coastal oceans through aquifers and pore waters. The resulting fluxes account for the biogeochemical transformation and modulation within the coastal aquifers that have occurred to the nutrients between groundwater recharge and SGD. A significant fraction of the net DIP and DIN discharge may originate from the remineralization of organic matter within the sediments, while a large portion of the net DSi discharge is likely to be released from aquifer solids (Knee and Paytan, 2011).

The first order estimates in this study provide an opportunity to compare SGD- and river-driven nutrient input fluxes to the ocean on a global scale, building on previous regional and local investigations. The estimated nutrient inputs through river discharge are from Global Nutrient Export from Watersheds (Global NEWS) model, which includes river-basin-scale models that can predict export of dissolved and particulate nutrients using a function of natural and anthropogenic biogeophysical properties of 5761 exoreic basins (Seitzinger et al., 2005, 2010). The fluxes of riverine DIN, DIP, and DSi are approximately 1.6 ± 0.2 Tmol yr^{-1}, 0.04 ± 0.006 Tmol yr^{-1}, and 5.1 ± 0.1 Tmol yr^{-1}, respectively (Seitzinger et al., 2005, 2010).

Therefore, total SGD-driven fluxes of DIN, DIP, and DSi are approximately 1.5-, 1.7-, and 0.7-fold of the river-driven fluxes to the global ocean, respectively (Figure 3.8). Assuming that the nutrients supplied by total SGD are fully utilized by biological production, production supported by the total SGD-driven DIN flux (2.4 Tmol yr^{-1}) could be potentially 16 Tmol C yr^{-1}. The estimated value accounts for approximately 20% of new production in continental shelf waters (Chen and Borges, 2009), but is likely to be larger considering the conservative approach to determine the SGD endmember in this study.

Estimates of nutrient fluxes from fresh groundwater have been attempted in previous studies (Beusen et al., 2013; Frings et al., 2016; Tréguer and De La Rocha, 2013). Based on the compiled dataset, combining the globally averaged fresh SGD of 1.85 Tm^3 yr^{-1} (Taniguchi et al., 2002; Slomp and Van Cappellen, 2004) with the endmember value of DIN in fresh groundwater (salinity = 0; 56 ± 23 μM), the resulting DIN flux from fresh component of SGD is 0.10 ± 0.04 Tmol yr^{-1}. This value agrees with the N input to the global ocean estimated by a land- and process-based modeling study (0.1 Tmol yr^{-1}, Beusen et al., 2013). Using the same method, the DIP (salinity = 0; endmember value of DIP = 0.6 ± 0.2 μM) and DSi (salinity = 0; endmember value of DSi = 131 ± 18 μM) fluxes via fresh-SGD are estimated to be 0.0012 ± 0.0004 Tmol yr^{-1} and 0.24 ± 0.03 Tmol yr^{-1}, respectively. The DIP flux through fresh SGD is reported here for the first time. The DSi flux estimated in this study is approximately 30% of that reported by upscaling results (Tréguer and De La

Rocha, 2013) from two regional studies, which used an average groundwater DSi value of 340 μM from southern Brazil (Niencheski et al., 2007) and Bengal Basin (Georg et al., 2009). However, the estimated global DSi endmember value in coastal groundwater (salinity = 0) is approximately 130 μM in this study, which is much lower than the value in the previous studies. The general consistency with the previous estimates for the fresh-SGD provides confidence that the globally compiled nutrient dataset is reasonable.

This study suggests that saline groundwater plays a dominant role in the net flux of SGD-driven nutrients to the coastal ocean and that the SGD-driven nutrients so far reported (Beusen et al., 2013; Tréguer and De La Rocha, 2013; Frings et al., 2016) based on fresh groundwater discharge significantly underestimate the actual fluxes by groundwater into the global ocean by excluding saline SGD. Therefore, further extensive SGD studies are necessary, particularly on (1) SGD magnitude changes in association with climate change, groundwater depletion, and sea-level rise, (2) SGD-driven fluxes of nutrients, trace elements, and organic matter depending on local contaminations and SGD magnitude changes, and (3) SGD effects on ecosystems, carbon sequestrations, acidification, and oxygen depletion in the coastal ocean.

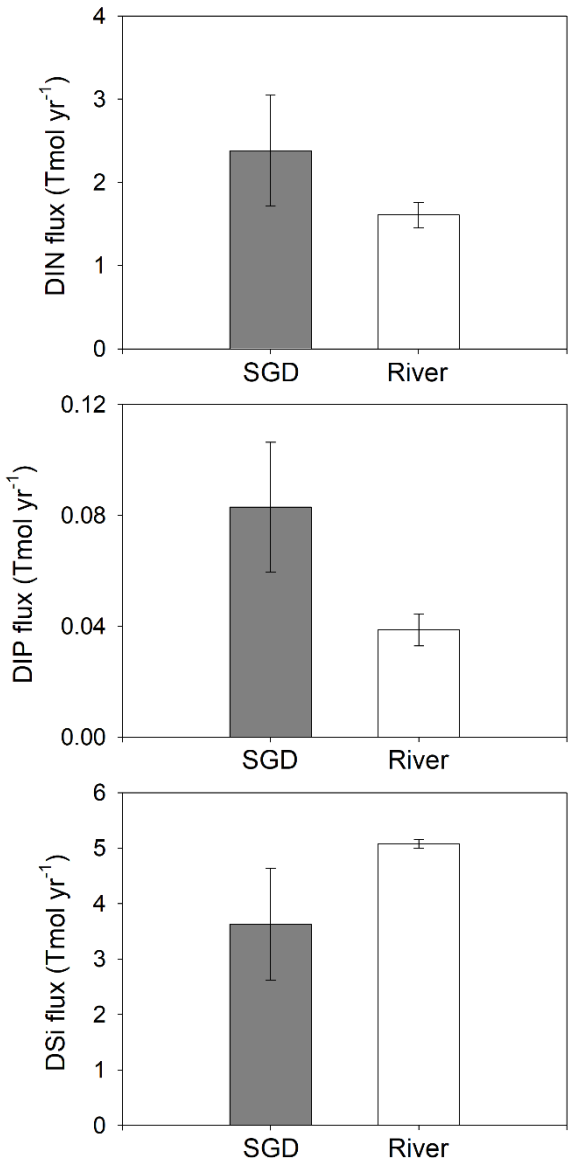

Figure 3.8. A comparison of global nutrient inputs to the ocean via SGD and river discharge. Fluxes via riverine inputs are obtained from the literatures (Seitzinger et al., 2005, 2010).

3.4. Conclusions

Fluxes of nutrients to the ocean have large impacts on biological production, carbon cycles, and deoxygenation in the ocean. While global nutrient fluxes via surface runoff are quite well known, those through SGD are poorly understood. In general, SFGD is known to contribute insignificant fluxes of nutrients to the global ocean, relative to the fluxes via rivers and atmospheric deposition. In this study, the global fluxes of nutrients via SGD, including submarine groundwater and pore water discharge, are comparable to those through rivers. These results suggest that SGD-derived DIN fluxes can potentially support approximately 20% of new production on continental shelves. This study presents that saline SGD is a volumetrically important for transporting dissolved nutrients (DIN, DIP, and DSi) into the global ocean.

4. Behaviors of silicate and phosphate in subterranean estuaries

4.1. Introduction

Submarine discharge of fresh and saline groundwater (or their composites) represents an important flux of nutrients to the ocean, comparable in magnitude to that transported by rivers as shown in several local and regional scales studies (Kim et al., 2005; Lee et al., 2012; Santos et al., 2014; Rodellas et al., 2015). In general, biogeochemical processes occurring in the mixing zone of fresh and saline groundwater (i.e., subterranean estuary, STE) significantly impact the chemical composition of groundwater discharging into the coastal ocean (Moore, 1999).

Fluxes of N through SGD and their behavior in STE have been investigated in a number of studies (e.g. Talbot et al., 2003; Kroeger and Charette, 2008). Since N is the most common groundwater pollutant worldwide (Spalding and Exner, 1993), increasing human activity has led to elevated groundwater N concentrations (e.g. Nolan, 2001; Choi et al., 2007). In STE, NO_3^- can be removed by denitrification under anoxic conditions. For example, denitrification accounted for up to 88% decrease in NO_3^- concentration in a STE in Cook Island (Erler et al., 2014). NH_4^+ can be effectively removed through nitrification (Kroeger and Charette, 2008) under oxic conditions and through anammox with NO_2 to form N_2 gas (Santoro, 2010).

Behaviors of P in estuaries are generally controlled by particle adsorption/desorption processes (Price et al., 2010; Li et al., 2013). In STE, phosphate can be removed by calcium phosphate precipitation (Cable et al., 2002; Slomp and Van Cappellen, 2004) and sorption onto Fe-oxides (Charette and Sholkovitz, 2002, 2006; Spiteri et al., 2008). Thus, particle-reactive characteristics of P are considered crucial process for controlling the availability of DIP to the biosphere. However, P can be desorbed from sediments under conditions where Si levels are high in pore-water. Tallberg et al. (2008) have suggested that P can be released from marine (sand-silt) sediments based on laboratory experiments with Si concentrations greater than 2000 μmol/L in pore-water. Similarly, excess Si produced by microbial mineralization of sinking diatoms (following diatom bloom events) resulted in the release of P from eutrophic lake sediments (Tuominen et al., 1996, 1998; Tallberg, 1999; Tallberg and Koski-Vähälä, 2001). Such an exchange of P and Si occurs because Si ions are capable of competing with P ions for sorption sites (Hingston et al., 1967; Obihara and Russell, 1972; Smyth and Sanchez, 1980).

However, this process has not yet been studied for Si levels lower than 400 μmol/L. Thus, in this study, the behavior of Si and associated behavior of P in STE was investigated based on the laboratory experiments. It is hypothesized that such a P-Si exchange could similarly occur in the STE, since Si concentrations in groundwater are generally high (20–400 μmol/L) (Ullman et al., 2003; Niencheski

et al., 2007; Johnson et al., 2008; Street et al., 2008; Lee et al., 2010; Kim et al., 2011; Lee et al., 2012; Liu et al., 2012; Godoy et al., 2013).

4.2. Materials and methods

4.2.1. Sampling

In order to investigate the adsorption and desorption of Si and P in STE, sandy sediment samples were collected using polypropylene buckets from eight coastal stations in the Korean Peninsula during low tide in the years 2010, 2011, 2013, and 2016 (Figure 4.1). After being homogenized, the bulk sediment samples were stored in the dark at +4°C until the laboratory experiments were started. The detailed geochemical characteristics controlling the magnitude of adsorption/desorption of Si and P are not compared in this study since the aim of this study is to determine general phenomenon occurring in STE for randomly collected samples.

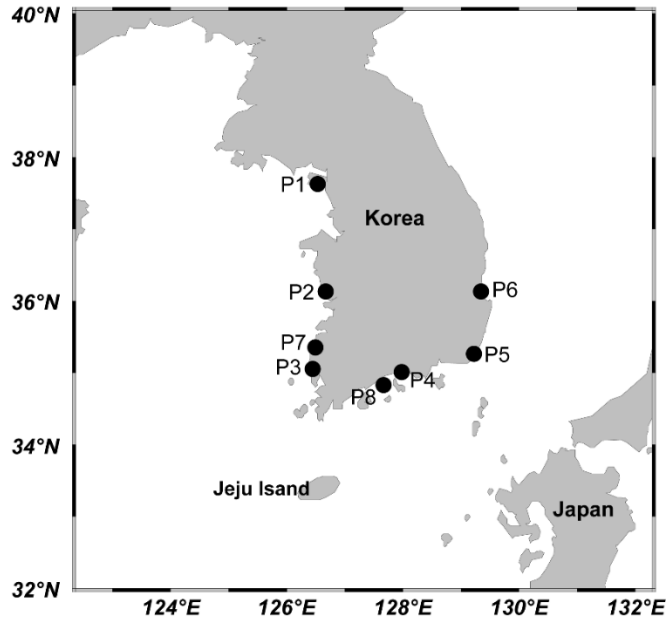

Figure 4.1. A map showing coastal sediment sampling stations. Eight samples were collected from the western (Eulwangri, P1; Chunjangdae, P2; Dongho, P7; Hampyeong, P3), southern (Bangjukpo, P8; Namildae, P4), and eastern (Ilgwang, P5; Bukbu, P6) coasts of Korea for phosphate desorption experiments.

4.2.2. Sediment column experiments

A sediment column (13 cm in diameter and 33 cm in height) was constructed to simulate natural groundwater seepage in an STE to observe phosphate release from permeable sediments (Figure 4.2). Artificial groundwater, which was prepared according to literature values reported for coastal groundwater (20 ppt NaCl, 200 μmol Si/L, pH ~7), was fed continuously into the sediment column at a speed of 0.3 L/h using a peristaltic pump (Figure 4.2). The concentrations of dissolved inorganic nutrients in the outflow were monitored every hour with Eco-LAB (EnviroTech, USA), a multi-channel real-time nutrient analyzer (Figure 4.3). This commercially available instrument uses the conventional colorimetric method, which is a well-established wet chemistry technique (Nam et al., 2005; Kim et al., 2006). Eco-LAB takes samples by withdrawing the syringe plunger at the inlet port, and the reagents are added by moving the valve to the corresponding ports, followed by retraction of the syringe plunger. After the samples and reagents are mixed in the syringe, color develops as the reaction progresses. The reaction product is then injected into the detector for measurements (Nam et al. 2005). The measurements of DIN were conducted using the same analyzer for two sets of experiments. For the analysis of nitrate, an activated cadmium column was used to reduce NO_3^- to NO_2^-. The calibration check was performed periodically, and the results were verified by measurements of random grab samples using the Alliance FUTURA Auto-Analyzer.

This experiment was conducted for six separate columns packed with sandy sediments collected from different coastal areas of Korea (P1-P6). Additionally, control experiments were carried out for two sediment columns (C1 from station P1 and C2 from station P3) with and without a Si spike for 100 hours.

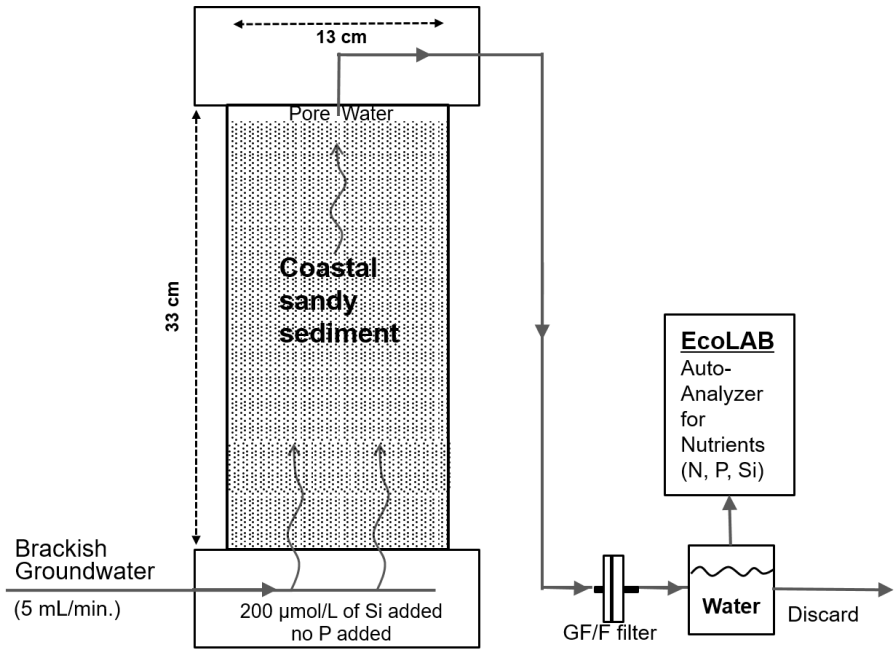

Figure 4.2. A schematic of the experimental setup for simulating submarine groundwater seepage conditions in an STE. Coastal sandy sediments were placed in each column, and artificial groundwater (20 ppt NaCl, 200 µmol Si/L, and pH 7) was fed into the sediment column (0.3 L/h) using a peristaltic pump. Concentrations of dissolved inorganic nutrients in the outflow were measured every hour using a real-time nutrient analyzer (Eco-LAB, EnviroTech, USA).

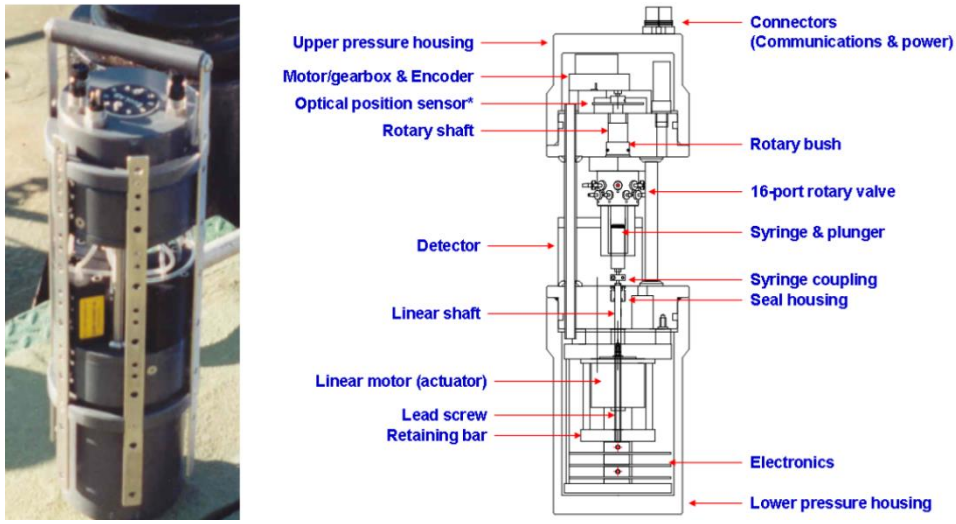

Figure 4.3. EcoLAB analyzer module with reagent housing (left) and a schematic diagram (right) of EcoLAB (EnviroTech, USA).

4.2.3. Beaker experiments

The P released from permeable sediments (P1-P6) was examined at different levels of pH, salinity, and Si. Specifically, in each of the test beakers, 50 g of homogenized sediments was mixed with 50 mL of test solution at room temperature (Figure 4.4). To test the effect of pH, the solution in each beaker was adjusted to pH 4, 5, 6, 7, and 8 (by using NaOH at ~200 µmol Si/L and ~20 ppt of NaCl). To test the effect of salinity, the solution in each beaker was adjusted to salinity 5, 10, 15, 20, 25, and 30 by diluting seawater at ~200 µmol Si/L and pH ~7. In order to examine the effect of Si levels on P-desorption, eight beakers were used for comparison, with the Si concentrations (in NaCl solutions) adjusted to 0, 25, 50, 75, 100, 200, 300, and 400 µmol/L at salinity ~20 and pH ~7. The sediments and solutions were mixed well every hour for 10 minutes over a period of ~24 hours followed by the collection of supernatants. Subsequently, the concentrations of DIP in the supernatants were analyzed using a spectrophotometer (X-ma 1000 HUMAN, Korea).

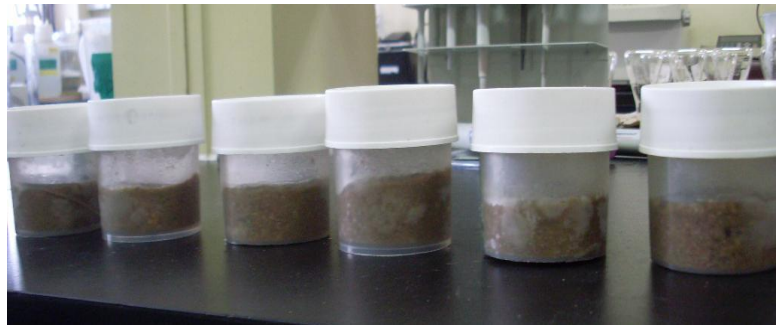

Figure 4.4. The photograph of experimental setup for the beaker experiments.

4.2.4. Bottle experiments

The method of bottle experiments is similar to the beaker experiments (chapter 4.2.3). However, in the experiments, 1,000 g of homogenized sediments from P2, P7, and P8 were mixed with 500 mL of experimental solutions with different conditions at room temperature (Figure 4.5). To test the effect of pH, deionized water solution in each 1L-bottle was adjusted to pH 4, 5, 6, 7, and 8 at 200 μmol Si/L. To test the effect of salinity, the solution in each bottle was adjusted to salinity 5, 10, 15, 20, 25, and 30 by diluting coastal seawater at 200 μmol Si/L and pH ~7. To examine the effect of Si levels on P-desorption, the solution in each bottle was adjusted to have Si concentrations of 0, 25, 50, 100, 200, and 400 μmol/L at pH ~7. The solutions and sediments were mixed well, and then the supernatants were collected after 1, 6, 12, and 24 hours in order to measure the pH and the concentrations of dissolved inorganic nutrients. The pH of each sample was measured using a portable multi-parameter sensor (Orion star A329, Thermo Scientific), and the concentrations of dissolved inorganic nutrients in each solution were analyzed using a nutrient auto-analyzer (QuAAtro39, SEAL).

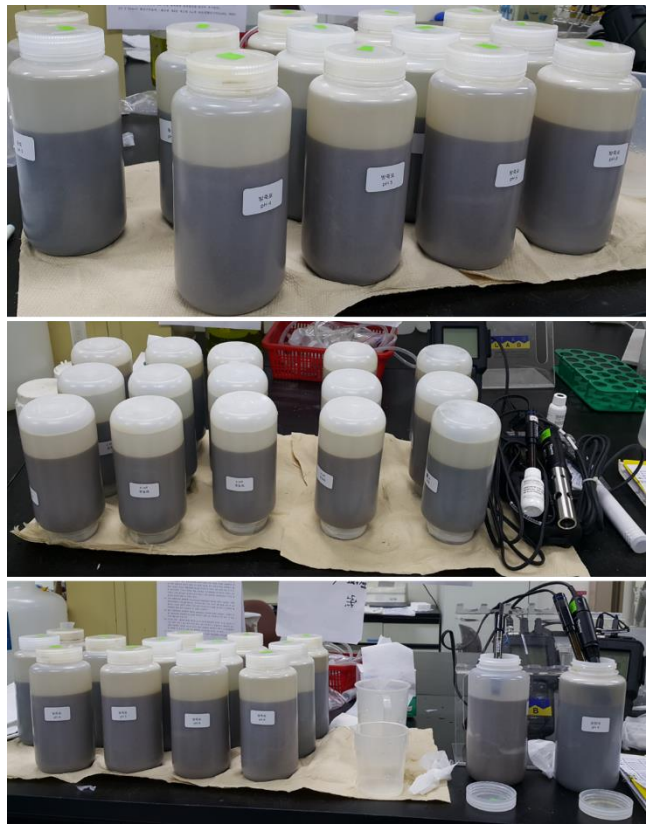

Figure 4.5. The photograph of experimental setup for the bottle experiments.

4.3. Results

4.3.1. Sediment column experiments

For long-term column experiments (> 150 hours), six different sediment columns showed consistent Si adsorption and P desorption trends, although the magnitudes and shapes differed based on sediment samples. As the saline solution (200 μmol Si/L, salinity 20) was loaded into the six columns, Si was 40−90% removed in the initial stage within the first 24 hours. Subsequently, the Si level in the outflow water increased slowly until it reached a saturation stage at 20−50 mg Si/kg-sediment. A wide range of time periods was taken to reach the saturation stage from 1–12 days (P1-P6; Figure 4.6). As Si adsorption increased, rapid desorption of P from sediments was observed in the outflow solutions (Figure 4.6). The loading solution did not contain P. However, P concentrations were 1–4 μmol/L for the initial outflow solutions. P concentrations reached maximum concentrations (6–20 μmol/L) within 20 to 80 hours depending on the sediment and then began to decrease to 2–10 μmol/L. These levels were still higher than the loading solution, when the experiments ended.

The control column experiments were conducted for two types of sediments (C1 and C2) over a period of 100 hours (Figure 4.7). The saline loading solution (200 μmol Si/L and no Si added) was used for each sediment column. As shown for previous column experiments, Si was almost fully removed in the initial stage with 80−90% removal in the initial 24 hours. As expected, rapid desorption of

P from sediments was observed in the outflow solutions as Si adsorption increased (Figure 4.7). Although the loading solution does not contain P, P concentrations were 4 µmol/L for C1 and 6 µmol/L for C2 in the initial outflow solutions. P concentrations reached a maximum of approximately 12 µmol/L within 50 to 60 hours. For solutions with added Si, the concentrations of N in outflow waters were almost zero for all monitoring periods. The concentrations of P, Si, and N remained constant for control experiments which did not contain Si over the entire experiment periods.

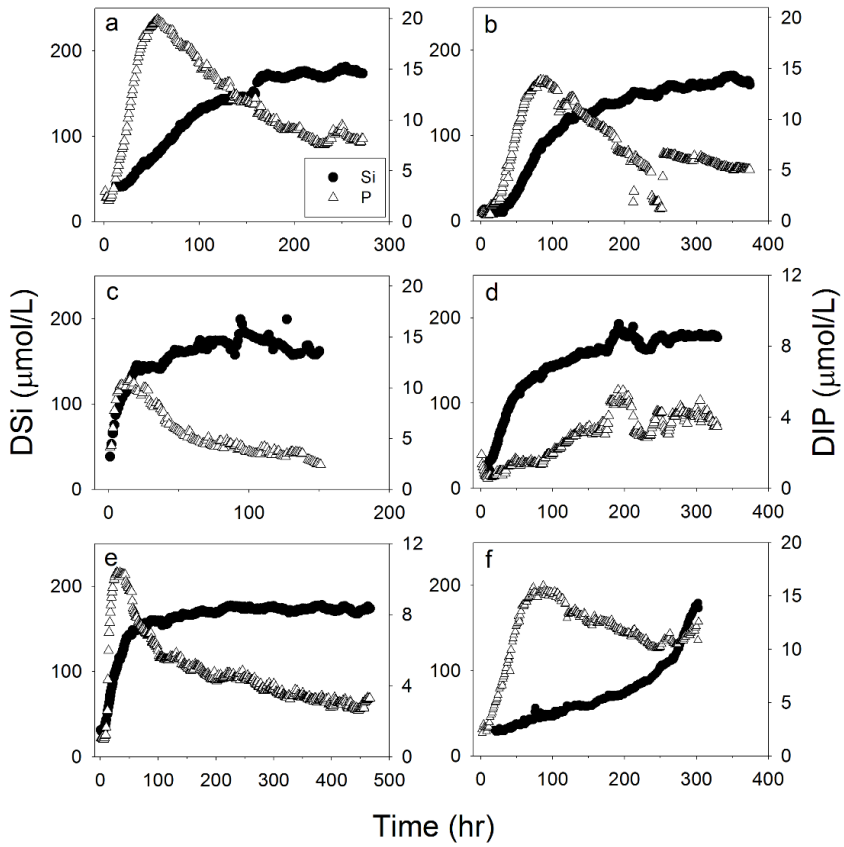

Figure 4.6. Long-term monitoring results of Si (●) adsorption and P (△) desorption from permeable sediments. Variations in desorbed phosphate from coastal sandy sediments ((a), P1; (b), P2; (c), P3; (d), P4; (e), P5; (f), P6) were observed over different time scales.

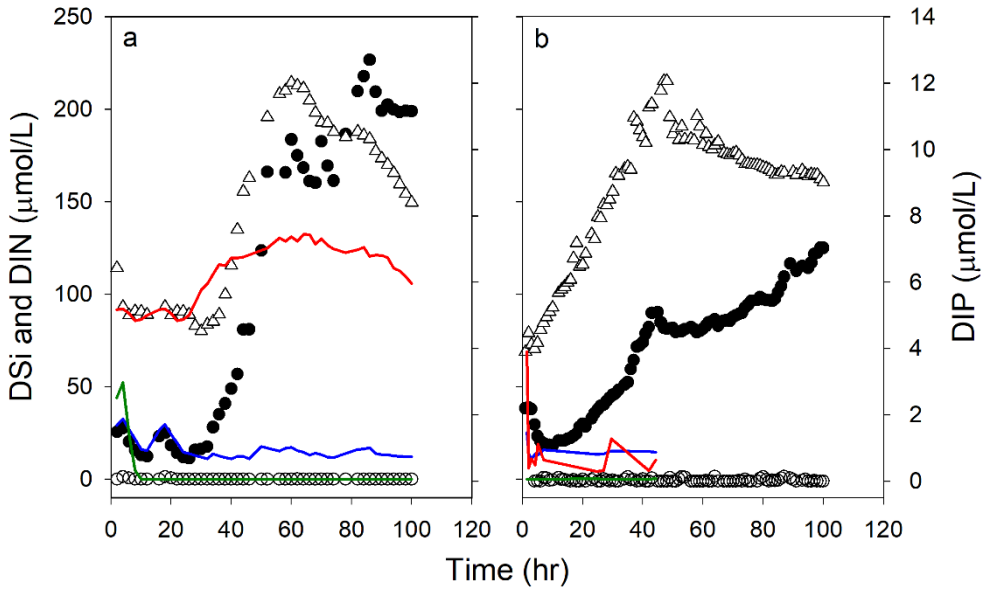

Figure 4.7. Long-term monitoring results of the behaviors of Si (●), P (△), and N (○) in seeping water with Si spiking in feeding groundwater, and those without Si spiking (line symbols- blue, Si; red, P; green, N) from permeable sediments from (a) P1 (column: C1) and (b) P3 (column: C2).

4.3.2. Beaker and bottle experiments

In order to examine P desorption from the sediments under different conditions, both beaker (50 g sediments, 50 mL 20 ppt NaCl) and bottle (1,000 g sediments, 500 mL deionized water) experiments were conducted. In all samples from the bottle experiment, pH values increased to 8.5−9.0 right after the sediments were mixed with the solution followed by a decrease to 8.0−9.0 and this was maintained for 24 hours. For both experiments, with 200 µmol Si/L loading solution, desorption of P (delta DIP) for pH 4–8 was nearly constant. Large difference in P desorption magnitude was observed depending on sediment samples (Figure 4.8). P desorption for different salinities, for both beaker and bottle experiments, was nearly constant, with large difference in P desorption magnitude for different sediments (Figure 4.8). As Si increased from 25 to 400 µmol/L at pH 8.3-8.7, desorption of P increased gradually from 60–180% for beaker experiments and from 40–90% for bottle experiments (Figure 4.8).

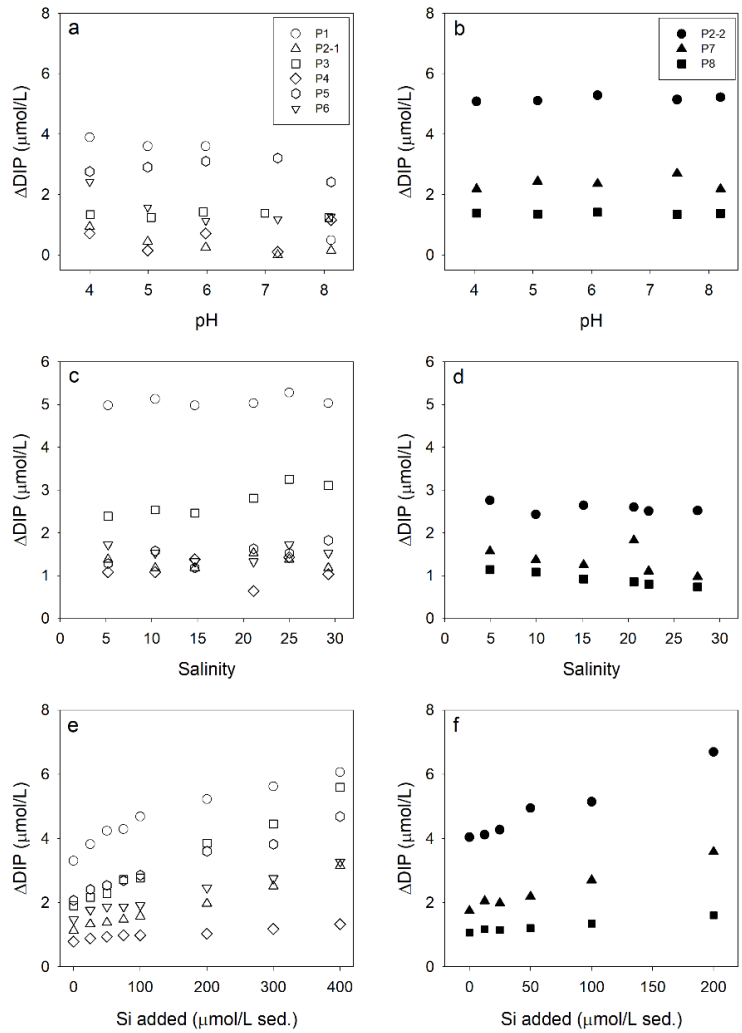

Figure 4.8. Effects of pH, salinity, and Si concentrations on phosphate releases for sediments collected from eight different coastal regions (P1–P8). P2-1 and P2-2 indicate sediment samples collected from different sites in region P2 in 2011 and 2016, respectively. The three panels (a, c, e) on the left show the results of beaker experiments (50 g of sediment and 50 mL of 20 ppt NaCl solution or diluted seawater). The three panels (b, d, f) on the right show the results of bottle

experiments (1,000 g of sediment and 500 mL of deionized water or diluted seawater).

4.4. Discussion

4.4.1. Adsorption of Si from groundwater to sediments

Si is generally conservative and increases in the course of weathering in groundwater (Corbett et al., 2002). At the sediment-water interface, Si ions are desorbed from sediments when the sediment particles encounter lower (0.15 μmol/L) silicate levels (Gehlen and Van Raaphorst, 2002), and adsorbed onto sediments when the concentration of Si in groundwater is high (225 μmol/L). In this study, the behavior of Si under typical saline groundwater conditions (200 μmol Si/L, 20 ppt salinity) occurring in STE was examined. The long-term column experiments for six different sediment columns showed that Si was almost fully removed in the initial stages, and Si levels in the outflow water gradually increased until it reached the saturation stage. Although Si removal occurs for all columns, the magnitudes of Si removal and the periods to reach the saturation stage vary significantly (Figure 4.6). This seems to be associated with differences in adsorption capacities of each sediment sample. In general, Fe/Mn-oxides, Al-oxides, carbonates, and organic matter are likely to influence the adsorption capacities of sediments for Si (Qin and Weng, 2006). However, in this study, specific factors controlling the adsorption of Si onto sediments were not determined since naturally occurring sandy sediments are mixtures of various sediment particle sizes and have different organic matter properties. Instead, it is attempted to establish a common phenomenon occurring in STE using samples from different coastal oceans.

These results suggest that Si is adsorbed onto sediments in STE when Si concentrations in groundwater are high. However, the magnitude of Si adsorption is greatly dependent on the conditions of STE, i.e. the levels of Si in groundwater, sediment mineralogical characteristics, organic matter content, seepage rates, tidal fluctuation of SGD pathways, etc.

4.4.2. Desorption of P from sediments to groundwater

In general, rapid desorption of P from sediments was observed in the outflow solutions as Si adsorption increased in six different sediment columns (Figure 4.6). P concentrations reached the maximum concentrations (6–20 μmol/L) within 20 to 80 hours, and decreased gradually with time (Figure 4.6). For the control experiments without added Si, the concentrations of P, Si, and N remained constant over the entire duration of the experiment. Furthermore, for Si added solutions, the concentrations of N in outflow waters were almost zero with little or no variations across all monitoring periods (Figure 4.7). Figure 4.8 shows that as Si increased from 25 to 400 μmol/L at pH 8.3-8.7, desorption of P increased gradually from 60–180% and from 40–90% for beaker and bottle experiments, respectively. These results are the first to suggest that the exchange of P can occur even at low levels of Si (25–50 μmol/L).

The decrease in P concentrations is thought to be due to the limitation of exchangeable P from the sediments in the column. The competitive P-Si interactions observed in the column experiments at pH 8.3-8.7 suggest that the increase in P concentrations in the outflow from sediment columns might be related to the exchange between P in sediments and Si in injected artificial groundwater. This observation implies that P desorption in sandy sediments in STE could be enhanced by Si in seeping groundwater. Despite similar trends of Si adsorption and P desorption, significant differences in time gaps between Si and P peaks were found

among different sediment columns. In addition, the amount of P desorption varied among sediments. These differences might be due to the heterogeneity in the sediments. If the increase in P concentrations was due to remineralization of organic matter, N concentrations should have increased as well (Figure 4.7). The control experiments also show that the level of Si control the level of P desorption from sediments. Thus, it is concluded that the P-Si exchange could also occur in the STE, under common Si levels in groundwater (e.g., 200 µmol/L). These results are consistent with previous studies where additions of inorganic Si (>200 µmol/L) increased the concentrations of dissolved P in the interstitial water of lake sediments (Koski-Vähälä et al., 2001; Tallberg and Koski-Vähälä, 2001) and marine sediments (Tallberg et al., 2008).

4.4.3. Effects of pH and salinity on P-Si exchange

For both beaker (50 g sediments, 50 mL 20 ppt NaCl, 200 μmol Si/L, 24 hours) and bottle (1,000 g sediments, 500 mL deionized water, 200 μmol Si/L, 24 hours) experiments, desorption of P (delta DIP) for pH 4–8 was almost constant. This seems to be due to high sediment to water ratios. At high solid concentration water (~1,700 mg/l), enhanced P mobilization is not observed at the pH range from 3 to 8.5 (Koski-Vähälä and Hartikainen, 2001). This result is different from calcium carbonate ($CaCO_3$) enriched sediments since $CaCO_3$-P fraction was entirely mobilized from sediments for a pH range of 9.5 to 5.5 (Gomez et al., 1999).

P desorption was also almost constant for different salinities for both beaker and bottle experiments. The amount of phosphate adsorption onto sediments is affected by salinity as well as grain size of the sediment particles (Meng et al., 2014). According to Meng et al.'s (2014) laboratory experiments, P adsorption onto sediments was maximum at salinity levels between 5 and 6 due to aggregations of particles. At higher salinities, anions (e.g., Cl^-, SO_4^{2-}, OH^-, and Br^-) would compete for adsorption sites on sediment surfaces to result in a decrease in phosphate adsorption. However, the salinity effect was negligible for larger particle grain size (fine silt → medium silt → coarse silt → sand) (Meng et al., 2014). Thus, the negligible effect of salinity obtained in this study seems to be due to sandy sediments used in this study (Figure 4.8). Therefore, these results suggest that P desorption

from sediments is predominantly controlled by Si levels of groundwater rather than pH and salinities in STE.

4.5. Conclusions

The laboratory experiments conducted in this study showed that P desorption from coastal sandy sediment to the water can be enhanced by high Si levels. P produced by P-Si exchange at the sediment-water interface might be an important mechanism controlling P flux to the ocean, although a major fraction of this P may originate from other marine sources. However, further research is necessary to determine the factors controlling the magnitudes of P desorption for different sediment characteristics as well as the real-world processes occurring in STE where sedimentary, oceanographic, and hydro-geochemical conditions are dynamic.

5. Contributions of groundwater-borne nutrients to coastal waters off a volcanic island

5.1. Introduction

SGD is particularly important nutrient transport pathway from land to the coastal ocean on tropical islands (e.g., Jeju Island, Hawaii, Balearic Islands, Mauritius, and etc.), where precipitation is large and rocks are highly permeable (Kim et al., 2003; Garcia-Solsona et al., 2010a; Knee et al., 2010; Kim et al., 2011; Povinec et al., 2012; Moosdorf et al., 2015). In this connection, nutrient fluxes through SGD are very important in coastal waters off islands standing in oligotrophic oceans.

In Flic-en-Flac lagoon, Mauritius Island, the concentrations of dissolved nitrate in wells were one order of magnitude greater than those in the lagoon and offshore waters (Povinec et al., 2012). In this region, the fluxes of SGD-derived DIN were estimated to be approximately 0.3×10^4 mmol m^{-1} day^{-1} along a shoreline. In Palma Bay of the island of Majorca, in the Mediterranean Sea, the fluxes of DIN via SGD were in the range of $0.01-1 \times 10^4$ mmol m^{-1} day^{-1}. In this bay, the amount of DIN supplied by SGD accounted fully for the excess nutrients (Rodellas et al., 2014). In Hawaii, N inputs through SGD were 2−100 times higher than N-fixation in coral reefs (Street et al., 2008). On Jeju Island, SGD-derived DIN fluxes were found to be

approximately 2×10^4 mmol m^{-1} day^{-1} in association with groundwater contamination (Kim et al., 2011).

Such a large input of nutrients through SGD could play a critical role in primary production in the coastal ocean. In the Balearic Islands, phytoplankton biomass in coastal waters seems to be sustained by consuming nutrients supplied from SGD (Garcia-Solsona et al., 2010a). As such, SGD from the highly permeability volcanic island, Jeju, is critical for feeding nutrients to coastal organisms (Kim et al., 2011). N inputs through SGD also contribute significantly to the biomass and succession of aquatic vegetation of reefs (Ishigaki Island, Japan, Umezawa et al., 2002). In the coral reefs of Hawaii, the SGD-derived DIN fluxes may support up to 100% of primary production (Street et al., 2008). However, too much nutrient loading via SGD often adversely affects coastal waters. For example, excess nutrient inputs from SGD resulted in benthic eutrophication in a semi-enclosed bay (Bangdu Bay) on Jeju Island (Hwang et al., 2005b). As such, enhanced nutrient loading by human activity via SGD can lead to reef degradation (Paytan et al., 2006).

In general, there are large variations in SGD magnitudes and groundwater quality depending on the precipitation and hydrogeological conditions of islands. In addition, nutrient conditions of open-ocean waters passing alongside the islands are dynamic and dependent on oceanographic conditions. However, the role of SGD in

different seasons with regard to changes in open-ocean water conditions is poorly understood. Thus, in this study, temporal changes in SGD and SGD-derived nutrient fluxes and budgets were observed in Hwasun Bay of Jeju Island. This island has high groundwater seepage rates, and the outer-bay water is upstream of the Kuroshio Current, which is very oligotrophic. Based on seasonal sampling campaigns, this study presents the relative contribution of SFGD and the outer-bay seawater to the nutrient loading and stoichiometry of Hwasun Bay.

5.2. Materials and methods

5.2.1. Study area

Jeju Island is located within approximately 140 km of the Korean Peninsula (Figure 5.1). This volcanic island has few streams in spite of high precipitation (1140−1960 mm yr^{-1}) because the island mostly consists of porous basalt (Hahn et al.. 1997). Hydrologic budget analyses show that approximately half of the total amount of rainfall contributes to groundwater recharge (1.7×10^9 m^3 yr^{-1}, Won et al., 2006). The SFGD flux calculated from the water mass balance on the island was 4.5 $\times 10^6$ m^3 day^{-1} (Lee and Kim, 2007a).

The study site, Hwasun Bay (1.4 km^2), is located in the southwestern part of the island (Figure 5.1). Since the low-permeability Seogwipo Formation is widely distributed under the thick basaltic layer in this region (Hahn et al., 1997; Koh et al., 2005), there are plenty of fresh groundwater springs that emerge from the aquifer. There is no continuous stream flow or river discharge into the bay. The total submarine groundwater (fresh and saline) inputs into the bay were estimated to be approximately 0.12 m^3 m^{-2} day^{-1} (Kim et al., 2011). The average depth of the bay is approximately 7 m (maximum ~15 m depth).

The coastal seawater near the bay is the Tsushima Current, which has high salinity (>35) and low nitrate concentrations (<1 μM) and originates from the north-flowing oligotrophic Kuroshio Current (Chang et al., 2000). The Tsushima Current

is diluted by Changjiang River diluted water (CDW), which has low salinity (<32), in summer and fall (Lie, 1984; Park, 1986; Chang and Isobe, 2003). The CDW has relatively high DIN concentrations relative to the DIP concentrations, with N:P ratios exceeding 100 (Tang et al., 1990; Wong et al., 1998).

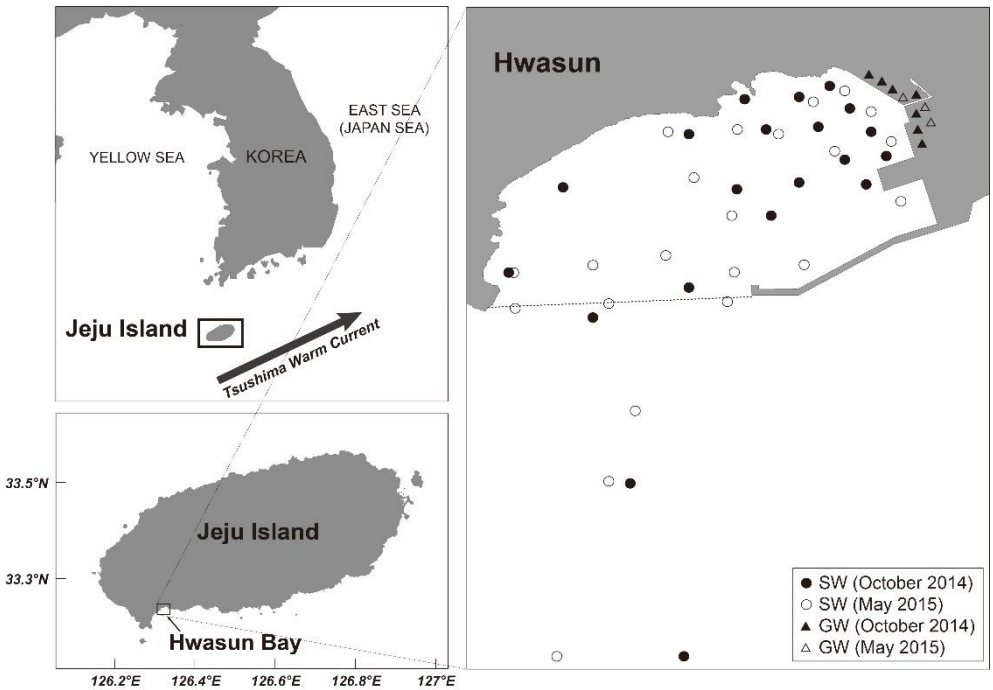

Figure 5.1. A map showing the sampling stations of coastal seawater (circle) and groundwater (triangle) in October 2014 and May 2015 in Hwasun Bay, Jeju Island. Sampling locations for groundwater and seawater from Hwasun Bay in August 2009 are shown in Fig. 1 in Kim et al. (2011).

5.2.2. Sampling and analyses

Bay seawater and coastal groundwater samples were collected for DIN, DIP, and DSi analyses. Seawater samples were collected in the bay from 20 and 22 stations in October 2014 and May 2015, respectively (Figure 5.1). The 2−4 seawater samples were collected for different depths at each site depending on water depths. The temperature and salinity of the seawater samples were measured onboard a ship using a conductivity-temperature-depth (CTD) instrument (Ocean Seven 304, IDRONAUT). Coastal groundwater samples (n = 7 and n = 3 in October 2014 and May 2015, respectively) were collected from beach wells along the shoreline. The temperature and salinity of groundwater samples were measured using a portable multi-parameter sensor (Orion star A329, Thermo Scientific).

Nutrient samples were collected in 50 mL conical tubes and filtered through 0.7-μm GF/F filters (Whatman, 45-mm diameter). The samples were frozen until the analysis was conducted. DIN (NO_3^- + NO_2^- + NH_4^+), DIP (PO_4^{3-}), and DSi ($Si(OH)_4^-$) were analyzed using nutrient auto-analyzers (FUTURA PLUS, Alliance and New QuAAtro39, SEAL).

In this study, the data from Kim et al. (2011) (August 2009) were also used together with the data from this study (October 2014 and May 2015) in order to examine the seasonal variations.

5.3. Results and discussion

5.3.1. Concentrations of nutrients in groundwater, outer-bay seawater, and bay seawater

In fresh groundwater, the mean concentrations of DIN were quite constant over the three periods (463 ± 275, 416 ± 142, and 551 ± 232 μM in August 2009, October 2014, and May 2015, respectively; Figure 5.2a). The mean concentrations of DIP in the fresh groundwater samples in August 2009 (3.8 ± 1.8 μM) were approximately 1.5-fold higher than those in October 2014 (2.7 ± 0.5 μM) and May 2015 (2.7 ± 0.4 μM; Figure 5.2b). The mean concentrations of DSi in fresh groundwater samples in October 2014 (513 ± 4 μM) and May 2015 (456 ± 56 μM) showed similar values, which were approximately four times lower than the value (2173 ± 1346 μM) in August 2009 (Figure 5.2c). This difference seems to be due to two extremely high values (SPL2, SPL3) in August 2009 (Kim et al., 2011). The DIN:DIP (N:P) ratios were similar for the three periods (158 ± 147, 162 ± 83, and 213 ± 106 μM in August 2009, October 2014, and May 2015, respectively; Figure 5.2d). The higher N:P ratios in groundwater suggest that SGD has a larger impact in N-limited water conditions. The temporal variations of nutrient concentrations in fresh groundwater were insignificant relative to spatial variations.

In the outer-bay seawater, the concentrations of DIN in May 2015 (3.6 ± 1.9 μM) were 2−3 times the values in August 2009 (1.8 ± 1.0 μM) and October 2014 (1.1 ± 0.1 μM; Figure 5.2a). DIP in the outer-bay seawater in October 2014 was

depleted, lower than the detection limit (< 0.05 μM), which was much lower than DIP concentrations in August 2009 (0.6 ± 0.5 μM) and May 2015 (0.1 ± 0.02 μM; Figure 5.2b). The concentrations of DSi (8.8 ± 1.4 μM) in the outer-bay seawater in May 2015 were twice as high as those in August 2009 (3.1 ± 1.6 μM) and October 2014 (4.3 ± 0.4 μM; Figure 5.2c). In August 2009, the outer-bay seawater were N-limited (N:P ratios <8), which seems to be due to the influence of N-depleted Tsushima Current passing along the island. In October 2014, the outer-bay seawater was extremely P-depleted (N:P ratios >100) owing to the input of P-depleted Changjiang River water to the Tsushima Current. During this period (October 2014), salinities for all seawater samples ranged from 29.2 to 29.7 (Figure 5.3), which indicates the influence of CDW. In May 2015, higher N:P ratios (>28) were observed in the outer-bay seawater, although the influence of CDW was not observed during this season. This seems to be due to excessive SFGD (high N:P ratios) inputs to the bay, as shown by the large salinity gradient in the bay and conservative behavior of both nutrients with respect to salinity (Figure 5.3).

In the bay seawater, the mean concentrations of DIN were similarly low in August 2009 (2.0 ± 0.2 μM) and October 2014 (3.2 ± 1.6 μM) compared to those in May 2015 (8.6 ± 11.8 μM; Figure 5.2a). The mean concentrations of DIP in the bay seawater were 0.6 ± 0.1 and 0.1 ± 0.04 μM in August 2009 and May 2015, respectively (Figure 5.2b), similar to those in the outer-bay seawater. Similar to the outer-bay seawater, DIP concentrations in the bay seawater in October 2014 were

below the detection limit (< 0.05 μM). The concentrations of DSi in the bay seawater were 11 ± 4, 6 ± 2, and 12 ± 8 μM in August 2009, October 2014, and May 2015, respectively (Figure 5.2c). The N:P ratios in the bay seawater were lower than the Redfield ratio (N:P = 16) in August 2009 (3.2 ± 0.4), while they were higher than the Redfield ratio in October 2014 (1031 ± 1332) and May 2015 (63 ± 50; Figure 5.2d).

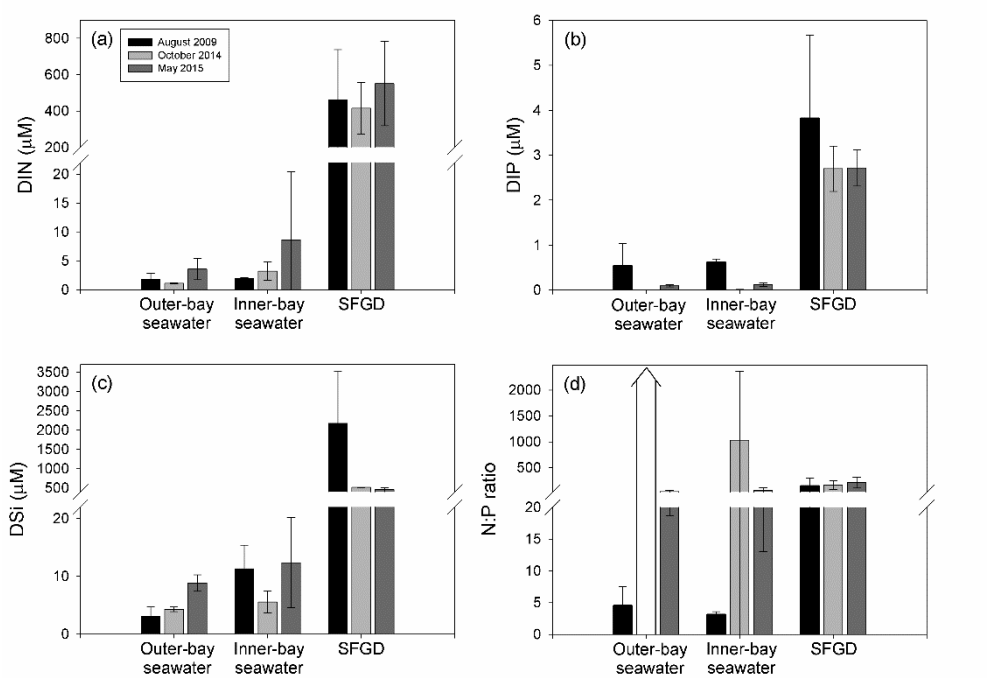

Figure 5.2. Bar graphs and error bars showing mean values and standard deviations of (a) DIN, (b) DIP, and (c) DSi, and (d) N:P ratios of outer- and inner-bay seawater, and coastal fresh groundwater. Black, grey, and dark grey bars represent samples in August 2009, October 2014, and May 2015, respectively.

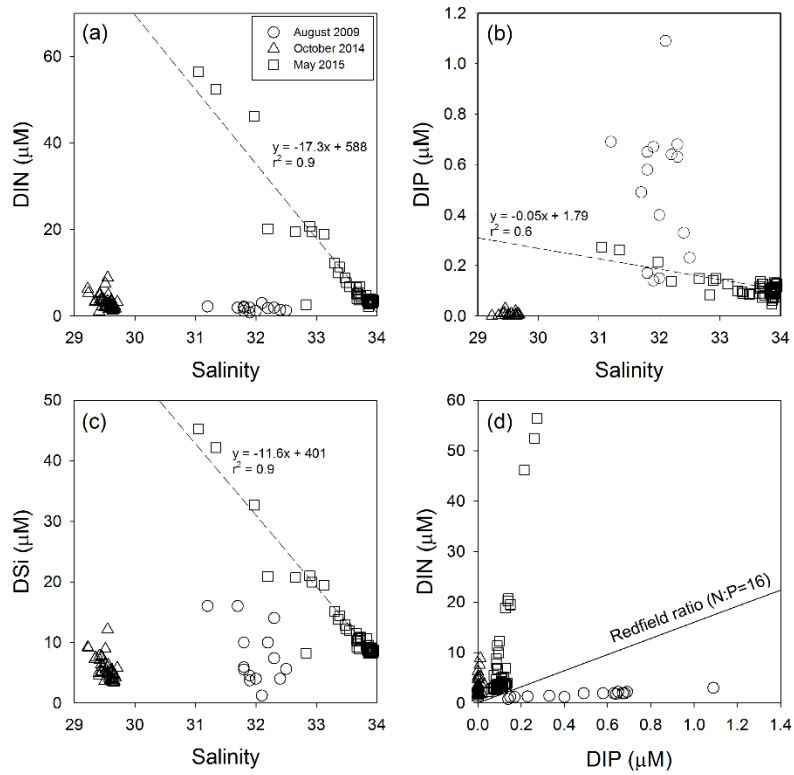

Figure 5.3. Plots of (a) DIN, (b) DIP, and (c) DSi versus salinity, and (d) N:P ratios of coastal seawater in Hwasun Bay. The data in Augutst 2009 were obtained from Kim et al. (2011).

5.3.2. Contributions of SGD on nutrient budgets

The concentrations of nutrients in coastal seawater decreased as salinity increased during all sampling periods. The seawater samples showed different salinity ranges of 31.2−32.5, 29.2−29.7, and 31.0−33.9 in August 2009, October 2014, and May 2015, respectively (Figure 5.3). The largest anomalies of salinity in the bay seawater were observed in May 2015 (Figure 5.4). Considering that there is no surface runoff in Hwasun Bay, the salinity anomalies reflect the input of SFGD into the bay. Thus, SFGD flux can be calculated based on salinity anomalies in the inner-bay seawater relative to the outer-bay seawater together with water residence times of the bay. The water residence time in this bay was calculated using a tidal prism model (Sanford et al. 1992; Moore et al. 2006). This model uses a function of the tidal range and the volume of bay seawater. In this calculation, it is assumed that the return flow is negligible since the velocity of the offshore current near the coast of Jeju Island is high (10-15 cm s^{-1}; Chang et al., 2000). The residence times of seawater were 2.5, 2.8, and 2.6 days in August 2009, October 2014, and May 2015, respectively. Based on these information, fresh groundwater fluxes were estimated to be 1.2×10^4, 0.2×10^4, and 4.2×10^4 m^3 day^{-1} in August 2009, October 2014, and May 2015, respectively.

The contribution of fresh groundwater inputs to Hwasun Bay seawater was estimated by multiplying SFGD-derived nutrient fluxes by the water residence time of bay water. The nutrient fluxes through SFGD were calculated by multiplying the

groundwater discharge by the end-member concentrations of fresh groundwater. The intercepts of salinity (salinity = 0) versus nutrient curves for groundwater and seawater were used as the endmember values of each nutrient (Figure 5.5). These correlations suggest that nutrient inputs through the diffusion from bottom sediments and saline groundwater discharge are insignificant in this system. Thus, the nutrient contributions to the bay seawater from SFGD can be compared to the background concentrations of the outer-bay seawater.

The entire range of extrapolated values was used as the fresh groundwater endmember values of each nutrient (194−630 μM for DIN, 1.8−3.3 μM for DIP, and 160−401 μM for DSi). In this estimation, two spring water samples (SPL2, SPL3) in August 2009 were regarded as outliers to avoid overestimation. The contribution of outer-bay seawater to the nutrient inventories of Hwasun Bay seawater was estimated by multiplying the mean concentration of nutrients in the outer-bay by the volume of bay seawater.

In August 2009, on the basis of this estimation, approximately 40% of the DIN inventory of the inner-bay was found to be from SFGD, whereas the contribution of outer-bay seawater to the DIP inventory of the inner-bay seawater was 99% (Figure 5.6a). DSi inputs via fresh groundwater contributed approximately 20% of the DSi inventory of the bay in August 2009 (Figure 5.6a). These results

show that inputs of DIN from SGD contributed significantly to biological production of this bay during this period as the outer-bay seawater was N-limited.

In October 2014, SFGD fluxes were lowest among the three sampling periods. During this period, DIP inputs through SFGD contributed about 100% of the DIP inventory of the bay. However, the outer-bay seawater contributed 80% and 95% of the DIN and DSi inventories in the bay, respectively (Figure 5.6b). This result suggests that even the small magnitude of DIP inputs (0.5×10^4 mmol day^{-1}) through SFGD regulated biological production of this bay during this time because DIP concentrations in the outer-bay seawater were not detectable.

In May 2015, approximately 60, 25, and 25% of the DIN, DIP, and DSi inventories of the inner-bay were respectively attributed to SFGD (Figure 5.6c). Because the concentrations of DIN, DIP, and DSi were conservative in this bay during this period due to the excessive inputs of nutrients through SGD, most of the nutrients from SGD seem to be conservatively transferred to the open ocean (Figure 5.7).

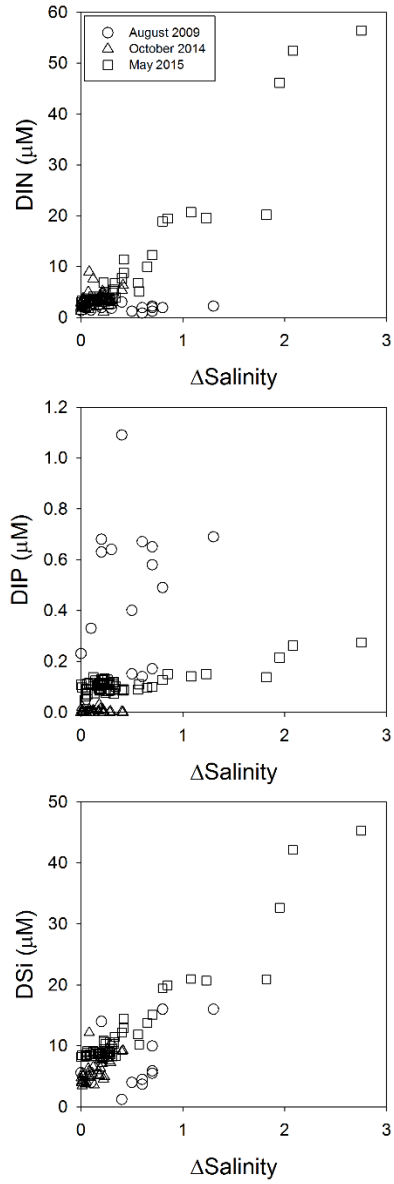

Figure 5.4. Plots of salinity anomalies versus concentrations of DIN, DIP, and DSi in bay seawater in Hwasun Bay, respectively.

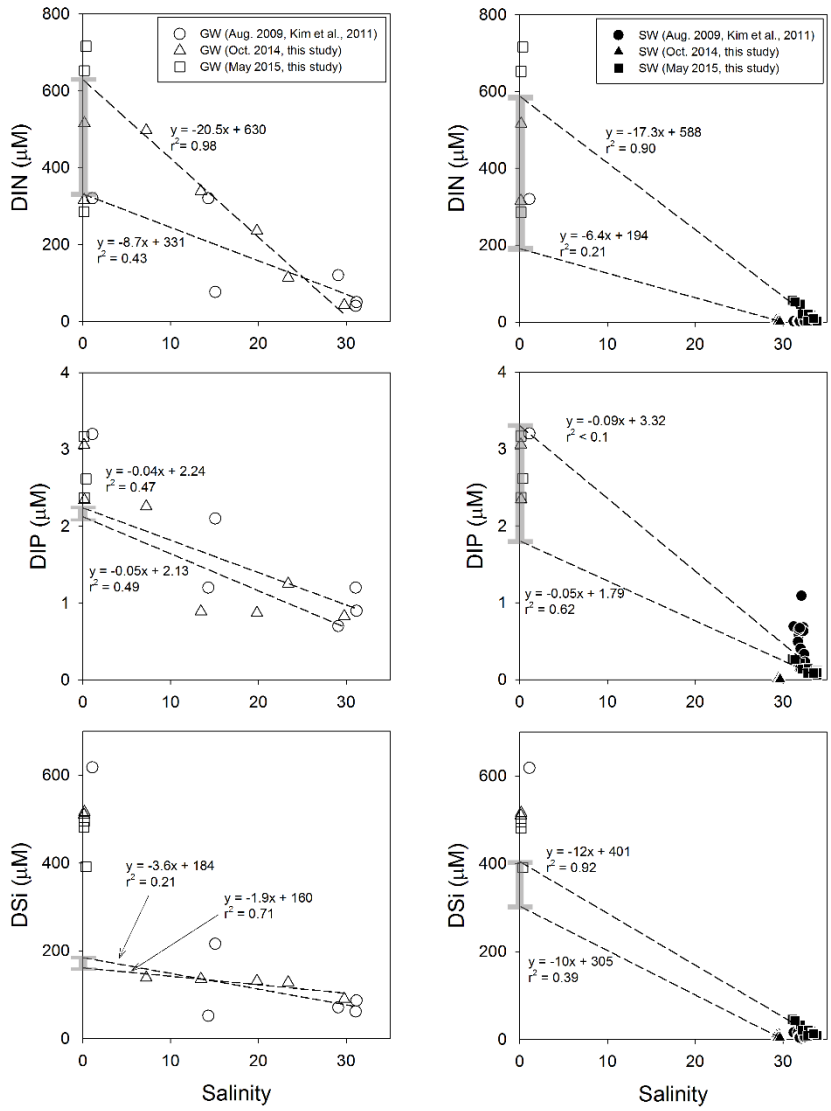

Figure 5.5. Plots of salinity versus DIN, DIP, and DSi concentrations in coastal groundwater (left 3 panels) and seawater (right 3 panels). The dashed lines in the left 3 panels and right 3 panels show linear regressions for salinity = 0 endmembers fitted through groundwater and seawater concentrations, respectively.

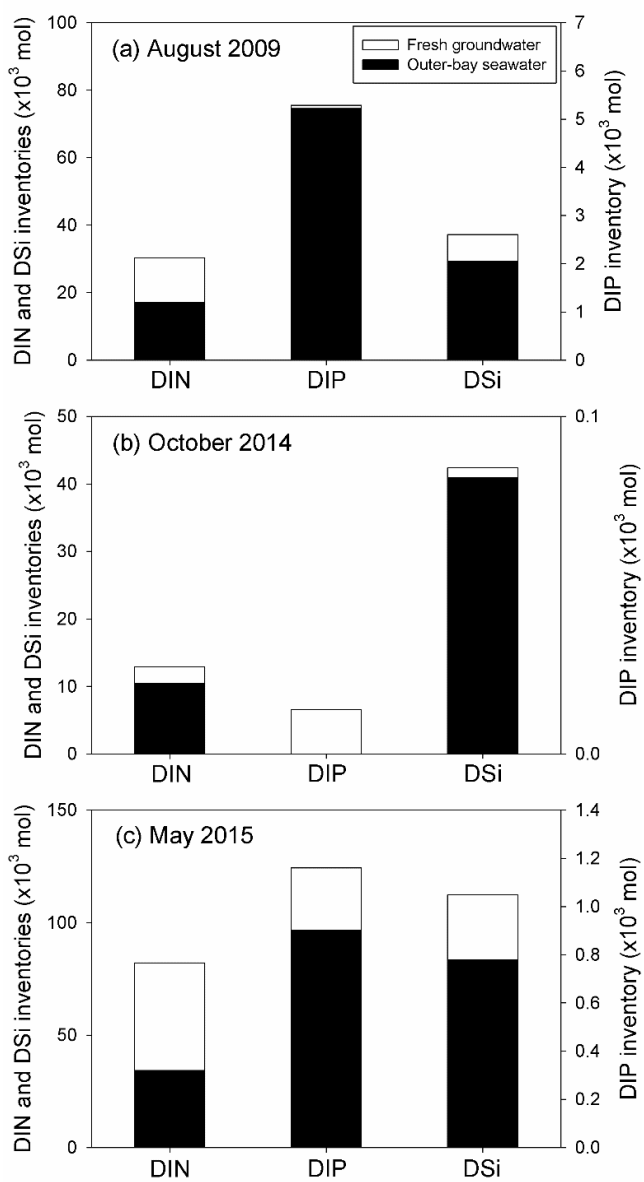

Figure 5.6. Nutrient inventories (×10^3 mol) in Hwasun Bay in (a) August 2009, (b) October 2014, and (c) May 2015. The white and black bars represent the nutrient inventories originating from fresh groundwater inputs and outer-bay seawater, respectively.

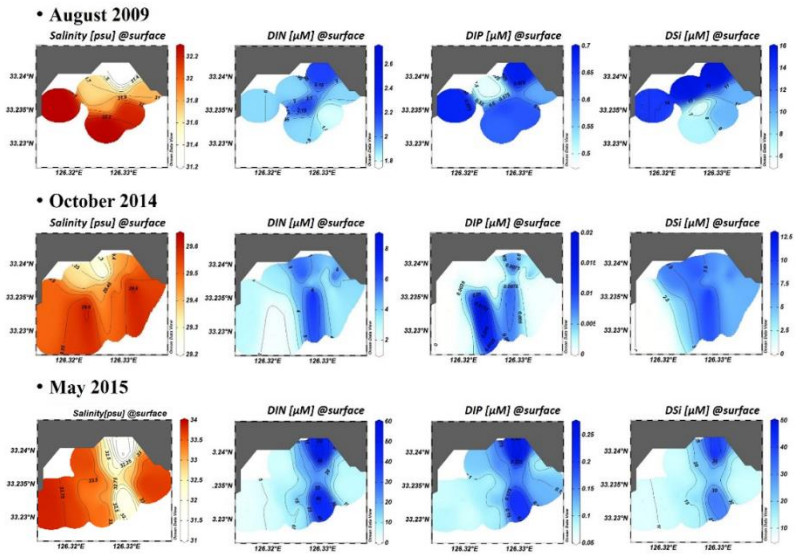

Figure 5.7 Distributions of salinity and concentrations of DIN, DIP, and DSi in surface seawater in Hwasun Bay in August 2009, October 2014, and May 2015.

5.4. Conclusions

In Hwasun Bay, the concentrations of nutrients in the coastal groundwater samples were similar for different seasons. However, the influence of SGD-derived nutrients on biological production was very different for the three sampling periods. In August 2009, SGD was the major source of DIN in N-limited bay waters influenced by N-limited Tsushima Current. In October 2014, SGD was the absolute source of DIP in P-depleted bay waters that were influenced by CDW. In May 2015, excessive inputs of nutrients from SGD resulted in almost complete transfer of SGD-derived nutrients to the open ocean. Further extensive studies are necessary for understanding large seasonal and spatial variations of SGD-derived nutrient inputs to the coastal ocean and their different roles in coastal production.

6. Summary and conclusions

Determining the global fluxes of SGD and SGD-derived nutrients to the ocean is difficult due to the lack of data for total SGD (fresh and saline) at the global scale. In this study, global fluxes of SGD are estimated using a Ra inverse modelling technique, and SGD-driven nutrient fluxes are calculated by multiplying nutrient/^{228}Ra ratios in coastal groundwater by the global ^{228}Ra flux via SGD. The results show that the global magnitude of SGD flux is approximately 1−1.5 times the river discharge. The estimated fluxes of nutrients via SGD to the global ocean are comparable to those through rivers.

The endmember concentrations of nutrients in SGD not only depend on the freshwater sources but also on the biogeochemical reactions that occur in the STE where freshwater and seawater interact (Moore, 1999). The investigation of factors controlling the mobility of P in SGD through STE is important since P is commonly a limiting nutrient for biological production and is particle-reactive. In this study, it is found that the P desorption from coastal sandy sediment in the STE to the coastal water can be enhanced by high Si levels in seeping groundwater. The occurrence of this process in the STE is important because this process influences P and Si fluxes through SGD to the coastal ocean.

The input of nutrients via SGD could play a critical role in primary production in the coastal ocean. In this study, it is found that the influence of SGD-

derived nutrients on biological production off the volcanic Jeju Island differed depending on open-ocean nutrient conditions, although the concentrations of nutrients in coastal groundwater were similar for different seasons.

This study presents that SGD is a volumetrically and chemically important vehicle for transporting DIN, DIP, and DSi into the coastal ocean and therefore plays a critical role in marine productivity at regional and global scales.

Bibliography

Anschutz, P., Charbonnier, C., Deborde, J., Deirmendjian, L., Poirier, D., Mouret, A., Buquet, D., Lecroart, P., 2016. Terrestrial groundwater and nutrient discharge along the 240-km-long Aquitanian coast. Marine Chemistry 185:38-47.

Basterretxea, G., Tovar-Sanchez, A., Beck, A. J., Masqué, P., Bokuniewicz, H. J., Coffey, R., Duarte, C. M., Garcia-Orellana, J., Garcia-Solsona, E., Martinez-Ribes, L., Vaquer-Sunyer, R., 2010. Submarine groundwater discharge to the coastal environment of a Mediterranean island (Majorca, Spain): ecosystem and biogeochemical significance. Ecosystems 13(5): 629-643.

Beck, A. J., Rapaglia, J. P., Cochran, J. K., Bokuniewicz, H. J., 2007a. Radium mass-balance in Jamaica Bay, NY: Evidence for a substantial flux of submarine groundwater. Marine Chemistry 106(3): 419-441.

Beck, A. J., Rapaglia, J. P., Cochran, J. K., Bokuniewicz, H. J., Yang, S., 2008. Submarine groundwater discharge to Great South Bay, NY, estimated using Ra isotopes. Marine Chemistry 109(3): 279-291.

Beck, A. J., Tsukamoto, Y., Tovar-Sanchez, A., Huerta-Diaz, M., Bokuniewicz, H. J., Sanudo-Wilhelmy, S. A., 2007b. Importance of geochemical transformations in determining submarine groundwater discharge-derived trace metal and nutrient fluxes. Applied Geochemistry 22(2): 477-490.

Beusen, A., Slomp, C., Bouwman, A., 2013. Global land–ocean linkage: direct inputs of nitrogen to coastal waters via submarine groundwater discharge. Environmental Research Letters 8(3): 034035.

Breier, J., Nidzieko, N., Monismith, S., Moore, W., Paytan, A., 2009. Tidally regulated chemical fluxes across the sediment-water interface in Elkhorn Slough, California: Evidence from a coupled geochemical and hydrodynamic approach. Limnology and Oceanography 54(6): 1964-1980.

Burnett, W. C., Bokuniewicz, H., Huettel, M., Moore, W. S., Taniguchi, M., 2003. Groundwater and pore water inputs to the coastal zone. Biogeochemistry 66(1-2): 3-33.

Burnett, W. C., Cowart, J. B., Deetae, S., 1990. Radium in the Suwannee River and estuary. Biogeochemistry 10(3): 237-255.

Burnett, W. C., Wattayakorn, G., Taniguchi, M., Dulaiova, H., Sojisuporn, P., Rungsupa, S., Ishitobi, T., 2007. Groundwater-derived nutrient inputs to the Upper Gulf of Thailand. Continental Shelf Research 27(2): 176-190.

Cable, J., Burnett, W., Chanton, J., Corbett, D. R., Cable, P., 1997. Field evaluation of seepage meters in the coastal marine environment. Estuarine, Coastal and Shelf Science 45(3): 367-375.

Cable, J., Corbett, D. R., Walsh, M., 2002. Phosphate uptake in coastal limestone aquifers: a fresh look at wastewater management. Limnology and Oceanography Bulletin 11(2): 1-4.

Chang, K. -I., Suk, M. -S., Pang, I. -C., Teague, W., 2000. Observations of the Cheju current. Journal-Korean Society of Oceanography 35(3): 129-152.

Chang, P. H., Isobe, A., 2003. A numerical study on the Changjiang diluted water in the Yellow and East China Seas. Journal of Geophysical Research: Oceans 108(C9).

Charette, M. A., Buesseler, K. O., 2004. Submarine groundwater discharge of nutrients and copper to an urban subestuary of Chesapeake Bay (Elizabeth River). Limnology and Oceanography 49(2): 376-385.

Charette, M. A., Henderson, P. B., Breier, C. F., Liu, Q., 2013. Submarine groundwater discharge in a river-dominated Florida estuary. Marine Chemistry 156: 3-17.

Charette, M. A., Sholkovitz, E. R ., 2002. Oxidative precipitation of groundwater-derived ferrous iron in the subterranean estuary of a coastal bay. Geophysical Research Letters 29(10).

Charette, M. A., Sholkovitz, E. R ., 2006. Trace element cycling in a subterranean estuary: Part 2. Geochemistry of the pore water. Geochimica et Cosmochimica Acta 70(4): 811-826.

Chen, C.-T. A., Borges, A. V., 2009. Reconciling opposing views on carbon cycling in the coastal ocean: continental shelves as sinks and near-shore ecosystems as sources of atmospheric CO_2. Deep Sea Research Part II: Topical Studies in Oceanography 56(8): 578-590.

Cho, H. M., Kim, G., 2016. Determining groundwater Ra end-member values for the estimation of the magnitude of submarine groundwater discharge using Ra isotope tracers. Geophysical Research Letters 43(8): 3865-3871.

Choi, W.-J., Han, G.-H., Lee, S.-M., Lee, G.-T., Yoon, K.-S., Choi, S.-M., Ro, H.-M., 2007. Impact of land-use types on nitrate concentration and $\delta^{15}N$ in unconfined groundwater in rural areas of Korea. Agriculture, Ecosystems & Environment 120(2): 259-268.

Church, T. M., 1996. An underground route for the water cycle. Nature 380: 579-580.

Cole, M. L., Kroeger, K. D., McClelland, J. W., Valiela, I., 2006. Effects of watershed land use on nitrogen concentrations and δ^{15} nitrogen in groundwater. Biogeochemistry 77(2): 199-215.

Corbett, D. R., Chanton, J., Burnett, W., Dillon, K., Rutkowski, C., Fourqurean, J. W., 1999. Patterns of groundwater discharge into Florida Bay. Limnology and Oceanography 44(4): 1045-1055.

Corbett, D. R., Dillon, K., Burnett, W., Schaefer, G., 2002. The spatial variability of nitrogen and phosphorus concentration in a sand aquifer influenced by onsite sewage treatment and disposal systems: a case study on St. George Island, Florida. Environmental Pollution 117(2): 337-345.

Costa Jr, O., Leao, Z., Nimmo, M., Attrill, M., 2000. Nutrification impacts on coral reefs from northern Bahia, Brazil. Island, Ocean and Deep-Sea Biology, Springer: 307-315.

Cuet, P., Atkinson, M., Blanchot, J., Casareto, B., Cordier, E., Falter, J., Frouin, P., Fujimura, H., Pierret, C., Susuki, Y., 2011. CNP budgets of a coral-dominated fringing reef at La Réunion, France: coupling of oceanic phosphate and groundwater nitrate. Coral Reefs 30(1): 45-55.

Davis, S. N., 1964. Silica in streams and ground water. American Journal of Science 262(7): 870-891.

Dillow, J. J., Banks, W. S., Smigaj, M. J., 2002. Ground-water quality and discharge to Chincoteague and Sinepuxent Bays adjacent to Assateague Island National Seashore, Maryland, US Department of the Interior, US Geological Survey.

Dollar, S., Atkinson, M., 1992. Effects of nutrient subsidies from groundwater to nearshore marine ecosystems off the island of Hawaii. Estuarine, Coastal and Shelf Science 35(4): 409-424.

Duce, R. A., LaRoche, J., Altieri, K., Arrigo, K. R., Baker, A. R., Capone, D. G., Cornell, S., Dentener, F., Galloway, J., Ganeshram, R. S., Geider, R. J., Jickells, T., Kuypers, M. M., Langlois, R., Liss, P. S., Liu, S. M., Middelburg, J. J., Moore, C. M., Nickovic, S., Oschlies, A., Pedersen, T., Prospero, J., Schlitzer, R., Seitzinger, S., Sorensen, L. L., Uematsu, M., Ulloa, O., Voss, M., Ward, B., Zamora, L., 2008. Impacts of atmospheric anthropogenic nitrogen on the open ocean. Science 320(5878): 893-897.

Dugdale, R.,Goering, J., 1967. Uptake of new and regenerated forms of nitrogen in primary productivity. Limnology and Oceanography 12(2): 196-206.

El-Gamal, A. A., Peterson, R. N., Burnett, W. C., 2012. Detecting freshwater inputs via groundwater discharge to Marina Lagoon, Mediterranean Coast, Egypt. Estuaries and Coasts 35(6): 1486-1499.

Elsinger, R. J., Moore, W. S., 1984. ^{226}Ra and ^{228}Ra in the mixing zones of the Pee Dee River-Winyah bay, Yangtze River and Delaware bay estuaries. Estuarine, Coastal and Shelf Science 18(6): 601-613.

Eneke, G., Ayonghe, S., Chandrasekharam, D., Ntchancho, R., Ako, A., Mouncherou, O., Thambidurai, P., 2011. Controls on groundwater chemistry in a highly urbanised coastal area. International Journal of Environmental Research 5(2): 475-490.

Erler, D. V., Santos, I. R., Zhang, Y., Tait, D. R., Befus, K. M., Hidden, A., Li, L., Eyre, B. D., 2014. Nitrogen transformations within a tropical subterranean estuary. Marine Chemistry 164: 38-47.

Frings, P. J., Clymans, W., Fontorbe, G., Christina, L., Conley, D. J., 2016. The continental Si cycle and its impact on the ocean Si isotope budget. Chemical Geology 425: 12-36.

Garcia-Solsona, E., García-Orellana, J., Masqué, P., Garcés, E., Radakovitch, O., Mayer, A., Estradé, S., Basterretxea, G., 2010a. An assessment of karstic submarine groundwater and associated nutrient discharge to a Mediterranean coastal area (Balearic Islands, Spain) using radium isotopes. Biogeochemistry 97(2-3): 211-229.

Garcia-Solsona, E., Garcia-Orellana, J., Masqué, P., Rodellas, V., Mejías, M., Ballesteros, B., Domínguez, J., 2010b. Groundwater and nutrient discharge through karstic coastal springs (Castelló, Spain). Biogeosciences 7(9): 2625-2638.

Garcia-Solsona, E., Masqué, P., Garcia-Orellana, J., Rapaglia, J., Beck, A., Cochran, J., Bokuniewicz, H., Zaggia, L., Collavini, F., 2008. Estimating submarine groundwater discharge around Isola La Cura, northern Venice Lagoon (Italy), by using the radium quartet. Marine Chemistry 109(3): 292-306.

Garcia, H., Locarnini, R., Boyer, T., Antonov, J., Baranova, O., Zweng, M., Reagan, J., Johnson, D., 2014. Dissolved inorganic nutrients (phosphate, nitrate, silicate). World Ocean Atlas 2013 volume 4: 25.

Garrison, G., Glenn, C., McMurtry, G., 2003. Measurement of submarine groundwater discharge in Kahana Bay, O'ahu, Hawaii. Limnology and Oceanography 48(2): 920-928.

Gehlen, M., Van Raaphorst, W., 2002. The role of adsorption–desorption surface reactions in controlling interstitial $Si(OH)_4$ concentrations and enhancing $Si(OH)_4$ turn-over in shallow shelf seas. Continental Shelf Research 22(10): 1529-1547.

Georg, R., West, A., Basu, A., Halliday, A., 2009. Silicon fluxes and isotope composition of direct groundwater discharge into the Bay of Bengal and

the effect on the global ocean silicon isotope budget. Earth and Planetary Science Letters 283(1): 67-74.

Gleeson, J., Santos, I. R., Maher, D. T., Golsby-Smith, L., 2013. Groundwater–surface water exchange in a mangrove tidal creek: evidence from natural geochemical tracers and implications for nutrient budgets. Marine Chemistry 156: 27-37.

Gobler, C. J., Sañudo-Wilhelmy, S. A., 2001. Temporal variability of groundwater seepage and brown tide blooms in a Long Island embayment. Marine Ecology Progress Series 217: 299-309.

Godoy, J. M., Souza, T. A., Godoy, M. L. D., Moreira, I., Carvalho, Z. L., Lacerda, L. D., Fernandes, F. C., 2013. Groundwater and surface water quality in a coastal bay with negligible fresh groundwater discharge: Arraial do Cabo, Brazil. Marine Chemistry 156: 85-97.

Gomez, E., Durillon, C., Rofes, G., Picot, B., 1999. Phosphate adsorption and release from sediments of brackish lagoons: pH, O_2 and loading influence. Water Research 33(10): 2437-2447.

Gonneea, M. E., Morris, P. J., Dulaiova, H., Charette, M. A., 2008. New perspectives on radium behavior within a subterranean estuary. Marine Chemistry 109(3): 250-267.

Gu, H., Moore, W. S., Zhang, L., Du, J., Zhang, J., 2012. Using radium isotopes to estimate the residence time and the contribution of submarine groundwater

discharge (SGD) in the Changjiang effluent plume, East China Sea. Continental Shelf Research 35: 95-107.

Hahn, J., Lee, Y., Kim, N., Hahn, C., Lee, S., 1997. The groundwater resources and sustainable yield of Cheju volcanic island, Korea. Environmental Geology 33(1): 43-53.

Haines, T., Lloyd, J., 1985. Controls on silica in groundwater environments in the United Kingdom. Journal of hydrology 81(3-4): 277-295.

Hingston, F., Atkinson, R., Posner, A., Quirk, J., 1967. Specific adsorption of anions. Nature 215: 1459-1461.

Hosono, T., Ono, M., Burnett, W. C., Tokunaga, T., Taniguchi, M., Akimichi, T., 2012. Spatial distribution of submarine groundwater discharge and associated nutrients within a local coastal area. Environmental Science & Technology 46(10): 5319-5326.

Hu, C., Muller-Karger, F. E., Swarzenski, P. W., 2006. Hurricanes, submarine groundwater discharge, and Florida's red tides. Geophysical Research Letters 33(11).

Hwang, D.-W., Kim, G., Lee, Y.-W., Yang, H.-S., 2005a. Estimating submarine inputs of groundwater and nutrients to a coastal bay using radium isotopes. Marine Chemistry 96(1): 61-71.

Hwang, D. W., Lee, Y. W., Kim, G., 2005b. Large submarine groundwater discharge and benthic eutrophication in Bangdu Bay on volcanic Jeju Island, Korea. Limnology and Oceanography 50(5): 1393-1403.

Ji, T., Du, J., Moore, W. S., Zhang, G., Su, N., Zhang, J., 2013. Nutrient inputs to a Lagoon through submarine groundwater discharge: The case of Laoye Lagoon, Hainan, China. Journal of Marine Systems 111: 253-262.

Jickells, T., 1998. Nutrient biogeochemistry of the coastal zone. Science 281(5374): 217-222.

Johannes, R., 1980. Ecological significance of the submarine discharge of groundwater. Marine Ecology Progress Series 3(4): 365-373.

Johannes, R., Hearn, C., 1985. The effect of submarine groundwater discharge on nutrient and salinity regimes in a coastal lagoon off Perth, Western Australia. Estuarine, Coastal and Shelf Science 21(6): 789-800.

Johnson, A. G., Glenn, C. R., Burnett, W. C., Peterson, R. N., Lucey, P. G., 2008. Aerial infrared imaging reveals large nutrient-rich groundwater inputs to the ocean. Geophysical Research Letters 35(15).

Kay, E. A. Lau, L., Stroup, E., Dollar, S., Fellows, D., Young, R., 1977. Hydrologic and ecologic inventories of the coastal waters of west Hawaii. Technical Report-Water Resources Research Center, University of Hawaii (USA).

Kelly, R., Moran, S., 2002. Seasonal changes in groundwater input to a well-mixed estuary estimated using radium isotopes and implications for coastal nutrient budgets. Limnology and Oceanography 47(6): 1796-1807.

Kim, G., Hwang, D. W., 2002. Tidal pumping of groundwater into the coastal ocean revealed from submarine ^{222}Rn and CH_4 monitoring. Geophysical Research Letters 29(14): 23-21-23-24.

Kim, G., Kim, J.-S., Hwang, D.-W., 2011. Submarine groundwater discharge from oceanic islands standing in oligotrophic oceans: Implications for global biological production and organic carbon fluxes. Limnology and Oceanography 56(2): 673-682.

Kim, G., Lee, K. K., Park, K. S., Hwang, D. W., Yang, H. S., 2003. Large submarine groundwater discharge (SGD) from a volcanic island. Geophysical Research Letters 30(21).

Kim, G., Lee, Y. W., Joung, D. J., Kim, K. R., Kim, K., 2006. Real-time monitoring of nutrient concentrations and red-tide outbreaks in the southern sea of Korea. Geophysical Research Letters 33(13).

Kim, G., Ryu, J.-W., Hwang, D.-W., 2008. Radium tracing of submarine groundwater discharge (SGD) and associated nutrient fluxes in a highly-permeable bed coastal zone, Korea. Marine Chemistry 109(3): 307-317.

Kim, G., Ryu, J.-W., Yang, H.-S., Yun, S.-T., 2005. Submarine groundwater discharge (SGD) into the Yellow Sea revealed by ^{228}Ra and ^{226}Ra isotopes: Implications for global silicate fluxes. Earth and Planetary Science Letters 237(1): 156-166.

Kim, G., Swarzenski, P.W., 2010. Submarine ground-water discharge (SGD) and associated nutrient fluxes to the coastal ocean. In, Carbon and Nutrient

Fluxes in Continental Margins: A Global Synthesis; in, K.-K. Liu, L. Atkinson, R. Quinones, and L. Talaue-McManus, eds.: Springer-Verlag, New York, pp. 529-538.

Kim, T.-H., Waska, H., Kwon, E., Suryaputra, I. G. N., Kim, G., 2012. Production, degradation, and flux of dissolved organic matter in the subterranean estuary of a large tidal flat. Marine Chemistry 142: 1-10.

Kitheka, J. U., Mwashote, B., Ohowa, B., Kamau, J., 1999. Water circulation, groundwater outflow and nutrient dynamics in Mida creek, Kenya. Mangroves and Salt Marshes 3(3): 135-146.

Knee, K., Paytan, A., 2011. Submarine groundwater discharge: A source of nutrients, metals, and pollutants to the coastal ocean. Treatise on Estuarine and Coastal Science 4: 205-234.

Knee, K. L., Street, J. H., Grossman, E. E., Boehm, A. B., Paytan, A., 2010. Nutrient inputs to the coastal ocean from submarine groundwater discharge in a groundwater-dominated system: relation to land use (Kona coast, Hawai'i, USA). Limnology and Oceanography 55(3): 1105.

Koh, D. C., Chang, H. W., Lee, K. S., Ko, K. S., Kim, Y., Park, W. B., 2005. Hydrogeochemistry and environmental isotopes of ground water in Jeju volcanic island, Korea: implications for nitrate contamination. Hydrological Processes 19(11): 2225-2245.

Koski-Vähälä, J., Hartikainen, H., 2001. Assessment of the risk of phosphorus loading due to resuspended sediment. Journal of Environmental Quality 30(3): 960-966.

Koski-Vähälä, J., Hartikainen, H., Tallberg, P., 2001. Phosphorus mobilization from various sediment pools in response to increased pH and silicate concentration. Journal of Environmental Quality 30(2): 546-552.

Krest, J. M., Moore, W., Gardner, L., Morris, J., 2000. Marsh nutrient export supplied by groundwater discharge: Evidence from radium measurements. Global Biogeochemical Cycles 14(1): 167-176.

Kroeger, K., Charette, M., 2008. Nitrogen biogeochemistry of submarine groundwater discharge. Limnology and Oceanography 53(3): 1025.

Kroeger, K. D., Swarzenski, P. W., Greenwood, W. J., Reich, C., 2007. Submarine groundwater discharge to Tampa Bay: Nutrient fluxes and biogeochemistry of the coastal aquifer. Marine Chemistry 104(1): 85-97.

Kwon, E. Y., Kim, G., Primeau, F., Moore, W. S., Cho, H. -M., DeVries, T., Sarmiento, J. L., Charette, M. A., Cho, Y. K., 2014. Global estimate of submarine groundwater discharge based on an observationally constrained radium isotope model. Geophysical Research Letters 41(23): 8438-8444.

Lapointe, B. E., 1997. Nutrient thresholds for bottom-up control of macroalgal blooms and coral reefs. Limnology and Oceanography 44: 1586-1592.

Lapointe, B. E., Clark, M. W., 1992. Nutrient inputs from the watershed and coastal eutrophication in the Florida keys. Estuaries and Coasts 15(4): 465-476.

Lee, C. M., Jiao, J. J., Luo, X., Moore, W. S., 2012. Estimation of submarine groundwater discharge and associated nutrient fluxes in Tolo Harbour, Hong Kong. Science of the Total Environment 433: 427-433.

Lee, J. M., Kim, G., 2007a. Estimating submarine discharge of fresh groundwater from a volcanic island using a freshwater budget of the coastal water column. Geophysical Research Letters 34(11).

Lee, Y. -W., Hwang, D. -W., Kim, G., Lee, W. -C., Oh, H. -T., 2009. Nutrient inputs from submarine groundwater discharge (SGD) in Masan Bay, an embayment surrounded by heavily industrialized cities, Korea. Science of the Total Environment 407(9): 3181-3188.

Lee, Y. -W., Kim, G., 2007b. Linking groundwater-borne nutrients and dinoflagellate red-tide outbreaks in the southern sea of Korea using a Ra tracer. Estuarine, Coastal and Shelf Science 71(1): 309-317.

Lee, Y. -W., Kim, G., Lim, W. -A., Hwang, D. -W., 2010. A relationship between submarine-groundwater borne nutrients traced by Ra isotopes and the intensity of dinoflagellate red-tides occurring in the southern sea of Korea. Limnology and Oceanography 55(1): 1.

Lewis, J. B., 1987. Measurements of groundwater seepage flux onto a coral reef: Spatial and temporal variations. Limnology and Oceanography 32(5): 1165-1169.

Li, L., Barry, D., Stagnitti, F., Parlange, J. Y., 1999. Submarine groundwater discharge and associated chemical input to a coastal sea. Water Resources Research 35(11): 3253-3259.

Li, M., Whelan, M., Wang, G., White, S., 2013. Phosphorus sorption and buffering mechanisms in suspended sediments from the Yangtze Estuary and Hangzhou Bay, China. Biogeosciences 10(5): 3341-3348.

Li, Y. -H., Mathieu, G., Biscaye, P., Simpson, H. J., 1977. The flux of ^{226}Ra from estuarine and continental shelf sediments. Earth and Planetary Science Letters 37(2): 237-241.

Lie, H. -J.,1984. A note on water masses and general circulation in the Yellow Sea (Hwanghae). The Journal of the Oceanological Society of Korea 19: 187-194.

Liu, Q., Dai, M., Chen, W., Huh, C.-A., Wang, G., Li, Q., Charette, M. A., 2012. How significant is submarine groundwater discharge and its associated dissolved inorganic carbon in a river-dominated shelf system? Biogeosciences 9: 1777-1795.

Luo, X., Jiao, J. J., Moore, W., Lee, C. M., 2014. Submarine groundwater discharge estimation in an urbanized embayment in Hong Kong via short-

lived radium isotopes and its implication of nutrient loadings and primary production. Marine Pollution Bulletin 82(1): 144-154.

Makings, U., Santos, I. R., Maher, D. T., Golsby-Smith, L., Eyre, B. D., 2014. Importance of budgets for estimating the input of groundwater-derived nutrients to an eutrophic tidal river and estuary. Estuarine, Coastal and Shelf Science 143: 65-76.

Mejías, M., Ballesteros, B. J., Antón-Pacheco, C., Domínguez, J. A., Garcia-Orellana, J., Garcia-Solsona, E., Masqué, P., 2012. Methodological study of submarine groundwater discharge from a karstic aquifer in the Western Mediterranean Sea. Journal of Hydrology 464: 27-40.

Meng, J., Yao, Q., Yu, Z., 2014. Particulate phosphorus speciation and phosphate adsorption characteristics associated with sediment grain size. Ecological Engineering 70: 140-145.

Moore, D. G., Scott, M. R., 1986. Behavior of ^{226}Ra in the Mississippi River mixing zone. Journal of Geophysical Research: Oceans 91(C12): 14317-14329.

Moore, W. S., 1981. Radium isotopes in the Chesapeake Bay. Estuarine, Coastal and Shelf Science 12(6): 713-723.

Moore, W. S., 1996. Large groundwater inputs to coastal waters revealed by ^{226}Ra enrichments. Nature 380(6575): 612-614.

Moore, W. S., 1999. The subterranean estuary: a reaction zone of ground water and sea water. Marine Chemistry 65(1): 111-125.

Moore, W. S., 2006. The role of submarine groundwater discharge in coastal biogeochemistry. Journal of Geochemical Exploration 88(1): 389-393.

Moore, W. S., Astwood, H., Lindstrom, C., 1995. Radium isotopes in coastal waters on the Amazon shelf. Geochimica et Cosmochimica Acta 59(20): 4285-4298.

Moore, W. S., Blanton, J. O., Joye, S. B., 2006. Estimates of flushing times, submarine groundwater discharge, and nutrient fluxes to Okatee Estuary, South Carolina. Journal of Geophysical Research: Oceans 111(C9).

Moore, W. S., Sarmiento, J. L., Key, R. M., 2008. Submarine groundwater discharge revealed by ^{228}Ra distribution in the upper Atlantic Ocean. Nature Geoscience 1(5): 309-311.

Moosdorf, N., Stieglitz, T., Waska, H., Dürr, H. H., Hartmann, J., 2015. Submarine groundwater discharge from tropical islands: a review. Grundwasser 20(1): 53-67.

Moran, S., Stachelhaus, S., Kelly, R., Brush, M., 2014. Submarine groundwater discharge as a source of dissolved inorganic nitrogen and phosphorus to coastal ponds of Southern Rhode Island. Estuaries and Coasts 37(1): 104-118.

Nam, S., Kim, G., Kim, K. -R., Kim, K., Cheng, L. O., Kim, K.-W., Ossi, H., Kim, Y.-G., 2005. Application of real-time monitoring buoy systems for physical and biogeochemical parameters in the coastal ocean around the Korean peninsula. Marine Technology Society Journal 39(2): 70-80.

Niencheski, L. F. H., Windom, H. L., Moore, W. S., Jahnke, R. A., 2007. Submarine groundwater discharge of nutrients to the ocean along a coastal lagoon barrier, Southern Brazil. Marine Chemistry 106(3): 546-561.

Nolan, B. T., 2001. Relating nitrogen sources and aquifer susceptibility to nitrate in shallow ground waters of the United States. Ground Water 39(2): 290-299.

Nozaki, Y., Yamamoto, Y., Manaka, T., Amakawa, H., Snidvongs, A., 2001. Dissolved barium and radium isotopes in the Chao Phraya River estuarine mixing zone in Thailand. Continental Shelf Research 21(13): 1435-1448.

Obihara, C., Russell, E., 1972. Specific adsorption of silicate and phosphate by soils. Journal of Soil Science 23(1): 105-117.

Oga, M. S, Marlin, C., Dever, L., Filly, A., Njitchoua, R., 2008. Hydrochemical and isotopic characteristics of coastal groundwater near Abidjan (southern Ivory Coast), Applied groundwater studies in Africa, eds Adelana S, MacDonald A(Taylor and Francis, London), pp 371-389.

Oki, D. S., 1999. Geohydrology and numerical simulation of the ground-water flow system of Kona, Island of Hawaii, Geological Survey (US).

Park, Y. -H., 1986. Water characteristics and movements of the Yellow Sea Warm Current in summer. Progress in Oceanography 17(3): 243-254.

Paytan, A., Shellenbarger, G. G., Street, J. H., Gonneea, M. E., Davis, K., Young, M. B., Moore, W. S., 2006. Submarine groundwater discharge: An important source of new inorganic nitrogen to coral reef ecosystems. Limnology and Oceanography 51(1): 343-348.

Peterson, R. N., Burnett, W. C., Taniguchi, M., Chen, J., Santos, I. R., Ishitobi, T., 2008. Radon and radium isotope assessment of submarine groundwater discharge in the Yellow River delta, China. Journal of Geophysical Research: Oceans (1978–2012) 113(C9).

Povinec, P. P., Burnett, W. C., Beck, A., Bokuniewicz, H., Charette, A., Gonneea, M. E., Groening, M., Ishitobi, T., Kontar, E., Kwong, L. L. W., 2012. Isotopic, geophysical and biogeochemical investigation of submarine groundwater discharge: IAEA-UNESCO intercomparison exercise at Mauritius Island. Journal of Environmental Radioactivity 104: 24-45.

Price, R. M., Savabi, M. R., Jolicoeur, J. L., Roy, S., 2010. Adsorption and desorption of phosphate on limestone in experiments simulating seawater intrusion. Applied Geochemistry 25(7): 1085-1091.

Qin, Y. -C., Weng, H. -X., 2006. Silicon release and its speciation distribution in the surficial sediments of the Pearl River Estuary, China. Estuarine, Coastal and Shelf Science 67(3): 433-440.

Rajmohan, N., Al-Futaisi, A., Al-Touqi, S., 2009. Geochemical process regulating groundwater quality in a coastal region with complex contamination sources: Barka, Sultanate of Oman. Environmental Earth Sciences 59(2): 385-398.

Rapaglia, J., Ferrarin, C., Zaggia, L., Moore, W. S., Umgiesser, G., Garcia-Solsona, E., Garcia-Orellana, J., Masqué, P., 2010. Investigation of residence time and groundwater flux in Venice Lagoon: comparing radium

isotope and hydrodynamical models. Journal of Environmental Radioactivity 101(7): 571-581.

Rapaglia, J. P., Bokuniewicz, H. J., 2009. The effect of groundwater advection on salinity in pore waters of permeable sediments. Limnology and Oceanography 54(2): 630-643.

Reay, W. G., Gallagher, D. L., Simmons, G. M., 1992. Groundwater discharge and its impact on surface water quality in a Chesapeake Bay inlet1, Wiley Online Library.

Rengarajan, R., Sarma, V., 2015. Submarine groundwater discharge and nutrient addition to the coastal zone of the Godavari estuary. Marine Chemistry 172: 57-69.

Rodellas, V., Garcia-Orellana, J., Masqué, P., Feldman, M., Weinstein, Y., 2015. Submarine groundwater discharge as a major source of nutrients to the Mediterranean Sea. Proceedings of the National Academy of Sciences 112(13): 3926-3930.

Rodellas, V., Garcia-Orellana, J., Masqué, P., Font-Muñoz, J. S., 2015. The influence of sediment sources on radium-derived estimates of Submarine Groundwater Discharge. Marine Chemistry 171: 107-117.

Rodellas, V., Garcia-Orellana, J., Tovar-Sánchez, A., Basterretxea, G., López-Garcia, J. M., Sánchez-Quiles, D., Garcia-Solsona, E., Masqué, P., 2014. Submarine groundwater discharge as a source of nutrients and trace metals

in a Mediterranean bay (Palma Beach, Balearic Islands). Marine Chemistry 160: 56-66.

Sanford, L. P., Boicourt, W. C., Rives, S. R., 1992. Model for estimating tidal flushing of small embayments. Journal of Waterway, Port, Coastal, and Ocean Engineering 118(6): 635-654.

Santoro, A. E., 2010. Microbial nitrogen cycling at the saltwater–freshwater interface. Hydrogeology Journal 18(1): 187-202.

Santos, I. R., Bryan, K. R., Pilditch, C. A., Tait, D. R., 2014. Influence of porewater exchange on nutrient dynamics in two New Zealand estuarine intertidal flats. Marine Chemistry 167: 57-70.

Santos, I. R., Burnett, W. C., Chanton, J., Mwashote, B., Suryaputra, I., Dittmar, T., 2008. Nutrient biogeochemistry in a Gulf of Mexico subterranean estuary and groundwater-derived fluxes to the coastal ocean. Limnology and Oceanography 53(2): 705.

Santos, I. R., Cook, P. L. M., Rogers, L., Weys, J. d., Eyre, B. D., 2012. The "salt wedge pump": Convection-driven pore-water exchange as a source of dissolved organic and inorganic carbon and nitrogen to an estuary. Limnology and Oceanography 57(5): 1415-1426.

Santos, I. R., Weys, J. d., Tait, D. R., Eyre, B. D., 2013. The contribution of groundwater discharge to nutrient exports from a coastal catchment: post-flood seepage increases estuarine N/P ratios. Estuaries and Coasts 36(1): 56-73.

Santos, I. R., Lechuga-Deveze, C., Peterson, R. N., Burnett, W. C., 2011. Tracing submarine hydrothermal inputs into a coastal bay in Baja California using radon. Chemical Geology 282(1): 1-10.

Seitzinger, S., Harrison, J., Dumont, E., Beusen, A. H., Bouwman, A., 2005. Sources and delivery of carbon, nitrogen, and phosphorus to the coastal zone: An overview of Global Nutrient Export from Watersheds (NEWS) models and their application. Global Biogeochemical Cycles 19(4).

Seitzinger, S., Mayorga, E., Bouwman, A., Kroeze, C., Beusen, A., Billen, G., Van Drecht, G., Dumont, E., Fekete, B., Garnier, J., 2010. Global river nutrient export: A scenario analysis of past and future trends. Global Biogeochemical Cycles 24(4).

Senal, M. I. S., Jacinto, G. S., San Diego-McGlone, M. L., Siringan, F., Zamora, P., Soria, L., Cardenas, M. B., Villanoy, C., Cabrera, O., 2011. Nutrient inputs from submarine groundwater discharge on the Santiago reef flat, Bolinao, Northwestern Philippines. Marine Pollution Bulletin 63(5): 195-200.

Slomp, C. P.,Van Cappellen, P., 2004. Nutrient inputs to the coastal ocean through submarine groundwater discharge: controls and potential impact. Journal of Hydrology 295(1): 64-86.

Smyth, T. J., Sanchez, P. A., 1980. Effects of lime, silicate, and phosphorus applications to an Oxisol on phosphorus sorption and ion retention. Soil Science Society of America Journal 44(3): 500-505.

Spalding, R. F., Exner, M. E., 1993. Occurrence of nitrate in groundwater—a review. Journal of Environmental Quality 22(3): 392-402.

Spiteri, C., Van Cappellen, P., Regnier, P., 2008. Surface complexation effects on phosphate adsorption to ferric iron oxyhydroxides along pH and salinity gradients in estuaries and coastal aquifers. Geochimica et Cosmochimica Acta 72(14): 3431-3445.

Stewart, B. T., Santos, I. R., Tait, D. R., Macklin, P. A., Maher, D. T., 2015. Submarine groundwater discharge and associated fluxes of alkalinity and dissolved carbon into Moreton Bay (Australia) estimated via radium isotopes. Marine Chemistry 174: 1-12.

Stieglitz, T. C., Rapaglia, J., Krupa, S. C., 2007. An effect of pier pilings on nearshore submarine groundwater discharge from a (partially) confined aquifer. Estuaries and Coasts 30(3): 543-550.

Street, J. H., Knee, K. L., Grossman, E. E., Paytan, A., 2008. Submarine groundwater discharge and nutrient addition to the coastal zone and coral reefs of leeward Hawai'i. Marine Chemistry 109(3): 355-376.

Struyf, E., Dausse, A., Van Damme, S., Bal, K., Gribsholt, B., Boschker, H. T., Middelburg, J. J., Meire, P., 2006. Tidal marshes and biogenic silica recycling at the land-sea interface. Limnology and Oceanography 51(2): 838-846.

Su, N., Du, J., Moore, W. S., Liu, S., Zhang, J., 2011. An examination of groundwater discharge and the associated nutrient fluxes into the estuaries

of eastern Hainan Island, China using ^{226}Ra. Science of the Total Environment 409(19): 3909-3918.

Swarzenski, P. W., Izbicki, J. A., 2009. Coastal groundwater dynamics off Santa Barbara, California: Combining geochemical tracers, electromagnetic seepmeters, and electrical resistivity. Estuarine, Coastal and Shelf Science 83(1): 77-89.

Swarzenski, P. W., Simonds, F. W., Paulson, A. J., Kruse, S., Reich, C., 2007a. Geochemical and geophysical examination of submarine groundwater discharge and associated nutrient loading estimates into Lynch Cove, Hood Canal, WA. Environmental Science & Technology 41(20): 7022-7029.

Swarzenski, P. W., Reich, C., Kroeger, K. D., Baskaran, M., 2007b. Ra and Rn isotopes as natural tracers of submarine groundwater discharge in Tampa Bay, Florida. Marine Chemistry 104(1): 69-84.

Tait, D. R., Erler, D. V., Santos, I. R., Cyronak, T. J., Morgenstern, U., Eyre, B. D., 2014. The influence of groundwater inputs and age on nutrient dynamics in a coral reef lagoon. Marine Chemistry 166: 36-47.

Talbot, J., Kroeger, K., Rago, A., Allen, M., Charette, M., 2003. Nitrogen flux and speciation through the subterranean estuary of Waquoit Bay, Massachusetts. The Biological Bulletin 205(2): 244-245.

Tallberg, P.,1999. The magnitude of Si dissolution from diatoms at the sediment surface and its potential impact on P mobilization. Archiv für Hydrobiologie 144(4): 429-438.

Tallberg, P, Koski-Vähälä, J., 2001. Silicate-induced phosphate release from surface sediment in eutrophic lakes. Archiv für Hydrobiologie 151(2): 221-245.

Tallberg, P., Tréguer, P., Beucher, C., Corvaisier, R., 2008. Potentially mobile pools of phosphorus and silicon in sediment from the Bay of Brest: interactions and implications for phosphorus dynamics. Estuarine, Coastal and Shelf Science 76(1): 85-94.

Tang, R., Dong, H., Wang, F., 1990. Biogeochemical behavior of nitrogen and phosphate in the Changjiang estuary and its adjacent waters. Biogeochemical study of the Changjiang estuary: 322-334.

Taniguchi, M., Burnett, W. C., Cable, J. E., Turner, J. V., 2002. Investigation of submarine groundwater discharge. Hydrological Processes 16(11): 2115-2129.

Taniguchi, M., Burnett, W. C., Dulaiova, H., Siringan, F., Foronda, J., Wattayakorn, G., Rungsupa, S., Kontar, E. A., Ishitobi, T., 2008. Groundwater discharge as an important land-sea pathway into Manila Bay, Philippines. Journal of Coastal Research 24(sp1): 15-24.

Taniguchi, M., Ishitobi, T., Burnett, W. C., 2009. Global assessment of submarine groundwater discharge. From headwaters to the ocean: hydrological changes and watershed management: 613-617.

Taniguchi, M., Ishitobi, T., Burnett, W. C., Wattayakorn, G., 2007. Evaluating ground water–sea water interactions via resistivity and seepage meters. Groundwater 45(6): 729-735.

Taniguchi, M., Ishitobi, T., Shimada, J., 2006. Dynamics of submarine groundwater discharge and freshwater-seawater interface. Journal of Geophysical Research: Oceans (1978–2012) 111(C1).

Tay, C., Kortatsi, B., 2008. Groundwater quality studies: A Case study of the Densu Basin, Ghana. West African Journal of Applied Ecology 12(1).

Tovar-Sánchez, A., Basterretxea, G., Rodellas, V., Sánchez-Quiles, D., García-Orellana, J., Masqué, P., Jordi, A., López, J. M., Garcia-Solsona, E., 2014. Contribution of groundwater discharge to the coastal dissolved nutrients and trace metal concentrations in Majorca Island: karstic vs detrital systems. Environmental Science & Technology 48(20): 11819-11827.

Tréguer, P. J., De La Rocha, C. L., 2013. The world ocean silica cycle. Annual Review of Marine Science 5: 477-501.

Tse, K. C., Jiao, J. J., 2008. Estimation of submarine groundwater discharge in Plover Cove, Tolo Harbour, Hong Kong by ^{222}Rn. Marine Chemistry 111(3): 160-170.

Tuominen, L., Hartikainen, H., Kairesalo, T., Tallberg, P., 1998. Increased bioavailability of sediment phosphorus due to silicate enrichment. Water Research 32(7): 2001-2008.

Tuominen, L., Kairesalo, T., Hartikainen, H., Tallberg, P., 1996. Nutrient fluxes and microbial activity in sediment enriched with settled seston. Hydrobiologia 335(1): 19-31.

Ullman, W. J., Chang, B., Miller, D. C., Madsen, J. A., 2003. Groundwater mixing, nutrient diagenesis, and discharges across a sandy beachface, Cape Henlopen, Delaware (USA). Estuarine, Coastal and Shelf Science 57(3): 539-552.

Umezawa, Y., Miyajima, T., Kayanne, H., Koike, I., 2002. Significance of groundwater nitrogen discharge into coral reefs at Ishigaki Island, southwest of Japan. Coral Reefs 21(4): 346-356.

Urquidi-Gaume, M., Santos, I. R., Lechuga-Deveze, C., 2016. Submarine groundwater discharge as a source of dissolved nutrients to an arid coastal embayment (La Paz, Mexico). Environmental Earth Sciences 75(2): 1-13.

Van Drecht, G., Bouwman, A., Knoop, J., Beusen, A., Meinardi, C., 2003. Global modeling of the fate of nitrogen from point and nonpoint sources in soils, groundwater, and surface water. Global Biogeochemical Cycles 17(4).

Wang, X., Du, J., Ji, T., Wen, T., Liu, S., Zhang, J., 2014. An estimation of nutrient fluxes via submarine groundwater discharge into the Sanggou Bay—A typical multi-species culture ecosystem in China. Marine Chemistry 167: 113-122.

Waska, H., Kim, G., 2011. Submarine groundwater discharge (SGD) as a main nutrient source for benthic and water-column primary production in a large

intertidal environment of the Yellow Sea. Journal of Sea Research 65(1): 103-113.

Webster, I. T., Hancock, G. J., Murray, A. S., 1995. Modelling the effect of salinity on radium desorption from sediments. Geochimica et Cosmochimica Acta 59(12): 2469-2476.

Won, J. -H., Lee, J. -Y., Kim, J. -W., Koh, G. -W., 2006. Groundwater occurrence on Jeju Island, Korea. Hydrogeology Journal 14(4): 532-547.

Wong, G., Gong, G., Liu, K., Pai, S., 1998. 'Excess Nitrate'in the East China Sea. Estuarine, Coastal and Shelf Science 46(3): 411-418.

Young, M. B., Gonneea, M. E., Fong, D. A., Moore, W. S., Herrera-Silveira, J., Paytan, A., 2008. Characterizing sources of groundwater to a tropical coastal lagoon in a karstic area using radium isotopes and water chemistry. Marine Chemistry 109(3): 377-394.

Zektser, I., Dzhamalov, R., Safronova, T., 1983. Role of submarine groundwater discharge in the water balance of Australia. IAHS-AISH Publication(142): 209-219.

Abstract (in Korean)

해저 지하수 유출은 강물과 더불어 해양으로 영양염을 공급하는 주요 공급원이다. 많은 지역적 연구에 의하면 해저 지하수를 통한 영양염 유출량은 강물을 통한 영양염 공급량과 비슷한 수준이라 알려져 있다. 해저 지하수를 통한 해양으로의 영양염 유입에 대한 연구는 주로 지역적으로 이루어졌으며, 자료의 한계로 인해 전 지구적 규모에서는 연구가 부족한 실정이다. 본 연구에서는 지하수 중 라듐 동위원소(n >500)의 농도가 염분에 비례한다는 성질을 고려하여 라듐 단성분 값을 재 산정하였고, 그 값을 사용하여 전 지구적 해저 지하수 유출량을 재평가 하였다. 그 결과, 전 지구 해양으로 유입되는 지하수의 양은 $(5.6 \pm 1.5) \times 10^{13}\ m^3\ yr^{-1}$로, 강물 유출량의 2 배이며, 기존 연구에 의한 전 지구적 해저 지하수 유출량은 2-3 배 가량 과대평가 되었음을 밝혔다. 또한 대서양과 인도-태평양으로 유입되는 해저 지하수를 통한 영양염 플럭스는 강물에 의한 유출량과 비슷하다는 것을 밝혀냈다. 해저 지하수를 통해 전 지구 해양으로 유입되는 용존무기질소(2.4 $Tmol\ yr^{-1}$)가 생물생산에 모두 사용된다고 가정하였을 때, 이는 전체 대륙붕에서 일어나는 신 생물생산(new production)의 약 20%를 차지한다는 것을 알 수 있다.

전 지구 해저 지하수 중 영양염 (n >700)의 단성분 값 또한 염분에 따른 농도 차이를 크게 보였다. 육상 기원의 영양염과 재순환된 해수를 통해 대수층으로 유입된 영양염은 모두 해양으로 유입되기 전 여러 지화학적 반응을

거친다. 일반적으로 규소는 지하수가 유출되는 과정에서 보존적인 거동을 보인다고 알려져 있으나, 본 연구에서는 담지하수 중 고농도로 존재하는 규산염이 사질 퇴적물을 통과하면서 그 농도가 24 시간 이내에 40–90% 이상 감소하는 것을 실험실 실험을 통해서 관찰하였다. 반면, 인산염의 농도는 증가(5–20 μmol/L) 하였다. 본 연구 결과는 지하수 중 상대적으로 고농도로 존재하는 규산염이 사질 퇴적층을 통과하면서 제거되는 동시에 퇴적물로부터 인산염을 탈착시켜 해양으로 유출시키는데 영향을 미칠 수 있음을 시사한다.

이러한 지하수 기원의 영양염은 연안 지역의 생물생산 및 생물 군집 조성 등에 중요한 영향을 미치며, 과잉의 영양염 공급은 연안 해역의 부영양화와 유해 적조를 일으키기도 한다. 해저 지하수를 통한 영양염 공급은 큰 강의 영향이 없는 섬 지역에서 특히 더 중요하다. 제주도 남서부에 위치한 화순만은 빈 영양 해역으로 둘러싸여 있으며, 만 내로 유입되는 강이나 하천수의 영향이 없으며, 외해수의 영양염 농도 조건이 계절별로 다른 특성을 가진다. 본 연구에서는 지하수를 통한 영양염 공급이 화순만 내 영양염 물질수지에 미치는 영향을 시기별로 비교하였다. 그 결과, 2009 년 8 월에는 지하수를 통한 질산염 공급이 만 내 질산염 인벤토리의 40%를 차지하였고, 2014 년 10 월에는 지하수를 통한 인산염 공급이 만 내 인산염 인벤토리의 100%를 차지하였다. 그리고 조사 시기 중 가장 많은 양의 담지하수 유출($4.2 \times 10^4\ m^3\ day^{-1}$)을 보인 2015 년 5 월에는 지하수를 통한 과잉의 영양염 공급이 외해수까지 영향을 미치는 것으로 나타났다.

주요어: 해저지하수, 영양염, 해저하구, 영양염 플럭스, 연안, 해양

학번: 2009-22956

Appendix

Table A. Activities of ^{228}Ra and ^{226}Ra in global coastal groundwater, which is combined with the data reported by Kwon et al. (2014) and Moore et al. (2008) to calculate the globally averaged SGD ^{228}Ra and ^{226}Ra endmembers.

Location	Salinity	^{228}Ra (dpm m^{-3})	^{226}Ra (dpm m^{-3})	Reference
Southwestern coast of Korea				Kim et al. (2005)
1	15.3		592	
2	30.7		1095	
3	25.6		905	
4	27.3		563	
5	31.5		408	
6	1.6		2697	
7	25.2		648	
8	23.7		1208	
9	20.5		1085	
10	17.2		1155	
11	21		560	
Yeoja Bay, Korea				Hwang et al. (2005a)
B	3.9		200	
C	15.9		490	
D	0		90	
E	19.7		870	
F	27.3		270	
G	28.5		490	
Jeju Island, Korea				Hwang et al. (2005b)
A	33.3		172	
B	35.9		170	
C	30.5		136	
D	33.8		138	
E	32.7		162	
Yeongil Bay, eastern coast of Korea				Kim et al. (2008)
1	5.9		560	
2	18.8		720	
3	20.6		360	
4	7.8		320	
Florida estuary				Charette et al. (2013)
GW1		87	490	

GW2	2799	4852
GW2B	9454	24439
GW3	322	4281
GW4	593	3080
GW5	876	7350
GW6	904	21608
GW7	156	863
GW8	99	1541
GW9	434	15277
GW10	304	1621
GW11	218	4926
GW12	212	1288
GW13	243	2555
GW14	470	34455
GW15	795	12143
GW16	943	3426
GW17	1296	1417
GW18	203	2349
PZ2	1423	1438
PZ3	416	2230
GW1	136	980
GW2B	2497	8908
GW2	907	1268
GW4	417	2506
GW5	1876	1640
GW6	815	16479
GW7	257	1506
GW8	468	3765
GW9	363	14323
GW10	250	1923
GW11	202	3987
GW12	273	1528
GW13	248	3062
GW14	745	9036
GW15	385	27314
GW16	930	2553
GW17	1227	1261
GW18	275	2732
PZ4	9009	99454
PZ5	12754	85324
PZ6	4634	22449

PZ7		286	1131
PZ8		345	1503
GW2B		3011	11002
GW3		424	4416
GW5		1485	11556
GW6		978	22573
GW9		323	11419
GW10		148	934
GW11		193	5198
GW13		344	3112
PZ9		5354	58532
PZ10		29666	225453
PZ11		3828	40344
PZ12		531	2282
PZ13		537	1846
GW2		301	1100
GW2B		2638	10324
GW3		287	3344
GW5		1796	13131
GW6		872	18849
GW9		542	24568
GW10		462	1675
GW11		334	5898
GW13		304	3867
Yellow River delta			Peterson et al. (2008)
DO-34	3	710	
DO-33	0.7	32	
N-10	3.2	440	
N-10	12.4	726	
N-8	16.3	685	
N-12	55	590	
N-6	21	189	
N-7	9.1	805	
N-8	15.8	344	
N-10	17.9	950	
PW-2	27.1	780	
PW-4a	28.3	560	
Hawaii			Street et al. (2008)
GW(Spr.)	2.9	19	
GW(pit)	32.2	72	
GW(pit)	34.9	69.9	

GW(Spr.)	18.4	97.1	
GW(pond)	13.5	83.3	
GW(pond)	13.6	89	
GW-fed pond	14.2	86.1	
GW-fed pond	13.7	81.1	
shore spring	13.2	57.4	
inland spring	11.9	70.3	
shore spring	15.1	68.6	
GW(pit)	11.6	45.7	
GW(pond)	12.7	34.4	
GW Spr. #1	2.9	25.2	
GW Spr. #2	3.1	21.6	
GW	33.4	100.5	
GW (pond)	0.5	60.4	
Chongming Island, China			Gu et al. (2012)
Porewater	1.9	169	
Porewater	0.7	75	
Porewater	12.5	569	
Porewater	11.8	473	
Porewater	7.9	471	
Porewater	10	485	
Shengsi Islands, China			
Well	0.1	133	
Spring	0.2	166	
Spring	0.2	69	
Spring	0.2	152	
Well	0.2	166	
Well	0.5	267	
Well	0.4	191	
Well	0.3	116	
Well	0.1	90	
Well	0.6	294	
Spring	0.5	1214	
Well	0.7	451	
Well	0.2	1299	
Well	0.4	160	
Tolo Harbour Hong Kong			Lee et al. (2012)
1	11.3	550	

1	5.4		694.7	
2	33.9		607.9	
3	19.7		176	
3	18.8		721.6	
3	29.6		695.2	
3	28		1198.4	
6	0.04		220	
7	9.4		211.2	
8	25.2		739.2	
9	0.3		81.4	
10	0.6		37.4	
11	33.2		104.2	
11	34.4		405.3	
North inlet salt marsh South Carolina				Krest et al. (2000)
Borehole ID#1	36.7	13290	2180	
Borehole ID#2	33.3	11360	1380	
Borehole ID#3	31.2	4650	430	
Borehole ID#4	31	5160	580	
Borehole ID#5	32.1	8790	900	
Borehole ID#6	30.9	360	160	
Borehole ID#7	26.5	2220	190	
Borehole ID#8	24.5	3770	570	
Borehole ID#9	28.3	6310	500	
Borehole ID#10	20.8	2350	150	
Borehole ID#2	27.2	10150	1560	
Borehole ID#2	32.9	10500	1670	
Great South Bay, NY				Beck et al. (2008)
GP	5	1290	420	
GP	0	1550	940	
RA	26	1900	1100	
RA	7	7460	3020	
RA	0	5850	2010	
BB	24	420	320	
BB	0	280	390	
WS	25	410	330	
Kangaroo Island mangrove tidal creek, Australia				Gleeson et al. (2013)
Winter 1	28.2		538	
Winter 2	28.1		780	

Winter 3	30.5		1159	
Winter 4	31.5		592	
Summer 1	32		953	
Summer 2	35		545	
Summer 3	27		565	
Summer 4	21		626	
Summer 5	23		502	
Arraial do Cabo, Brazil				Godoy et al. (2013)
W1	3.1	243	101.4	
W2	12.5	1746	352.2	
W3	1.2	208.2	210	
W4	1.2	5.472	456.6	
W5	0.9	204.6	13.68	
W6	0.6	217.8	125.4	
W7	0.6	259.2	45.48	
W8	0.6	424.2	40.44	
W9	2.2	562.8	107.4	
W1	0.5	131.4	107.4	
W2	1.1	5.604	346.2	
W3	12.9	1452	273.6	
S1	34.7	380.4	750	
S2	34.5	343.2	192.6	
S3		135.6	428.4	
S4	34.7	256.8	272.4	
S5	30.5	138	185.4	
W1	0.7	180	90.6	
W2	0.4	17.4	151.2	
W3	0.6	38.7	70.8	
W4	11.8	1428	100.8	
W5	1	169.8	110.4	
W6	1.3	215.4	68.4	
W7	0.5	41.4	11.1	
S1	33.6	183.6	188.4	
S2	33.6	163.2	147	
S3	33.6	116.4	105.6	
S4	33.6	822	559.2	
S5	33.6	298.8	612	
Sanggou Bay, China				Wang et al. (2014)
GW-1	0.4	145	115	
GW-2	1	490	737	
GW-3	0.6	517	254	

GW-4	0.5	62.2	68	
GW-5	0.5	582	361	
GW-6	0.6	440	279	
PW	30.4	1240	548	
Venice Lagoon, Adriatic Sea				Garcia-Solsona et al. (2008)
Seepage 1	25	1510	237	
Seepage 15	27	980	307	
Marsh well 1	33.7	1970	610	
Marsh well 2	27.5	2340	1260	
Marsh well 3	34.9	1420	710	
Marsh well 5	30.9	3060	1100	
marsh pz.-10	34.8	8700	2270	
marsh pz.-25	34.2	14540	2660	
marsh pz.-80	30.9	3150	1480	
marsh pz.-30	32	5840	1480	
marsh pz.-60	32.6	8170	3110	
marsh pz.-80	32.9	6610	2570	
marsh pz.-90	30.8	5410	2730	
marsh pz.-130	27.1	5180	1990	
Alcalfar Cove W. Mediterranean Sea				Garcia-Solsona et al. (2010a)
sp1	26.9	173	164	
sp2	23.4	167	160	
sp3	23.2	204	157	
sp4	23.2	246	140	
sp4	25.7	180	215	
Pz1-und(45cm)	24.2	910	202	
Pz2-beach(45cm)	24.2	580	182	
Nwell	3.2	530	383	
Masan Bay, Korea				Lee et al. (2009)
G1	28.3		467	
G2	32.5		433	
G3	22.2		625	
G1	23.7		338	
G2	25.6		295	
G3	17.1		211	
G4	25.7		782	
G5	21.4		504	
G6	24		324	
G7	22.6		223	

G8	7.9		222	
G9	3.9		219	
G2	24		146	
G3	30		392	
G4	23		534	
G5	18.1		312	
G6	26		187	
G7	19.3		694	
G8	18.4		555	
G9	30.9		72	
P1	26.3		85	
P2	27		72	
P3	20.2		164	
P5	21.8		560	
P6	14.5		176	
P7	23		167	
P8	25.8		191	
P9	10		486	
P10	20		271	
Celestun Lagoon, Yucatan, Mexico				Young et al. (2008)
X	20	976	25700	
X	17	966	23900	
X	15	567	9040	
X	21	1063	25610	
X	28	1101	34680	
X	28	1162	29830	
X	26	1361	33180	
X	24	1101	31550	
X	22.4	1300	36600	
X	20.2	1180	27020	
Y	20	1280	30800	
Y	15	1210	27200	
Y	30.5	1670	41340	
Y	22.3	961	28570	
Z	3.8	327	5920	
Z	10	254	5090	
Z	12	310	4910	
Narragansett Bay, southern Rhode Island				Kelly and Moran (2002)
A	11.664		3400	

B	0.318	2100	
C	23.962	7000	
D	29.728	5200	
E	30.529	1700	
Hampyeong Bay, Korea			Waska and Kim (2011)
PW1	27.3	760	
PW2	9.6	710	
PW3	14.7	500	
PW4	23.6	750	
PW5	10.5	450	
PW6	18.8	900	
PW7	14.4	1180	
PW1	15.2	430	
PW2	7.1	870	
PW3	8.9	1460	
PW4	7.7	1160	
PW5	30	690	
PW6	27.6	1060	
PW7	24.1	760	
PW8	9	810	
PW9	17.9	1960	
PW10	24.4	3100	
PW11	5.9	1770	
PW1	32.7	600	
PW2	33.1	1050	
PW3	33.3	1150	
PW4	33.3	940	
PW5	32.6	580	
PW6	33.5	340	
PW7	33.4	1380	
PW8	33.7	1460	
PW9	32.8	660	
PW11	31.7	1760	
PW12	34.1	1680	
PW13	32.7	970	
PW14	32.7	960	

Table B. A list of data sources for DIN, DIP, and DSi in world-wide coastal groundwater.

Ocean	Study site	Reference
North Pacific Ocean	Yeongil Bay, Korea	Kim et al. (2008)
	Jeju Island, Korea	Hwang et al. (2005b)
		Kim et al. (2011)
	Southern coast of Korea	Kim et al. (2005)
	Yeoja Bay, Korea	Hwang et al. (2005a)
		Lee et al. (2010)
	Masan Bay, Korea	Lee et al. (2009)
	Hampyeong Bay, Korea	Waska and Kim (2011)
	Mt. Chokai volcanic coast, Japan	Hosono et al. (2012)
	Laoye lagoon, Hainan Island, China	Ji et al. (2013)
	Bamen Bay, South China Sea	Su et al. (2011)
	Northern South China Sea shelf	Liu et al. (2012)
	Tolo Harbour, Hong Kong	Lee et al. (2012)
		Luo et al. (2014)
	Sanggou Bay, China	Wang et al. (2014)
	Maui, Molokai, and Hawaii islands	Street et al. (2008)
	West coast of Hawaii	Dollar and Atkinson (1992)
		Johnson et al. (2008)
	Concepcion Bay, Baja California, Mexico	Santos et al. (2011)
	La Paz Bay, Baja California, Mexico	Urquidi-Gaume et al. (2016)
	West Beach, Santa Barbara, California, USA	Swarzenski and Izbicki (2009)
	Elkhorn Slough of Monterey Bay, California, USA	Breier et al. (2009)
	Lynch Cove, USA	Swarzenski et al. (2007a)
	Santiago Island, Philippines	Senal et al. (2011)

	Manila Bay, Philippines	Taniguchi et al. (2008)
South Pacific Ocean	Moreton Bay, Australia	Gleeson et al. (2013)
		Stewart et al. (2015)
	Caboolture River estuary, Moreton Bay, Australia	Makings et al. (2014)
	Muri lagoon, Cook Islands	Tait et al. (2014)
		Erler et al. (2014)
	Tauranga Harbor, New Zealand	Santos et al. (2014)
	Yarra River estuary, Australia	Santos et al. (2012)
	Tuckean Swamp	Santos et al. (2013)
North Atlantic Ocean	Florida estuary, USA	Charette et al. (2013)
	Marina lagoon, Egypt	El-Gamal et al. (2012)
	Maryland coastal bays, USA	Dillow et al. (2002)
	Cape Henlopen, Delaware, USA	Ullman et al. (2003)
	Tampa Bay, USA	Swarzenski et al. (2007b)
	Rhode Island, USA	Moran et al. (2014)
	Pettaquamscutt estuary, Rhode Island, USA	Kelly and Moran (2002)
	Alcalfar Cove	Garcia-Solsona et al. (2010a)
	Chesapeake Bay, USA	Charette and Buesseler (2004)
	Waquoite Bay, Massachusetts, USA	Kroeger and Charette (2008)
	Badum coastal area, Spain	Garcia-Solsona et al. (2010b)
	Port of Maó	Rodellas et al. (2015)
	Palma Beach, Majorca, Balearic Islands	Rodellas et al. (2014)
	The coast of Majorca Island, Spain	Tovar-Sánchez et al. (2014)
	Península, Spain	Mejías et al. (2012)
	Gulf of Mexico subterranean estuary	Santos et al. (2008)
	West Neck Bay, Long Island	Beck et al. (2007b)

	Ivory coast, Abidjan, Western Africa	Oga et al. (2008)
	Densu basin, Ghana	Tay and Kortatsi (2008)
	Douala Bain, Western Africa	Eneke et al. (2011)
	Alfacs Bay, Spain	Unpublished data (Rodellas et al.)
	Argentona, Catalonia, Spain	Unpublished data
	El Gorguel, Spain	Unpublished data
South Atlantic Ocean	Patos-Mirim lagoon, Brazil	Niencheski et al. (2007)
	Arraial do Cabo, Brazil	Godoy et al. (2013)
	Eastern Brazilian shelf, Bahia, Brazil	Costa Jr. et al. (2000)
Indian Ocean	Mauritius Island	Povinec et al. (2012)
	Marmion lagoon, Western Australia	Johannes and Hearn (1985)
	Barka, Gulf of Oman	Rajmohan et al. (2009)
	St-Gilles La Saline fringing reef, La Re´union	Cuet et al. (2011)
	Godavari estuary, India	Rengarajan and Sarma (2015)
	Mida creek, Kenya	Kitheka et al. (1999)

Publications and Presentations

Publications:

H. -M. Cho, Y. -L. Hong, and G. Kim* (2011) Atmospheric depositional fluxes of cosmogenic ^{35}S and ^{7}Be: Implications for the turnover rate of sulfur through the biosphere, *Atmospheric Environmen*t, 45, 4230-4234.

G. Yan, **H. -M. Cho**, I. Lee, and G. Kim* (2012) Significant emissions of ^{210}Po by coal burning into the Urban Atmosphere of Seoul, Korea, *Atmospheric Environment*, 59, 117-124.

E. Y. Kwon, G. Kim*, F. Primeau, W. S. Moore, **H. -M. Cho**, T. DeVries, J. L. Sarmiento, M. A. Charette, and Y. K. Cho (2014) Global estimate of submarine groundwater discharge based on an observationally constrained radium isotope model, *Geophysical Research Letters*, 41, doi:10.1002/2014GL061574.

J. Kim, **H. -M. Cho**, and G. Kim* (2015) ^{228}Ra flux in the Northwestern Pacific marginal seas: Implications for disproportionally large submarine groundwater discharge, *Ocean Science Journal*, 50(2), 195-202.

H. -M. Cho, and G. Kim* (2016) Determining groundwater Ra endmember values for the estimation of the magnitude of submarine groundwater discharge using Ra isotope tracers, *Geophysical Research Letters*, 43(8), 3865-3871.

H. -M. Cho, and G. Kim* (2017) Large temporal changes in contributions of groundwater-borne nutrients to coastal waters off a volcanic island, *Ocean Science Journal*–online published)

H. -M. Cho, G. Yan, and G. Kim (2017) Adsorption and desorption behaviors of silicate and phosphate in subterranean estuaries, submitted to *Biogeochemistry* (under review)

H. -M. Cho, G. Kim*, E. Y. Kwon, N. Moosdorf, J. Garcia-Orellana, and I. R. Santos (2017) Submarine solute flux as a major source of nutrients to the global ocean, submitted to *Proceedings of the National Academy of Sciences* (under review).

Presentations:

International presentations

H. -M. Cho and G. Kim (2011. 7) Dissolved phosphorus flow into the ocean enhanced by silicate in groundwater, *IUGG general meeting 2011,* Melbourne, Australia. **(INVITED)**

H. -M. Cho and G. Kim (2011. 11) Inputs of nutrients to the ocean through the subterranean estuary, *SNU-HU Joint Symposium*, Seoul, Korea. (Oral)

H. -M. Cho and G. Kim (2012. 9) Behavior of silica and phosphorus in subterranean estuary, *A Europole Mer Gordon-like Conference*, L'Aber Wrac'h, Brittany, France. (Poster)

H. -M. Cho and G. Kim (2012, 12) Inputs of nutrients to the ocean through the subterranean estuary, *SNU-HU Joint Symposium*, Hokkaido, Japan. (Oral)

H. -M. Cho and G. Kim (2015. 2) Behavior of dissolved silicate in a subterranean estuary, *2015 Aquatic Sciences Meeting*, Granada, Spain. (Poster)

G. Kim, **H. -M. Cho**, and J.H. Kim (2015. 4) Application of Ra-228 as a quantitative

tracer of submarine groundwater discharge over global and regional scales, *Tenth International Conference on Methods and Applications of Radioanalytical Chemistry*, Hawaii, USA.

G. Kim, **H. -M. Cho**, and I. Kim (2015. 8) Biogeochemical effects of submarine groundwater discharge in coastal waters. *Goldschmidt 2015*, Prague, Czech Republic.

H. -M. Cho and G. Kim (2016. 8) Role of submarine groundwater discharge (SGD) on biological production in coastal waters off a volcanic island, Jeju, Korea. *AOGS 2016*, Beijing, China. (Poster)

Domestic presentations

조형미, 방희근, 김규범 (2010. 6) 지하수가 유출되는 연안 사질 퇴적층 공극수에서 규산염의 거동, 2010 한국해양과학기술협의회 공동학술대회 (포스터 발표)

조형미, 김규범 (2011. 6) 연안 지하수에서 규산염과 인산염의 거동과 해양학적 중요성, 2011 한국해양과학기술협의회 공동학술대회 (구두 발표)

조형미, 김규범 (2015. 5) 해저 지하수 유출이 제주도 연안 생태계에 미치는 영향, 2015 한국해양학회 춘계학술발표대회 (구두 발표)

조형미, 김규범 (2016. 10) Large temporal changes in the contribution of submarine groundwater discharge to nutrient budgets in coastal waters off a

volcanic island, Jeju, Korea, 2016 한국해양학회 추계학술발표대회 (포스터 발표)